Laser Microfabricated Polymer Microelectrodes for Intraspinal Microstimulation

by

David A. Roszko

A thesis submitted in partial fulfillment of the requirements for the degree of

Master of Science

Neuroscience
University of Alberta

Abstract

Intraspinal microstimulation (ISMS) is a neural prosthetic technique which can restore locomotor function in models of severe spinal cord injury (SCI). Historically, ISMS has been implemented with microwire electrodes or rigid multielectrodes, which suffer from limitations related to either functionality or biocompatibility. Microwire electrodes, although demonstrating chronic biocompatibility, are functionally limited in that they can only electrically stimulate one discrete location - at the deinsulated tip. Multielectrodes, although capable of stimulating multiple discrete sites along the device shank, are typically large and constructed from stiff materials which can increase tissue damage and exacerbate foreign body responses. A recent trend in neural interface research has focused on developing flexible multisite electrodes for the nervous system which can stimulate multiple targets while reducing foreign body responses caused by mechanical mismatch between the implanted device and the nervous system.

In this research, a flexible polymer-substrate penetrating multielectrode for the spinal cord was developed as a way to improve the efficacy and biocompatibility of ISMS. Polymer multielectrodes were created from platinum-iridium foil and a polydimethylsiloxane-based substrate using laser microfabrication methods. Electrochemical properties of the laser-deinsulated multielectrode stimulating sites were assessed with standard electrochemical methods, including electrochemical impedance spectroscopy, cyclic voltammetry, and voltage transients, and were compared against microwire electrodes in phosphate buffered saline and *in vivo* in domestic pigs. Multielectrode mechanical properties were characterized through standard compression tests, in which the buckling force and theoretical Young's modulus were compared against those of microwire electrodes. Lastly, multielectrode functionality was verified *in vivo* in

a pig model of spinal cord injury by stimulating within the spinal cord and measuring evoked isometric joint torques and joint kinematics.

Polymer multielectrodes were shown to be significantly more flexible than microwire electrodes, owing to their exceptionally flexible PDMS substrates. Multielectrode laser-roughened stimulating sites were shown to have higher charge storage capacities than microwire electrodes in phosphate buffered saline and higher charge injection limits than microwire electrodes *in vivo*. When stimulating within the pig spinal cord, polymer multielectrodes were capable of producing joint torques and kinematics similar to those previously generated by microwire electrodes. However, acute tissue damage from implanting the multielectrodes with rigid insertion aids generated significantly more acute tissue damage than the microwire electrodes - suggesting that other insertion aid methods should be explored. Overall, these results suggest that this new polymer multielectrode design may improve targeting, functionality and biointegration in models of spinal cord injury.

Preface

This thesis is an original work by David A. Roszko. The research project in this thesis received research ethics approval from the University of Alberta Research Ethics Board, Project Name "Mechanical Stability of Intraspinal Implants in Large Animal Models", Protocol AUP00000799, Feb. 3, 2014.

All experiments were conducted in the lab of Dr. Vivian K. Mushahwar. This study was conceived by Dr. Vivian K. Mushahwar and David A. Roszko. David A. Roszko and Vivian K. Mushahwar designed the polymer multielectrodes. David A. Roszko fabricated and characterized all multielectrode and microelectrode samples in the laboratory. D. Wilson created the force measurement system used to assess the mechanical properties of the multielectrodes and microelectrodes. David A. Roszko, N. Tyreman, S. Mirkiani, and Vivian K. Mushahwar assisted with the surgical procedures and *in vivo* data collection. N. Tyreman completed the tissue processing. David A. Roszko analyzed all data.

The literature review in chapter 1 was written by David A. Roszko. Chapter 2 was written by David A. Roszko, with feedback from co-authors. Chapter 3 was written by David A. Roszko.

Acknowledgements

This thesis research was completed with the financial support of the Canadian Institutes of Health Research (CIHR), the Canada Foundation for Innovation (CFI), and the generous support of Jim and Nancy Hutton and Leo Broks through the University Hospital Foundation. I was personally supported by a National Sciences and Engineering Research Council of Canada (NSERC) Canada Graduate Scholarship - Master's (CGS-M) and an Alberta Graduate Excellence Scholarship (AGES). Only through the generous financial contributions of these agencies and private donors was this work possible.

I would like to acknowledge my supervisor, Dr. Vivian K. Mushahwar, for her support in the development and execution of this research project. Even when things went wrong, she was a constant advocate for my success and ensured that I could be resilient and excel in my research. You have my sincerest thanks.

I would like to acknowledge Michel Gauthier, Neil Tyreman, Don Wilson, and Rod Gramlich, for training me on lab equipment and techniques, for developing equipment related to my project, and for assisting with animal experiments. I would also like to acknowledge Soroush Mirkiani for being available to discuss problems related to the manufacturing and design of neural interfaces.

Lastly, I would like to thank my wife, Ashley Roszko, for supporting me while I pursue my research endeavors.

Table of Contents

List of Tables

List of Figures

List of Symbols and Abbreviations

AIROF - activated iridium oxide films

AIS - American Spinal Injury Association Impairment Scale

ASIA - American Spinal Injury Association

BCP - block copolymer

CIL - charge injection limit

CSC_c - cathodic charge storage capacity

CV - cyclic voltammetry

EDS - energy-dispersive x-ray spectroscopy

EIS - electrochemical impedance spectroscopy

E_{mc} - maximum cathodic polarization

eSCS - epidural spinal cord stimulation

FBR - foreign body response or reaction

FES - functional electrical stimulation

ISMS - intraspinal microstimulation

LCP - liquid crystal polymer

LIPSS - laser-induced periodic surface structures

MR - magnetic resonance

PBS - phosphate-buffered saline

PDMS - polydimethylsiloxane

PEDOT - poly(3,4-ethylenedioxythiophene)

PEG - polyethylene glycol

pFES - peripheral functional electrical stimulation

PtIr - platinum-iridium

PtIr-FW - platinum-iridium flat wire

SCI - spinal cord injury

SEM - scanning electron microscopy

SLIP - structured laser interference patterning

TIVA - total intravenous anesthesia

tSCI - traumatic spinal cord injury

VT - voltage transients

Quote

"We have a habit in writing articles published in scientific journals to make the work as finished as possible, to cover up all the tracks, to not worry about the blind alleys or describe how you had the wrong idea first, and so on. So there isn't any place to publish, in a dignified manner, what you actually did in order to get to do the work." - Richard P. Feynman, Nobel Lecture, 1966

Chapter 1: Introduction

Overview

The overall goal of my thesis research was to design, fabricate and characterize a new, implantable neural interface for the spinal cord which could be used to restore mobility after severe spinal cord injury. My research aimed to explore how recent trends in flexible polymer neural interface designs for intracortical and intrafascicular neural interfaces can be applied to the spinal cord to achieve improved device functionality and biocompatibility. Herein, I explored the fabrication and functionality of a new intraspinal multielectrode created with a new, exceptionally flexible smart-polymer substrate recently described by Gökaltun et al. for biomicrofluidics [1]. Through this initial characterization, I aimed to demonstrate the mechanical flexibility of these newly created devices compared to traditional microwire implants, compare the electrochemical properties of these devices to microwire implants, and demonstrate functionality of these implants in an animal model of spinal cord injury (SCI). I hope that this research will establish the groundwork for testing these devices further *in vitro* and *in vivo* to assess how these devices may improve biocompatibility compared to traditional implant designs.

In this introductory chapter, I will begin by exploring SCI and current treatment options. This will be followed by an introduction into neural interfaces used to restore mobility after paralysis caused by SCI. I will then focus on intraspinal microstimulation - the technology which I focused on for my research - and discuss some of the considerations involved in designing intraspinal neural interfaces. Lastly, I will discuss how polymer multielectrodes may address some of the current challenges faced by intraspinal implants.

Spinal Cord Injury

Spinal cord injury is a devastating condition that can result in paralysis, loss of sensation, and many other life-altering secondary complications [2]. In Canada, the estimated incidence of SCI is 3,675 cases per year, with a prevalence of 85,556 persons [3]. The impacts of SCI are multifaceted, with physical [2], [4], social, and economic dimensions [5]. In terms of the economic impact, the costs associated with traumatic SCI (tSCI), where injury is due to an external physical impact, are estimated to be between $1.5 - $3.0 million per person, costing the Canadian healthcare system $2.67 billion annually [6]. Although the priorities of people with

SCI differ depending on the level and extent of injury, regaining mobility has often been listed as a high priority [7].

Treatment Options for SCI

Currently, there is no cure for SCI, although various treatment options have been developed to preserve or improve function after injury. Treatment options under investigation for SCI often fall into three major categories: neuroprotection, neuroregeneration and rehabilitative or assistive devices. Neuroprotection, which aims to prevent further damage from occurring after the initial injury, can be accomplished with surgical techniques, such as surgical decompression, or by administering anti-inflammatory drugs [8]. Neuroregeneration, which aims to improve recovery after injury by regenerating neural tissue, can be accomplished through experimental drug and cell therapies [9], [10]. Lastly, rehabilitative or assistive devices, which seek to restore function after injury, can be realized through a wide range of clinically available technologies and approaches such as with wheelchairs or exercise training, or through experimental procedures involving exoskeletons or functional electrical stimulation (FES) to restore lost function or augment remaining function [11].

FES Systems to Restore Lower Limb Mobility after SCI

In the context of lower limb mobility, FES systems for both the peripheral and central nervous system are under development to restore the ability to stand, step and walk after SCI [12], [13]. These FES devices exist on a spectrum of invasiveness and specificity, where more specific electrical stimulation may come at the cost of increasingly invasive surgeries.

Peripheral Functional Electrical Stimulation

For peripheral FES (pFES) systems, surface stimulators and implantable devices can stimulate peripheral nerves to activate muscles paralyzed due to a SCI. In people with American Spinal Injury Association (ASIA) Impairment Scale (AIS) A-C injuries, a pFES system, implemented with a combination of intramuscular and epimysial electrodes, was able to achieve standing times of greater than 30 minutes for 3 participants and median standing times of 3.33 minutes for all 11 participants [14]. In another study, a similar pFES system allowed a participant with an

AIS A injury to walk distances of up to approximately 100 m, completed over the course of multiple 3-6 minute walking sessions in one day, and stand for 15 minutes [15]. Although promising, the major limitation of pFES systems is rapid muscle fatigue due to the reversed recruitment order of motor units, where large diameter axon, fast-fatigable motor units are recruited first instead of small diameter axon, fatigue-resistant motor units [16]. However, recent techniques have demonstrated that fatigability may be reduced with pFES systems by adjusting stimulation parameters, such as pulse amplitude and frequency, or by employing interleaved stimulation through multiple electrodes to reduce motor unit discharge rates or recruit motor units in a more physiologically normal order [17].

Epidural Spinal Cord Stimulation

For the central nervous system, the dominant FES technology available is epidural spinal cord stimulation (eSCS). Historically developed for treating pain, eSCS involves the placement of multicontact electrodes on the surface of the dura mater to electrically stimulate the posterior spinal cord [18]. More recently, epidural stimulators have produced some locomotor recovery in people with SCI [19], [20]. In three landmark studies, eSCS paired with rigorous locomotor training for 15 to 85 weeks resulted in participants with AIS A-B injuries walking up to 102 m and participants with AIS C-D injuries walking up to 1 km [13], [21], [22]. After training and when eSCS was turned off, participants with less severe injuries (AIS C-D) experienced neurological recovery which had not been attained through previous rehabilitative training alone, such as the ability to walk several steps without assistive devices or stimulation and the recovery of some voluntary leg movements [13]. However, when eSCS was turned off for participants with motor complete injuries (AIS A-B), the ability to walk overground or step independently on a treadmill was lost [21], [22]. These studies have created considerable excitement regarding the potential of paired exercise training and FES for restoring function after SCI.

Intraspinal Microstimulation

Another experimental technique for stimulating the central nervous system is intraspinal microstimulation (ISMS). ISMS is a more invasive procedure than eSCS, involving the implantation of hair-like microdevices directly into the spinal cord parenchyma to achieve focal

electrical stimulation [23], [24]. By electrically stimulating within the spinal cord, ISMS can activate locomotor networks to produce flexion, extension, alternation, and synergistic movements in the legs [25]. ISMS is believed to produce these movements and synergies by activating a combination of motoneurons, pre-motor networks, fibers-in-passage, interneurons, and sensory afferents [26], [27]. The location of these locomotor targets within the spinal cord have been shown to be consistent within species [28] and across species, such as in the rat [29], cat [23], pig [30] and in non-human primates [31]. These functional locomotor regions within the spinal cord exhibit a similar functional arrangement to the motoneuronal pools within the lumbosacral spinal cord [31]. Hip flexion and knee extension can be produced by electrically stimulating within the rostral lumbosacral cord while movements such as hip extension, ankle extension, and knee flexion can be produced by stimulating more caudally [31]. In preclinical studies, average standing durations of 20.89 minutes [32] and overground walking distances of 609 m - 835 m [33] have been achieved.

Comparing FES Technologies for Restoring Lower Limb Mobility after SCI

Compared to eSCS and some pFES systems, ISMS is one of the most invasive techniques proposed for restoring motor function after SCI. pFES and eSCS systems have both been successfully validated in humans for partially restoring locomotor function in people paralyzed by SCI, whereas ISMS systems for restoring locomotor function have not yet been translated to humans. Both pFES and eSCS systems have been capable of producing walking distances of around 100 m in people with severe SCI, however this was achieved without rest using eSCS and with rest using pFES [15], [21], [22]. Comparing these FES technologies in preclinical models, ISMS can produce longer durations of standing than pFES by selectively recruiting motor units in a graded and nearly normal physiological recruitment order [29], [32]. Additionally, pFES systems are known to experience lead wire breakage as they are implanted in regions of the body that may experience considerable movement, such as the limbs [34]. Because eSCS and ISMS systems are implanted in a small and relatively fixed position above or inside the spinal cord respectively, movement-associated implant damage may be reduced with these systems. Comparing eSCS and ISMS, ISMS can produce immediate locomotor function through the application of electrical stimulation within the spinal cord [33], [35], without the need for excessive, paired locomotor training required by eSCS [22]. However, locomotor function

generated by ISMS would likely be involuntary and controlled by an implanted stimulator, in contrast to voluntary locomotor recovery which can be facilitated by eSCS [13]. Lastly, ISMS can produce long distances of walking in models of severe SCI [33], which may not be possible with eSCS [21], [22] or pFES [97]. Thus, although considerable work is still required to translate ISMS to humans to restore locomotor function after SCI, ISMS remains an exciting area of spinal cord neural prosthesis research which may demonstrate some functional advantages over pFES and eSCS systems in terms of fatigue resistance and achievable walking distances.

Neural Interfaces used in Intraspinal Microstimulation

Several different neural interface designs have been used to implement ISMS. Typically, microwire arrays, fabricated by hand from 30 - 50 μm diameter stainless steel or platinum-iridium alloy microwires coated in polyimide or Teflon, have been used [24], [36], [37]. Microwire arrays have been shown to produce minimal functional deficits in chronic experiments in the cat [24] and produce minor foreign body responses in chronic experiments in the rat [38]. Minimal tissue damage was likely observed due to the relatively small size and flexibility of microwire implants. However, microwires are limited in that they can only electrically stimulate at one discrete location within the spinal cord - at the deinsulated tip. If a desired locomotor target is missed by the microwire electrode upon first implantation, the microwire must be implanted again until an adequate target is reached, which may result in multiple spinal cord penetrations and increased potential for tissue damage. When creating functional locomotor maps of the macaque spinal cord, it was noted that approximately 45% of microwire implant sites produced no locomotor activity when electrically stimulated [31], demonstrating that reaching the correct target is of paramount importance.

Accurately implanting ISMS microwire electrodes is challenging, requiring submillimeter precision in the rostrocaudal, dorsoventral, and mediolateral axes. Generally, arrays can be fabricated based on average spinal cord dimensions determined by atlases [39]. More accurate dimensions can be attained by first completing pre-operative magnetic resonance (MR) imaging to obtain precise dimensions of the target spinal cord [36]. Based on this information, a microwire array can be constructed to the exact specifications of the spinal cord to improve the chances of proper array placement and functionality. Additionally, to improve targeting

accuracy, image-guided implantation systems have been developed which employ MR imaging [40] or ultrasound imaging [41] to ensure microwire electrodes are implanted in the proper location intraoperatively.

Due to the design of microwire arrays, where multiple electrodes are separated rostrocaudally by a specified distance (2 - 4 mm), rostrocaudal targeting specificity is addressed by implanting multiple microelectrodes in the spinal cord. Moreover, because most ISMS microwire arrays allow for the individual placement of each microwire electrode separately, mediolateral positioning of each microwire electrode can be adjusted intraoperatively as required. Dorsoventral targeting with microwire electrodes, however, can only be addressed during the manufacturing process, as each microwire implant is fabricated with a specific implantation depth and can only stimulate at the tip of the electrode. Thus, it becomes difficult to modify the dorsoventral position of a microwire implant.

To solve this problem, researchers have investigated the use of multisite devices for the spinal cord, such as cylindrical multielectrodes constructed on an optical fiber core substrate [42] or multisite silicon microelectrode arrays [43] - [45] which have multiple electrical stimulation sites along each device shank. With these devices, a single electrode insertion can effectively reach multiple dorsoventral targets, increasing the likelihood that a suitable locomotor target is reached after the first spinal cord penetration. Although these devices solve the problem of dorsoventral targeting specificity within the spinal cord, their fabrication methods inevitably lead to larger and stiffer devices, which can increase tissue displacement and exacerbate foreign body responses.

Lastly, a key consideration for intraspinal implants is how the relative motion of the spinal cord and spinal column affect implant integrity. In domestic pig cadavers, which have a similar spinal column range of motion to that of humans, Toossi et al. showed that the lumbar enlargement experienced a change in length of 5.64 ± 0.59 mm when transitioned from hyperextension to hyperflexion [46]. Similarly, it was shown that the L2 lamina, which would act as a rigid fixation point for the ISMS lead wires, underwent a displacement of 5.66 ± 0.57 mm relative to the adjacent spinal cord when transitioned from hyperextension to hyperflexion [46]. For a rigidly implanted ISMS device, where the electrode is implanted in the spinal cord and the lead wire is fixed to the L2 spinous process, the combination of spinal cord strain and relative displacement between the spinal cord and spinal column could produce tethering forces sufficient to explant

the intraspinal device [46] or cause tissue damage [47], [48]. To overcome this problem, strain-relief systems [46] and wireless designs [49] have been proposed for intraspinal implants.

Foreign Body Reponses of Neural Interfaces

Implanting a device into the nervous system leads to a natural cellular and immune response known as the foreign body response or reaction (FBR). Upon implantation into neural tissue, damage to the blood brain barrier leads to blood-plasma proteins adhering to the device, followed by a cascade of microglia and astrocyte activation which seek to encapsulate the device in a glial scar [50]. Although inflammation has recently been shown to be unexpectedly beneficial in promoting functional recovery after injury by enhancing neural plasticity [95], FBR is generally considered an unwanted response for neural interfaces and a key reason why neural implants, especially systems for recording single unit neural activity, fail over time. Glial encapsulation and chronic inflammation can lead to either migration or death of neurons near the implant [51], resulting in reduced efficacy of the device. To decrease FBR and improve the biocompatibility and functionality of neural interfaces, several implant modifications have been tested. At the surface level, hydrophilic coatings such as polyethylene glycol (PEG) [52], bioactive coatings [53] and anti-inflammatory drugs [54] can modulate or reduce FBR. Mechanically, it has been shown that tethering forces and implant size also exacerbate FBR [48]. Thus, reduced implant size and strain relief mechanisms [46], [55] have been explored. Lastly, implant stiffness and mechanical mismatch between the implant and tissue have been shown to exacerbate FBR [56], [57], leading to the development of implants which strive to be as flexible as the brain or spinal cord.

Electrochemical Safety Requirements for Neural Interfaces

Electrochemical considerations play a key role in device safety when stimulating within the nervous system. Generally, the mechanisms of how electrical stimulation causes neural tissue damage can be understood by two main theories: 1) mass action theory, which claims that electrically-induced neuronal activation can lead to cellular or environmental changes, such as excitotoxicity, which result in neuronal death, or 2) electrochemical theories, which claim that toxic electrochemical byproducts caused by charge injection mechanisms can lead to cell death

[58]. When electrically stimulating neural tissue, current may be delivered through a combination of capacitive mechanisms, involving the redistribution of charge at the electrode surface and within the electrolyte, and Faradaic mechanisms, which achieve charge transfer via redox reactions at the electrode/tissue interface [58], [59]. Faradaic charge injection mechanisms in particular can create electrochemical byproducts involved in electrochemical theories of tissue damage.

Focusing on electrochemical theories of tissue damage, experimental evidence has shown that tissue damage can be reduced or eliminated by operating stimulating electrodes within strict limits based on the charge per phase and charge density of the stimulating sites [60] - [62]. Based on experimental data, electrochemical limits have been historically described for reducing tissue damage, such as maintaining charge densities below 30 $\mu C/cm^2$ or reducing charge per phase below 4 nC/ph [62], [63]. Yet most studies assessing tissue damage from electrical stimulation fail to capture the multitude of parameters which may affect damage, such as stimulation frequency, pulse duration and duty cycle, electrode geometry and size, or current densities, and exceptions to these firm electrochemical limits, where electrodes may operate beyond known limits and produce minimal damage, may exist [62]. A commonly accepted approach to reduce tissue damage from electrical stimulation involves employing biphasic, charge-balanced stimulation waveforms and restricting the potentials of stimulating devices within safe limits (such as between -0.6 - 0.8 V for platinum alloys, relative to Ag|AgCl) to prevent water hydrolysis; through these restrictions, cytotoxic electrochemical byproducts stemming from water hydrolysis and other non-reversible faradaic reactions can be reduced [58], [59].

Methods for Improving the Electrochemical Properties of Neural Electrodes

Several surface modifications can be applied to stimulating electrodes to improve their electrochemical properties and allow devices to inject more charge safely into neural tissue, such as by applying activated iridium oxide films (AIROF) [64], hydrogels or conductive polymers such as poly(3,4-ethylenedioxythiophene) (PEDOT) [65], [66], or graphene oxide coatings [96]. In chronic stimulation experiments, iridium oxide and hydrogel coatings have demonstrated persistent advantages over bare platinum electrodes, although graphene oxide coatings may have reduced efficacy at chronic timepoints [96]. These modifications may be critical for reaching

required stimulation levels *in vivo* to produce functional responses while remaining within safe potential limits, especially considering that charge injection capabilities *in vivo* are typically reduced compared to *in vitro* measurements [67].

Electrochemical Assessments for Neural Electrodes

Neural electrodes can be electrochemically assessed with a number of common techniques, including electrochemical impedance spectroscopy (EIS), cyclic voltammetry (CV) and voltage transients (VT) [59]. EIS characterizes the electrochemical impedance of an electrode over a range of stimulating frequencies, which can be a useful measure for comparing electrodes in terms of how much current they may be capable of delivering while remaining within safe potential limits. CV can be used to assess how much current can be delivered through an electrode when the potential is ramped at a constant rate between predefined potential limits; by integrating the cathodic current over time, the amount of reversible cathodic charge which can be stored on at the electrode-tissue interface - termed the cathodic charge storage capacity (CSC_c) - can be calculated. And lastly, VT can be used to assess the maximum cathodic and anodic potentials of an electrode during a stimulation pulse to determine the maximum charge injection limit (CIL) of the electrode before potentials exceed safe limits.

Polymer Microelectrodes

To improve the biocompatibility of neural implants, a recent trend in neural interface research has centered around the use of polymer substrates to create flexible, implantable devices [68] - [70]. These devices, known as polymer microelectrodes, utilize a wide range of common and experimental polymer materials to produce implants with lower Young's moduli than that of metal or silicon. These materials have Young's moduli ranging from 10.6 GPa for liquid crystal polymer (LCP) to as low as 0.1-0.5 MPa for polydimethylsiloxane (PDMS) [71]. When compared to traditional microelectrode materials such as silicon, which has a Young's modulus of 190 GPa [69], these polymer materials are much closer to matching the modulus of nervous tissue, which can be as low as 5 kPa for the spinal cord [72]. Devices have been fabricated with polyimide substrates [73], parylene-C substrates [74], and LCP substrates [75], [76]. PDMS, one of the lowest modulus polymers available, has been used as the substrate of non-penetrating

neural interfaces [77]. However, PDMS has less commonly been used as the substrate for penetrating neural interfaces [78] - [80], and has never been used as the substrate of penetrating electrodes for the spinal cord. One likely reason for this is because the extremely low modulus of PDMS makes it exceptionally difficult to insert into tissue.

Insertion Methods for Polymer Microelectrodes

Due to their high flexibility, polymer microelectrodes become nearly impossible to insert into neural tissue on their own. Instead, researchers have used strategies such as temporary insertion guides or shuttles [79], [81], dissolvable stiffeners [82] - [84], smart polymers or shape memory polymers that exhibit lower moduli after insertion [56], [85], or tunable liquid metal probes [80] to help insert these probes into the nervous system. In some cases, this requires modifying the surface characteristics of the polymer substrate in order to achieve better adhesion between the implant and any dissolvable stiffener [83].

Laser fabrication methods for neural interfaces

To construct polymer microelectrodes, traditional microfabrication and nanofabrication techniques are often utilized, such as spin coating, photolithography, chemical vapor deposition, physical vapor deposition methods, and reactive ion etching [68], [69]. Yet these traditional techniques can be costly and time consuming, requiring multiple lithographic masks to be developed for each design iteration. Laser microfabrication has been established as a rapid and cost-effective prototyping method for developing neural interfaces and neural prostheses [86], [87]. Lasers can be used to machine metals, polymers, ceramics, and composites by selectively heating, melting, vaporizing, or ablating the target material [88]. Laser microfabrication techniques have been utilized to create prototype devices for retinal prostheses [86], [87], peripheral nerve and intrafascicular interfaces [74], [89], and intracortical interfaces [82], [90]. The biocompatibility of laser microfabricated microelectrode arrays constructed from PDMS and platinum foil and has also been assessed, where it was shown that the byproducts of laser microfabrication, typically consisting of metal oxides and silicon oxides, do not cause further biological responses compared to the unmachined materials [91]. Additionally, laser microfabrication techniques have also been used to improve the electrochemical properties of

stimulating electrodes. This has been achieved by increasing stimulating electrode surface areas through techniques such as structured laser interference patterning (SLIP) [74] or creating laser-induced periodic surface structures (LIPSS) [92].

Polymer Microelectrodes in the Context of ISMS

In the context of intraspinal micro-implants, multisite devices are favorable over microwires because they can deliver electrical stimuli to multiple regions within the spinal cord. Multisite devices eliminate the need for multiple electrodes to be implanted at the same rostrocaudal/mediolateral position to excite multiple dorsoventral targets and reduce the possibility of incorrect electrode placement and reinsertion tissue damage. Yet these devices are typically larger and stiffer than microwires and may exacerbate FBR. Improving the flexibility of neural interfaces has been shown to improve biocompatibility by reducing implant/tissue strains [56], [57]. Therefore, a flexible polymer implant with multiple stimulation sites may satisfy both the efficacy requirement (i.e., requiring multiple stimulation sites) and the safety requirement (i.e., displaying adequate flexibility to reduce FBR) needed to implement ISMS effectively. PDMS is a common biocompatible polymer used for constructing non-penetrating neural interfaces, yet it has been less commonly used as the substrate of penetrating multielectrode neural interfaces because of its exceptional flexibility [69]. With the addition of poly(dimethylsiloxane) dimethylsiloxane-ethylene block copolymer (PDMS-PEG BCP) [1], PDMS substrates may have the additional advantage of reducing protein and cell adhesion *in vivo*. This added feature, although not directly assessed in this thesis, may provide an additional advantage for these devices by modulating glial cell adhesion *in vivo* and reducing FBR, and should be investigated in future research.

Goal and Aims

In light of the above information, the goal of my thesis research was to design, fabricate and characterize a new, polymer microelectrode with multiple stimulation sites (termed polymer multielectrode) for the spinal cord in an effort to improve the efficacy and biocompatibility of ISMS compared to when ISMS is implemented with traditional 50 μm diameter, platinum-iridium (80%/20%) microwire electrodes. I have selected to machine these prototype polymer

multielectrodes using laser microfabrication, which has been validated as a rapid prototyping method for neural interfaces for the cortex and peripheral nerve [74], [82]. To improve the efficacy of the device compared to microwire implants, the polymer multielectrode was fabricated with 3 stimulating sites separated dorsoventrally along the shank, allowing the multielectrode to electrically stimulate 3x more dorsoventral regions than a single microwire electrode. Based on evidence showing that flexible neural interfaces exhibit decreased FBR [56], [57], the polymer multielectrode was fabricated with a flexible PDMS-based substrate - PDMS being one of the most flexible, traditional polymer materials used in neural interfaces [71] - in an effort to maximize its flexibility compared to microwire implants and other multielectrode designs. Adding to the novelty of this design, the substrate was modified through the addition of a low percentage of PDMS-PEG BCP [1] in an effort to modulate FBR. Although this feature was not directly assessed in this thesis, we plan to assess this modification in subsequent studies on *in vitro* and *in vivo* glial cell adhesion and FBR.

Through this research, I sought to address the following three aims:

1) I aimed to make a device more flexible than traditional microwire electrodes commonly used in ISMS to improve device biocompatibility.
2) I aimed to create multielectrode stimulating sites that would perform similarly to microwire electrodes in terms of their electrochemical properties and charge injection capabilities.
3) I aimed to demonstrate that functional responses could be generated by the polymer multielectrodes when implanted within the lumbosacral enlargement of the pig in the context of ISMS as seen previously for microwire implants.

Aim (1) was assessed by measuring the buckling forces [83] of both microwire implants and polymer multielectrodes, clamped end-to-end in a custom compression-sensing device inspired by a force sensor developed by Qu et al. [93]. A lower buckling force would indicate that the electrode is more flexible. Due to the inherent flexibility of PDMS, polymer multielectrodes fabricated with PDMS/PDMS-PEG substrates were expected to exhibit improved mechanical flexibility compared to traditional microwire implants.

Aim (2) was assessed using EIS, CV and VT [59] to compare the electrochemical impedance, CSC_c, and CIL of microwire electrodes and polymer multielectrodes in both phosphate buffered saline and *in vivo* in a domestic pig model. Domestic pigs were selected as the animal model for this study due to their similar spinal cord neuroanatomy to humans [39] and previous use in ISMS research [30], [46], [94].

Aim (3) was assessed by implanting polymer multielectrodes *in vivo* in a domestic pig model and electrically stimulating within the quadriceps motor pool. A force transducer (Scottsdale, AZ, USA) firmly held in place proximal to the ankle was used to record isometric joint torques as a function of stimulation current amplitude. Kinematics and electrode responses were also assessed.

Along with addressing these three aims, I also report the laser microfabrication process parameters and outcomes that were developed during this study to inform future researchers when developing neural interfaces with laser fabrication methods. Micromachined materials and implants were assessed with scanning electron microscopy (SEM) and energy-dispersive x-ray spectroscopy (EDS) (ThermoScientific, MA, USA) to assess surface features, surface elements, and the minimum feature size of the devices.

References

[1] A. Gökaltun, Y. B. A. Kang, M. L. Yarmush, O. B. Usta, and A. Asatekin, "Simple surface modification of poly(dimethylsiloxane) via surface segregating smart polymers for biomicrofluidics," *Scientific Reports*, vol. 9, 7377, 2019.

[2] C. S. Ahuja, J. R. Wilson, S. Nori, M. R. N. Kotter, C. Druschel, A. Curt, and M. G. Fehlings, "Traumatic spinal cord injury," *Nature Reviews Disease Primers*, vol. 3, no. 1, Apr., pp. 1-21, 2017.

[3] V. K. Noonan, M. Fingas, A. Farray, D. Baxter, A. Singh, M. G. Fehlings, and M. F. Dvorak, "Incidence and prevalence of spinal cord injury in Canada: A national perspective," *Neuroepidemiology*, vol. 38, no. 4, June, pp. 219-226, 2012.

[4] R. Sweis, and José Biller, "Systemic complications of spinal cord injury," *Current Neurology and Neuroscience Reports*, vol. 17, art. 8, Feb., pp. 1-8, 2017.

[5] I. H. Tsai, D. E. Graves, W. Chan, C. Darkoh, M-S. Lee, and L. A. Pompeii, "Environmental barriers and social participation in individuals with spinal cord injury," *Rehabilitation Psychology*, vol. 62, no. 1, Feb., pp. 36-44, 2017.

[6] H. Krueger, V. K. Noonan, L. M. Trenaman, P. Joshi, and C. S. Rivers, "The economic burden of traumatic spinal cord injury in Canada," *Chronic diseases and injuries in Canada*, vol. 33, no. 3, June, pp. 1-26, 2013.

[7] L. A. Simpson, J. J. Eng, J. T. C. Hsieh, D. L. Wolfe, and the SCIRE Research Team, "The health and life priorities of individuals with spinal cord injury: A systematic review," *Journal of Neurotrauma*, vol. 29, no. 8, May, pp. 1548-1555, 2012.

[8] M. G. Fehlings, L. A. Tetreault, J. R. Wilson, B. K. Kwon, A. S. Burns, A. R. Martin, G. Hawryluk, and J. S. Harrop, "A clinical practice guideline for the management of acute spinal cord injury: Introduction, rationale, and scope," *Global Spine Journal*, vol. 7, no. 3, Sep., pp. 84S-94S, 2017.

[9] A. K. Varma, A. Das, G. Wallace IV, J. Barry, A. A. Vertegel, S. K. Ray, and N. L. Banik, "Spinal cord injury: A review of current therapy, future treatments, and basic science frontiers," *Neurochemical Research*, vol. 38, Mar., pp. 895-905, 2013.

[10] M. M. Zavvarian, A. Toossi, M. Khazaei, J. Hong, and M. G. Fehlings, "Novel innovations in cell and gene therapies for spinal cord injury," *F1000Research*, vol. 9, Apr., pp. 1-11, 2020.

[11] K. E. Musselman, M. Shah, and J. Zariffa, "Rehabilitation technologies and interventions for individuals with spinal cord injury: Translational potential of current trends," *Journal of NeuroEngineering and Rehabilitation*, vol. 15, art. 40, May., pp. 1-8, 2018.

[12] C. H. Ho, R. J. Triolo, A. L. Elias, K. L. Kilgore, A. F. DiMarco, K. Bogie, A. H. Vette, M. Audu, R. Kobetic, S. R. Chang, K. M. Chan, S. Dukelow, D. J. Bourbeau, S. W. Brose, K. J. Gustafson, Z. Kiss, and V. K. Mushahwar, "Functional electrical stimulation and spinal cord injury," *Phys Med Rehabil Clin N Am.*, vol. 25, no. 3, Aug., pp. 1-30, 2014.

[13] F. B. Wagner, J-B. Mignardot, C. G. Le Goff-Mignardot, R. Demesmaeker, S. Komi, M. Capogrosso, A. Rowald, I. Seáñez, M. Caban, E. Pirondini, M. Vat, L. A. McCracken, R. Heimgartner, I. Fodor, A. Watrin, P. Seguin, E. Paoles, K. Van Den Keybus, G. Eberle, B. Schurch, E. Pralong, F. Becce, J. Prior, N. Buse, R. Buschman, E. Neufeld, N. Kuster, S. Carda, J. von Zitzewitz, V. Delattre, T. Denison, H. Lambert, K. Minassian, J. Bloch, and G. Courtine, "Targeted neurotechnology restores walking in humans with spinal cord injury," *Nature*, vol. 563, Oct., pp. 65-71, 2018.

[14] R. J. Triolo, S. N. Bailey, M. E. Miller, L. M. Rohde, J. S. Anderson, J. A. Jr. Davis, J. J. Abbas, L. A. DiPonio, G. P. Forrest, D. R. Jr. Gater, and L. J. Yang, "Longitudinal performance of a surgically implanted neuroprosthesis for lower extremity exercise, standing, and transfers after spinal cord injury," *Arch Phys Med Rehabil.*, vol. 93, no. 5, May, pp. 896-904, 2012.

[15] D. Guiraud, T. Stieglitz, K. P. Koch, J. L. Divoux, and P. Rabischong, "An implantable neuroprosthesis for standing and walking in paraplegia: 5-year patient follow-up," *J. Neural Eng.*, vol. 3, no. 4, Sept., pp. 269-275, 2006.

[16] E. Henneman, G. Somjen, and D. O. Carpenter, "Functional significance of cell size in spinal motoneurons," *J. Neurophys.*, vol. 28, no. 3, May, pp. 560-580, 1965.

[17] T. S. Barss, E. N. Ainsley, F. C. Claveria-Gonzalez, M. J. Luu, D. J. Miller, M. J. Wiest, and D. F. Collins, "Utilizing physiological principles of motor unit recruitment to reduce fatigability of electrically-evoked contractions: A narrative review," *Archives of Physical Medicine and Rehabilitation*, vol. 99, no. 4, Apr., pp. 779-791, 2018.

[18] R. B. North and J. P. Prager, "Chapter 45: History of spinal cord stimulation," in *Neuromodulation, 2nd Ed.*, E. S. Krames, P. H. Peckham, and A. R. Rezai, Eds. Elsevier, 2018, pp-587-596.

[19] R. Herman, J. He, S. D'Luzansky, W. Willis, and S. Dilli, "Spinal cord stimulation facilitates functional walking in a chronic, incomplete spinal cord injured," *Spinal Cord*, vol. 40, no. 2, Feb., pp. 65-68, 2002.

[20] M. R. Carhart, J. He, R. Herman, S. D'Luzansky, and W. T. Willis, "Epidural spinal-cord stimulation facilitates recovery of functional walking following incomplete spinal-cord injury," *IEEE Trans. Neural Syst. Rehabil. Eng.*, vol. 12, no. 1, Mar., pp. 32-42, 2004.

[21] M. L. Gill, P. J. Grahn, J. S. Calvert, M. B. Linde, I. A. Lavrov, J. A. Strommen, L. A. Beck, D. G. Sayenko, M. G. Van Straaten, D. I. Drubach, D. D. Veith, A. R. Thoreson, C. Lopez, Y. P. Gerasimenko, V. R. Edgerton, K. H. Lee, and K. D. Zhao, "Neuromodulation of lumbosacral spinal networks enables independent stepping after complete paraplegia," *Nature Medicine*, vol. 24, Nov., pp. 1677-1682, 2018.

[22] C. A. Angeli, M. Boakye, R. A. Morton, J. Vogt, K. Benton, Y. Chen, C. K. Ferreira, and S. J. Harkema, "Recovery of over-ground walking after chronic motor complete spinal cord injury," *New England Journal of Medicine*, vol. 379, Sep., pp. 1244-1250, 2018.

[23] V. K. Mushahwar and K. W. Horch, "Muscle recruitment through electrical stimulation of the lumbo-sacral spinal cord," *IEEE Trans. Rehabil. Eng.*, vol. 8, no. 1, Mar., pp. 22-29, 2000.

[24] V. K. Mushahwar, D. F. Collins, and A. Prochazka, "Spinal cord microstimulation generates functional limb movements in chronically implanted cats," *Experimental Neurology*, vol. 163, Feb., pp. 422-429, 2000.

[25] L. Guevremont, C. G. Renzi, J. A. Norton, J. Kowalczewski, R. Saigal, and V. K. Mushahwar, "Locomotor-related networks in the lumbosacral enlargement of the adult spinal cat: Activation through intraspinal microstimulation," *IEEE Trans. Neural Syst. Rehabil. Eng.*, vol. 14, no. 3, Sep., pp. 266-272, 2006.

[26] R. A. Guant, A. Prochazka, V. K. Mushahwar, L. Guevremont, and P. H. Ellaway, "Intraspinal microstimulation excites multisegmental sensory afferents at lower stimulus levels than local α-motoneuron responses," *J. Neurophysiol*, vol. 96, no. 6, Dec., pp. 2995-3005, 2006.

[27] D. Barthélemy, H. Leblond, and S. Rossignol, "Characteristics and mechanisms of locomotion induced by intraspinal microstimulation and dorsal root stimulation in spinal cats," *J. Neuophysiol*, vol. 97, no. 3, Mar., pp. 1986-2000, 2007.

[28] V. K. Mushahwar, and K. W. Horch, "Selective activation of muscle groups in the feline hindlimb through electrical microstimulation of the ventral lumbo-sacral spinal cord," *IEEE Trans. Rehabil. Eng.*, vol. 8, no. 1, Mar., pp. 11-21, 2000.

[29] J. A. Bamford, C. T. Putman, and V. K. Mushahwar, "Intraspinal microstimulation preferentially recruits fatigue-resistant muscle fibres and generates gradual force in rat," *J. Physiol*, vol. 569, no. 3, Dec., pp. 873-884, 2005.

[30] J. T. Hachmann, J. H. Jeong, P. J. Grahn, G. W. Mallory, L. Q. Evertz, A. J. Bieber, D. A. Lobel, K. E. Bennet, K. H. Lee, and J. L. Lujan, "Large animal model for development of functional restoration paradigms using epidural and intraspinal stimulation," *PLoS ONE*, vol. 8, no. 12, Dec., pp. 1-7, 2013.

[31] A. Toossi, D. G. Everaert, S. I. Perlmutter, and V. K. Mushahwar, "Functional organization of motor networks in the lumbosacral spinal cord of non-human primates," *Scientific Reports*, vol. 9, Sept., pp. 1-16, 2019.

[32] B. Lau, L. Guevremont, and V. K. Mushahwar, "Strategies for generating prolonged functional standing using intramuscular stimulation or intraspinal microstimulation," *IEEE Trans. Neural Syst. Rehabil. Eng.*, vol. 15, no. 2, June, pp. 273-285, 2007.

[33] B. J. Holinski, K. A. Mazurek, D. G. Everaert, A. Toossi, A. M. Lucas-Osma, P. Troyk, R. Etienne-Cummings, R. B. Stein, and V. K. Mushahwar, "Intraspinal microstimulation produces over-ground walking in anesthetized cats," *J. Neural Eng.*, vol. 13, no. 5, Sept., pp. 1-17, 2016.

[34] D. B. Popovic, "Functional electrical stimulation for lower extremities," in *Neural Prostheses: Replacing Motor Function After Disease or Disability*, R. B. Stein, P. H. Peckham, and D. B. Popovic, Eds. New York: Oxford Univ. Press, 1992, pp. 233-251.

[35] R. Saigal, C. Renzi, and V. K. Mushahwar, "Intraspinal microstimulation generates functional movements after spinal-cord injury," *IEEE Trans. Neural Syst. Rehabil. Eng.*, vol. 12, no. 4, Dec., pp. 430-440, 2004.

[36] J. A. Bamford, R. M. Lebel, K. Parseyan, and V. K. Mushahwar, "The fabrication, implantation, and stability of intraspinal microwire arrays in the spinal cord of cat and rat," *IEEE Trans. Neural Syst. Rehabil. Eng.*, vol. 25, no. 3, Mar., pp. 287-296, 2017.

[37] P. J. Grahn, K. H. Lee, A. Kasasbeh, G. W. Mallory, J. T. Hachmann, J. R. Dube, C. J. Kimble, D. A. Lobel, A. Bieber, J. H. Jeong, K. E. Bennet, and J. L. Lujan, "Wireless control of intraspinal microstimulation in a rodent model of paralysis," *J. Neurosurg.*, vol. 123, Jul., pp. 232-242, 2015.

[38] J. A. Bamford, K. G. Todd, and V. K. Mushahwar, "The effects of intraspinal microstimulation on spinal cord tissue in the rat," *Biomaterials*, vol. 31, Apr., pp. 5552-5563, 2010.

[39] A. Toossi, B. Bergin, M. Marefatallah, B. Parhizi, N. Tyreman, D. G. Everaert, S. Rezaei, P. Seres, J. C. Gatenby, S. I. Perlmutter, and V. K. Mushahwar, "Comparative neuroanatomy of the lumbosacral spinal cord of the rat, cat, pig, monkey, and human," *Scientific Reports*, vol. 11, Jan., pp. 1-15, 2021.

[40] P. J. Grahn, S. J. Goerss, J. L. Lujan, G. W. Mallory, B. A. Kall, A. A. Mendez, J. K. Trevathan, J. P. Felmlee, K. E. Bennet, and K. H. Lee, "MRI-guided stereotactic system for delivery of intraspinal microstimulation," *SPINE*, vol. 41, no. 13, July, pp. E806-E813, 2016.

[41] A. Toossi, D. G. Everaert, P. Seres, J. L. Jaremko, K. Robinson, C. C. Kao, P. E. Konrad, and V. K. Mushahwar, "Ultrasound-guided spinal stereotactic system for intraspinal implants," *J. Neurosurg Spine*, vol., 29, Sept., pp. 292-305, 2018.

[42] S. Snow, S. C. Jacobsen, D. L. Wells, and K. W. Horch, "Microfabricated cylindrical multielectrodes for neural stimulation," *IEEE Trans. Biomed. Eng.*, vol. 53, no. 2, Feb., pp. 320-326, 2006.

[43] V. Pikov, L. Bullara, and D. B. McCreery, "Intraspinal stimulation for bladder voiding in cats before and after chronic spinal cord injury," *J. Neural Eng.*, vol. 4, no. 4, Dec., pp. 356-368, 2007.

[44] S. Shahdoost, S. B. Frost, D. J. Guggenmos, J. A. Borrell, C. Dunham, S. Barbay, R. J. Nudo, and P. Mohseni, "A brain-spinal interface (BSI) system-on-chip (SoC) for closed-loop cortically-controlled intraspinal microstimulation," *Analog Integrated Circuits and Signal Processing*, vol. 95, Jan., pp. 1-16, 2018.

[45] V. Pikov, D. B. McCreery, and M. Han, "Intraspinal stimulation with a silicon-based 3D chronic microelectrode array for bladder voiding in cats," *Journal of Neural Engineering*, vol. 17, Dec., pp. 1-13, 2020.

[46] A. Toossi, D. G. Everaert, A. Azar, C. R. Dennison, and V. K. Mushahwar, "Mechanically stable intraspinal microstimulation implants for human translation," *Annals of Biomedical Engineering*, vol. 45, no. 3, Mar., pp. 681-694, 2017.

[47] R. Biran, D. C. Martin, and P. A. Tresco, "The brain tissue response to implanted silicon microelectrode arrays is increased when the device is tethered to the skull," *J. Biomed. Mater. Res. A.*, vol. 82, no. 1, Jul., pp. 169-178, 2007.

[48] J. Thelin, H. Jörntell, E. Psouni, M. Garwicz, J. Schouenborg, N. Danielsen, and C. E. Linsmeier, "Implant size and fixation mode strongly influence tissue reactions in the CNS," *PLoS ONE*, vol. 6, no. 1, Jan., 2011.

[49] A. Abdo, M. Sahin, D. S. Freedman, E. Cevik, P. S. Spuhler, and M. S. Unlu, "Floating light-activated micro electrical stimulators tested in the rat spinal cord," *Journal of Neural Engineering*, vol. 5, no. 5, Oct., pp. 1-21, 2011.

[50] F. Lotti, F. Ranieri, G. Vadalà, L. Zollo, and G. Di Pino, "Invasive intraneural interfaces: Foreign body reaction issues," *Frontiers in Neuroscience*, vol. 11, art. 497, Sept., 2017.

[51] V. S. Polikov, P. A. Tresco, and W. M. Reichert, "Response of brain tissue to chronically implanted neural electrodes," *Journal of Neuroscience Methods*, vol. 148, Aug., pp. 1-18, 2005.

[52] S. Sommakia, J. L. Rickus, and K. J. Otto, "Glial cells, but not neurons, exhibit a controllable response to a localized inflammatory microenvironment *in vitro*," *Frontiers in Neuroengineering*, vol. 7, art. 41, Nov., 2014.

[53] S. Sridar, M. A. Churchward, V. K. Mushahwar, K. G. Todd, and A. L. Elias, "Peptide modification of polyimide-insulated microwires: Towards improved biocompatibility through reduced glial scarring," *Acta Biomaterialia*, vol. 60, Jul., pp. 154-166, 2017.

[54] Y. Zhong, and R. V. Bellamkonda, "Dexamethasone coated neural probes elicit attenuated inflammatory response and neuronal loss compared to uncoated neural probes," *Brain Res.*, vol. 1148, May, pp. 15-27, 2007.

[55] S. Mirkiani, D. A. Roszko, R. Fox, P. R. Troyk, and V. K. Mushahwar, "Stretchable lead wires for long-term intraspinal microstimulation," presented at Neural Interfaces 2021: The NANS-NIC Joint Meeting (virtual), 2021.

[56] J. K. Nguyen, D. J. Park, J. L. Skousen, A. E. Hess-Dunning, D. J. Tyler, S. J. Rowan, C. Weder, and J. R. Capadona, "Mechanically-compliant intracortical implants reduce the neuroinflammatory response," *Journal of Neural Engineering*, vol. 11, no. 5, Aug., pp. 1-15, 2014.

[57] Z. J. Du, C. L. Kolarcik, T. D. Y. Kozai, S. D. Luebben, S. A. Sapp, X. S. Zheng, J. A. Nabity, and X. T. Cui, "Ultrasoft microwire neural electrodes improve chronic tissue integration," *Acta Biomaterialia*, vol. 53, Apr., pp. 46-58, 2017.

[58] D. R. Merrill, M. Bikson, and J. G. R. Jefferys, "Electrical stimulation of excitable tissue: Design of efficacious and safe protocols," *J. Neurosci. Methods*, vol. 141, pp. 171-198, 2005.

[59] S. F. Cogan, "Neural Stimulation and Recording Electrodes," *Annu. Rev. Biomed. Eng.*, vol. 10, Apr., pp. 275-309, 2008.

[60] D. B. McCreery, W. G. Agnew, T. G. H. Yuen, and L. Bullara, "Charge density and charge per phase as cofactors in neural injury induced by electrical stimulation," *IEEE Trans. Biomed. Eng.*, vol. 37, no. 10, Oct., pp. 996-1001, 1990.

[61] R. V. Shannon, "A model of safe levels for electrical stimulation," *IEEE Trans. Biomed. Eng.*, vol. 39, no. 4, Apr., pp. 424-426, 1992.

[62] S. F. Cogan, K. A. Ludwig, C. G. Welle, and P. Takmakov, "Tissue damage thresholds during therapeutic electrical stimulation," *Journal of Neural Engineering*, vol. 13, no. 2, Jan., pp. 1-13, 2016.

[63] D. McCreery, V. Pikov, and P. R. Troyk, "Neuronal loss due to prolonged controlled-current stimulation with chronically implanted microelectrodes in the cat cerebral cortex," *Journal of Neural Engineering*, vol. 7, no. 3, May, pp. 1-9, 2010.

[64] S. F. Cogan, P. R. Troyk, J. Ehrlich, and T. D. Plante, "In vitro comparison of the charge-injection limits of activated iridium oxide (AIROF) and platinum-iridium microelectrodes," *IEEE Trans. Biomed. Eng.,* vol. 52, no. 9, Sep., pp. 1612-1614, 2005.

[65] H. Vara and J. E. Collazos-Castro, "Enhanced spinal cord microstimulation using conducting polymer-coated carbon microfibers," *Acta Biomaterialia*, vol. 90, May, pp. 71-86, 2019.

[66] A. N. Dalrymple, U. A. Robles, M. Huynh, B. A. Nayagam, R. A. Green, L. A. Poole-Warren, J. B. Fallon, and R. K. Sheperd, "Electrochemical and biological performance of chronically stimulated conductive hydrogel electrodes," *Journal of Neural Engineering*, vol. 17, Apr., pp. 1-17, 2020.

[67] R. T. Leung, M. N. Shivdasani, D. A. X. Nayagam, and R. K. Shepherd, "In Vivo and in vitro comparison of the charge injection capacity of platinum macroelectrodes," *IEEE Trans. Biomed. Eng.*, vol. 62, no. 3, Mar., pp. 849-857, 2015.

[68] K. M. Szostak, L. Grand, and T. G. Constandinou, "Neural interfaces for intracortical recording: Requirements, fabrication methods, and characteristics," *Frontiers in Neuroscience*, vol. 11, art. 665, pp. 1-27, 2017.

[69] A. Weltman, J. Yoo, and E. Meng, "Flexible, penetrating brain probes enabled by advances in polymer microfabrication," *Micromachines*, vol. 7, no. 10, Oct., pp. 1-36, 2016.

[70] C. H. Thompson, T. A. E. Riggins, P. R. Patel, C. A. Chestek, W. Li, and E. Purcell, "Toward guiding principles for the design of biologically-integrated electrodes for the central nervous system," *J. Neural Eng.*, vol. 17, no. 2, Mar., 2020.

[71] C. Hassler, T. Boretius, and T. Steiglitz, "Polymers for neural implants," *Polymer Physics*, vol. 49, pp. 18-33, 2011.

[72] H. Ozawa, T. Matsumoto, T. Ohashi, M. Sato, and S. Kokubun, "Mechanical properties and function of the spinal pia mater," *J. Neurosurg. Spine*, vol. 1, Jul., pp. 122-127, 2004.

[73] K. C. Cheung, P. Renaud, H. Tanila, and K. Djupsund, "Flexible polyimide microelectrode array for in vivo recordings and current source density analysis," *Biosensors and Bioelectronics*, vol. 22, pp. 1783-1790, 2007.

[74] M. Mueller, N. de la Oliva, J. del Valle, I. Delgado-Martínez, X. Navarro, and T. Stieglitz, "Rapid prototyping of flexible intrafascicular electrode arrays by picosecond laser structuring," *Journal of Neural Engineering*, vol. 14, no. 6, Nov., pp. 1-11, 2017.

[75] S. Shin, J. H. Kim, J. Jeong, T. M. Gwon, S. H. Lee, and S. J. Kim, "Novel four-sided neural probe fabricated by a thermal lamination process of polymer films," *J. Neurosci. Methods*, vol. 278, pp. 25-35, 2017.

[76] R. T. Rihani, A. M. Stiller, J. O. Usoro, H. Lawson, H. Kim, B. J. Black, V. R. Danda, J. Maeng, V. D. Varner, T. H. Ware, and J. J. Pancrazio, "Deployable, liquid crystal elastomer-based intracortical probes," *Acta Biomaterialia*, vol. 111, pp. 54-64, 2020.

[77] I. R. Minev, P. Musienko, A. Hirsch, Q. Barraud, N. Wenger, E. M. Moraud, J. Gandar, M. Capogrosso, T. Milekovic, L. Asboth, R. F. Torres, N. Vachicouras, Q. Liu, N. Pavlova, S. Duis, A. Larmagnac, J. Vörös, S. Micera, Z. Suo, G. Courtine, and S. P. Lacour, "Electronic dura mater for long-term multimodal neural interfaces," *Science*, vol. 347, no. 6218, Jan., pp. 159-163, 2015.

[78] J. M. Kim, D. R. Oh, J. Sanchez, S. H. Kim, and J. M. Seo, "Fabrication of polydimethylsiloxane (PDMS) - based multielectrode array for neural interface,"*35th Annual International Conference of the IEEE EMBS*, Jul., pp. 1716-1719, 2013.

[79] T. D. Y. Kozai, and D. R. Kipke, "Insertion shuttle with carboxyl terminated self-assembled monolayer coatings for implanting flexible polymer neural probes in the brain," *J. Neurosci. Methods*, vol. 184, no. 2, Nov., pp. 199-205, 2009.

[80] X. Wen, B. Wang, S. Huang, T. Liu, M. -S. Lee, P. -S. Chung, Y. T. Chow, I. -W. Huang, H. G. Monbouquette, N. T. Maidment, and P. -Y. Chiou, "Flexible, multifunctional neural probe with liquid metal enabled, ultra-large tunable stiffness for deep-brain chemical sensing and agent delivery," *Biosens Bioelectron.*, vol. 131, Apr., pp. 37-45, 2019.

[81] S. H. Felix, K. G. Shah, V. M. Tolosa, H. J. Sheth, A. C. Tooker, T. L. Delima, S. P. Jadhav, L. M. Frank, and S. S. Pannu, "Insertion of flexible neural probes using rigid stiffeners attached with biodissolvable adhesive," *Journal of Visualized Experiments*, vol. 79, 50609, 2013.

[82] J. Agorelius, F. Tsanakalis, A. Friberg, P. T. Thorbergsson, L. M. E. Pettersson, and G. Schouenborg, "An array of highly flexible electrodes with a tailored configuration locked by gelatin during implantation - initial evaluation in cortex cerebri of awake rats," *Frontiers in Neuroscience*, vol. 9, art. 331, Sep., pp. 1-12, 2015.

[83] A. Lecomte, V. Castagnola, E. Descamps, L. Dahan, M. C. Blatché, T. M. Dinis, E. Leclerc, C. Egles, and C. Bergaud, "Silk and PEG as means to stiffen a parylene probe for insertion in the brain: Toward a double time-scale tool for local drug delivery," *J. Micromech. Microeng.*, vol. 25, 125003, 2015.

[84] Z. Zhao, X. Li, F. He, X. Wei, S. Lin, and C. Xie, "Parallel, minimally-invasive implantation of ultra-flexible neural electrode arrays," *J. Neural Eng.*, vol. 16, no. 3, Jun., 035001, 2019.

[85] A. M. Stiller, J. O. Usoro, J. Lawson, B. Araya, M. A. González-González, V. R. Danda, W. E. Voit, B. J. Black, and J. J. Pancrazio, "Mechanically robust, softening shape memory polymer probes for intracortical recording," *Micromachines*, vol. 11, no. 6, art. 619, Jun., 2020.

[86] M. Schuettler, B. V. King, and G. J. Suaning, "Fabrication of implantable microelectrode arrays by laser cutting of silicone rubber and platinum foil," *Journal of Neural Engineering*, vol. 2, no. 1, Feb., pp. S121-S128, 2005.

[87] C. W. D. Dodds, M. Schuettler, T. Guenther, N. H. Lovell, and G. J. Suaning, "Advancements in electrode design and laser techniques for fabricating micro-electrode arrays as part of a retinal prosthesis," *2011 Annual International Conference of the IEEE Engineering in Medicine and Biology Society*, Aug., pp. 636-639, 2011.

[88] G. Chryssolouris, *Laser Machining: Theory and Practice*. New York: Springer Science+Business Media, 1991.

[89] H. T. Lancashire, A. Canhoestenberghe, C. J. Pendegrass, Y. A. Ajam, E. Magee, N. Donaldson, and G. W. Blunn, "Microchannel neural interface manufacture by stacking silicone and metal foil laminae," *Journal of Neural Engineering*, vol. 13, no. 3, Mar., pp. 1-9, 2016.

[90] W. Shen, L. Karumbaiah, X. Liu, T. Saxena, S. Chen, R. Patkar, R. V. Bellamkonda, and M. G. Allen, "Extracellular matrix-based intracortical microelectrodes: Toward a microfabricated neural interface based on natural materials," *Microsystems & Nanoengineering*, vol. 1, art. 15010, Jun., pp. 1-12, 2015.

[91] R. A. Green, J. S. Ordonez, M. Schuettler, L. A. Poole-Warren, N. H. Lovell, and G. J. Suaning, "Cytotoxicity of implantable microelectrode arrays produced by laser micromachining," *Biomaterials*, vol. 31, no. 5, Feb., pp. 886-893, 2010.

[92] A. Kelly, N. Farid, K. Krukiewicz, N. Belisle, J. Grorke, E. M. Waters, A. Trotier, F. Laffir, M. Kilcoyne, G. M. O'Connor, and M. J. Biggs, "Laser-induced periodic surface structure enhances neuroelectrode charge transfer capabilities and modulates astrocyte function," *ACS Biomater. Sci. Eng.*, vol. 6, Mar., pp. 1449-1461, 2020.

[93] J. Qu, Q. Wu, T. Clancy, Q. Fan, X. Wang, and X. Liu, "3D-printed strain-gauge micro force sensors," *IEEE Sensors Journal*, vol. 20, no. 13, Jul., pp. 6971-6978, 2020.

[94] A. Toossi, D. G. Everaert, R. R. E. Uwiera, D. S. Hu, K. Robinson, F. S. Gragasin, and V. K. Mushahwar, "Effect of anesthesia on motor responses evoked by spinal neural prostheses during intraoperative procedures," *Journal of Neural Engineering*, vol. 16, Mar., pp. 1-18, 2019.

[95] E. Schmidt, P. Raposo, R. Vavrek, and K. Fouad, “Inducing inflammation following subacute spinal cord injury in female rats: A double-edged sword to promote motor recovery,” *Brain, Behavior, and Immunity*, vol. 93, Mar., pp. 55-65, 2021.

[96] A. N. Dalrymple, M. Huynh, U. A. Robles, J. B. Marroquin, C. D. Lee, A. Petrossians, J. J. Whalen III, D. Li, H. C. Parkington, J. S. Forsythe, R. A. Green, L. A. Poole-Warren, R. K. Shepherd, and J. B. Fallon, “Electrochemical and mechanical performance of reduced graphene oxide, conductive hydrogel, and electrodeposited Pt-Ir coated electrodes: an active in vitro study,” *Journal of Neural Engineering*, vol. 17, Dec., 016015, 2019.

[97] K. A. Mazurek, B. J. Holinski, D. G. Everaert, R. B. Stein, R. Etienne-Cummings, and V. K. Mushahwar, “Feed forward and feedback control for over-ground locomotion in anaesthetized cats,” *Journal of Neural Engineering*, vol. 9, Apr., 026003, 2012.

Chapter 2: Laser-microfabricated polymer multielectrodes for intraspinal microstimulation

INTRODUCTION

Spinal cord injury (SCI) is a devastating condition which can result in loss of mobility, loss of sensation, and a reduction in quality of life [2]. The estimated global prevalence of traumatic SCI (tSCI), where injury is due to an external physical impact, is between 250 - 906 per million, with national incidences between 8 - 49.1 per million reported globally [3]. The impacts of SCI are multifaceted, with physical [2], [4], economic [5], [7], and social dimensions [6]. In the United States, the estimated lifetime costs for someone living with SCI are between $1.1 - 4.7 million USD, depending on the age at injury and extent of injury [5]. Although the priorities of people living with SCI differ depending on the level and extent of injury, regaining mobility has often been listed as a high priority [8].

Intraspinal microstimulation (ISMS) is a neuroprosthetic technique under development for restoring locomotor function after SCI. It involves the implantation of microelectrodes directly into the lumbar region of the spinal cord where the locomotor networks reside [14], [22]. By electrically stimulating within the spinal cord, neural networks capable of producing lower limb flexion, extension, and synergistic movements can be recruited [16], [20], [47]. The locations of these locomotor targets are consistent within species [17], [20] and in different species such as the rat [18], cat [14], [47], pig [19], and in non-human primates [20], and are likely to be preserved in humans, thus providing a feasible target for ISMS.

ISMS recruits motor responses in a graded and nearly normal physiological recruitment order, where smaller fatigue resistant fibers which generate less force are preferentially recruited before larger fatigue resistant fibers [14], [18]. Due to the resulting fatigue resistance qualities, ISMS has achieved long durations of standing of 20.89 minutes in the cat [21] and produced long distances of overground walking of between 609 - 835 m in the cat [22]. If translated to humans, these qualities may permit ISMS to improve functional recovery, in terms of standing duration and walking distances, compared to other available neural prostheses implemented with peripheral functional electrical stimulation or epidural spinal cord stimulation, which are limited due to muscle fatigue [9] - [13]. Because of these compelling preclinical results, there has been ongoing efforts to translate ISMS to humans to restore lower limb mobility after SCI [20], [27], [32].

Traditionally, ISMS has been implemented with microwire electrode arrays, with electrode diameters between 30 - 50 μm [15], [24], [60]. These microwire arrays produce minimal functional deficits when implanted chronically in the cat [15] and produce minor foreign body responses (FBR) in the rat [25]. However, microwire electrodes are functionally limited as they can only electrically stimulate one region of the spinal cord - at the deinsulated tip. If a desired locomotor target is not activated by the microwire electrode, the device must be removed and implanted again until a proper response is attained, which may result in multiple spinal cord penetrations and an increased potential for tissue damage. This becomes especially challenging in the dorsoventral axis, as microelectrodes are fabricated with a fixed insertion length and therefore their insertion depth cannot be easily changed. When mapping the rhesus macaque spinal cord with microelectrodes, Toossi et al. noted that 45% of sites within the spinal cord produced no motor response when electrically stimulated, indicating that targeting accuracy of microwire implantation is essential for successful functioning of the system [20].

One solution to this challenge has been the use of multisite electrodes, with multiple stimulating electrodes on a single shank, to improve the chances of correct targeting when the device is first implanted. Researchers have used 4-channel cylindrical multielectrodes [28], fabricated with 85 μm diameter optic fiber core substrates, or silicon-based microelectrode arrays [29] - [31] to implement ISMS. Although these devices significantly improve the chances of correct targeting within the spinal cord, their fabrication methods and materials inevitably lead to larger and stiffer devices, which can increase tissue displacement and damage, as well as exacerbate FBR.

It is becoming increasingly clear that the mechanical properties of implanted neural interfaces greatly impact device biocompatibility [35], [36]. By fabricating devices with materials nearly as flexible as the central nervous system, such as biocompatible polymers [45], tissue damage stemming from device tethering forces or tissue micromotion can be reduced [35], [36], thus mitigating FBR and improving device functionality. Following this trend, increasingly flexible neural interface designs have been proposed for the cortex [35], [36] and peripheral nerves [49]. Devices have been fabricated using a wide range of common and experimental polymer materials to produce low modulus implants. These materials have Young's moduli ranging from 10.6 GPa for liquid crystal polymer (LCP) to as low as 0.1 - 0.5 MPa for poly(dimethylsiloxane) (PDMS) [45]. Devices have been commonly fabricated with polyimide substrates [48] or

parylene-C substrates [49]. However, PDMS substrates, which have been effectively used for creating flexible non-penetrating neural interfaces [50], have been less commonly used for penetrating neural interfaces [51] - [53]. This is likely because the very low modulus of PDMS makes it difficult to insert into tissue. Although the long-term functionality of polymer microelectrodes has seldom been reported for the cortex [44], bladder stimulators constructed with PDMS encapsulants have been reported to function for as long as 25 years *in vivo* with minimal material degradation [45]. Due to their remarkable flexibility, nearly all penetrating polymer microelectrodes require temporary insertion aids to be implanted into tissue [52], [54]. Typically, polymer microelectrodes are fabricated using standard microfabrication techniques [43], [44], although rapid and cost-effective prototyping methods, such as laser microfabrication, have also been reported [49], [55], [59]. In the context of the spinal cord, flexible polymer microelectrodes with multiple stimulation sites may improve dorsoventral targeting compared to microwire implants, while avoiding the mechanical tissue damage and strain caused by stiffer multielectrode designs.

In this study, we describe the fabrication and characterization of a flexible polymer multielectrode for the spinal cord to implement ISMS. With multiple stimulating electrodes and a flexible PDMS-based substrate, we predicted that this device would demonstrate improved functionality over traditional microwire electrodes while remaining highly flexible compared to other multielectrode or silicon microelectrode array designs. We characterized the mechanical and electrochemical properties of the polymer multielectrodes with respect to microwire electrodes and demonstrated device functionality *in vivo*.

METHODS

Multielectrode microfabrication

A three-channel polymer multielectrode was designed in AutoCAD 2020 (Autodesk, CA, USA) with a nominal implantation depth of 4 mm, width of 135 μm, and thickness of 120 μm. The medical-grade PDMS silicone elastomer MED-6215 (NuSil, CA, USA) was used for constructing the substrate of the multielectrodes. Dimethylsiloxane-(60-70% ethylene oxide) block copolymer (PDMS-PEG) (Gelest, PA, USA) was mixed into the bulk PDMS to improve

the surface hydrophilicity of the multielectrode substrate, as described for biomicrofluidics by Gökaltun et al. [1]. Platinum-iridium (80%/20%) flat wire (PtIr-FW) (California Fine Wire, CA, USA), with a thickness of 15 μm and width of 150 μm, was used for micromachining the conductive elements of the implants. Multielectrodes were fabricated using a combination of spin-coating (Laurell Technologies Corporation, PA, USA) and nanosecond exciplex laser (wavelength = 248 nm) micromachining (COMPex 110, Coherent, CA, USA). A pictorial description of the microfabrication procedure can be seen in Figure 1. A considerable amount of time was spent fine-tuning nanosecond laser process parameters, including demagnification, beam scanning speed, pulse energy, pulse frequency, and spot diameter, to achieve satisfactory metal and polymer machining (summarized in Table 1). As outlined by others, process parameters were first tested on cost-effective aluminum foil samples [59] before they were applied to more expensive PtIr-FW samples.

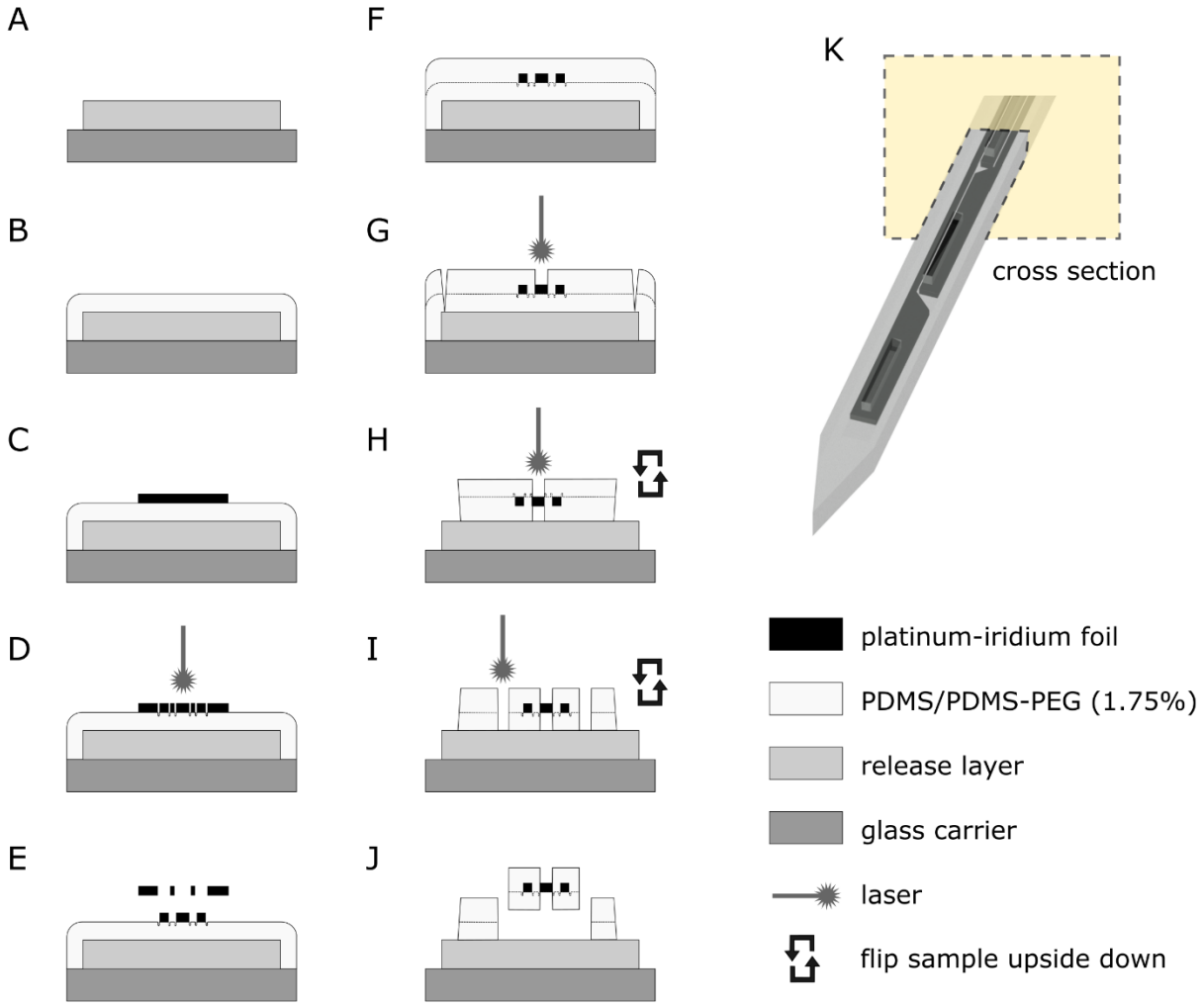

Figure 1: Sequential processing steps for the polymer multielectrodes, depicted as cross-sectional images of (K). (A) a glass carrier is coated in a release layer and (B) a PDMS/PDMS-PEG (1.75%) layer is spin coated onto the surface. (C) a platinum-iridium (80%/20%) foil layer is mounted onto the polymer layer, and (D) a nanosecond laser is used to machine the foil. (E) excess foil is removed, (F) the metal is encapsulated in another layer of PDMS/PDMS-PEG (1.75%), and (G)-(I) the laser is used to deinsulate stimulating sites on the top and bottom surfaces of the device and cut out the implant. (J) the implant is removed from the carrier. (K) a 3D rendered image of the implant is shown.

A glass carrier (either a microscope slide or glass coverslip) was coated in a cellophane tape release layer. A mixture of PDMS and PDMS-PEG was prepared, with a w/w ratio of 1.75% PDMS-PEG to PDMS. A layer of the PDMS mixture was spin-coated on the carrier surface at 1000 rpm for 1 minute. The polymer layer was vacuum desiccated for 30 minutes and allowed to partially cure at 65°C for 30 minutes. Samples of PtIr-FW, approximately 7 mm long, were mounted to the surface and the sample was then fully cured at 120°C for 1.5 hours. After curing, polymer-metal adhesion was suitable for laser machining. Using exciplex laser parameters suitable for cutting metal (Table 1), all features of the multielectrodes were machined into the PtIr-FW samples. Excess metal between electrical traces was removed manually and the samples were encapsulated in another layer of PDMS/PDMS-PEG (1.75%) via spin-coating at 3000 rpm for 1 minute. The samples were then cured at 120°C for 20 minutes. After curing, wire-bonding sites and stimulating sites on the top surface were deinsulated using laser parameters suitable for removing polymer layers without damaging the underlying metal surfaces (Table 1). The PDMS samples were then individually cut out using a scalpel blade and flipped upside down to expose the bottom surfaces. After flipping, the bottom stimulating sites were deinsulated with the laser. A low-intensity laser pulse (Table 1) was applied to the stimulating sites to remove surface contaminants caused by laser deinsulation. The samples were then flipped again to the original orientation and the border of the polymer multielectrode was machined using the laser, allowing the device to be removed from the glass carrier. Lastly, low-intensity laser pulses were used to remove surface contaminants from the wire-bonding sites (5 - 10 pulses) and the stimulating sites (1 pulse). To assess process parameters, polymer multielectrode samples underwent scanning electron microscopy (SEM) imaging and energy-dispersive X-ray spectroscopy (EDS) surface mapping (PhenomXL, ThermoScientific, MA, USA) at various stages during production.

Using a set of micromanipulators, conductive silver epoxy (EPO-TEK H22, Epoxy Technology Inc, MA, USA) was carefully deposited onto all wire-bonding sites and allowed to cure at 150°C for 15 minutes. Polyimide-insulated microwires, with a diameter of 30 μm, were then bonded to the polymer multielectrodes as lead wires to connect to external circuitry. Wire-epoxy junctions were cured at 150°C for 15 minutes. After all leads were bonded to the multielectrode, the lead junction was insulated with PDMS (Sylgard, Sigma-Aldrich, MO, USA). All samples were gently rinsed in 70% ethanol prior to electrochemical testing to remove any remaining surface contaminants.

Table 1: Nanosecond laser process settings used for micromachining metal layers, polymer layers, and surface contaminants.

	Metal Cutting	PDMS Deinsulation	PDMS Cutting	Surface Contaminant Removal
Demagnification	27.5X	27.5X	27.5X	27.5X
Scanning Speed [mm/s]	0.04-0.07	0.17	0.17	N/A
Pulse Energy [mJ/pulse]	215	150	200	150
Attenuator Transmission [%]	25	10	25	5
Pulse Frequency [Hz]	100	50	50	N/A
Spot Diameter [μm]	10	27.5	27.5	*variable

*Spot size for surface oxide and contaminant removal was set to the size of the site to be cleaned.

Microwire electrode microfabrication

Microwire electrodes were fabricated from 50 μm diameter polyimide-insulated platinum-iridium (80%/20%) wire (California Fine Wire, CA, USA). A nanosecond laser, with a wavelength of 248 nm, was used to deinsulate 400 μm at the tip of each microwire. Microwires were then beveled with a microelectrode beveler (BV-10, Sutter, CA, USA) to an angle of approximately 15°. For *in vivo* experiments, microwires were formed into 4-wire microwire arrays following methods previously described [23]. Briefly, microwire electrodes were bent at 90° to a predefined insertion depth of approximately 4.5 mm. All microwires were then

embedded within a silastic tube to maintain a rostrocaudal spacing of 4 mm and leads were secured together using epoxy and 6-0 suture.

Compression tests

A custom mechanical force measurement system was developed based on a 3D-printed strain gauge recently described by Qu et al. [61]. The mechanical measurement system was calibrated with 6 calibration weights to verify signal linearity. Polymer multielectrode samples were clamped vertically between two acrylic blocks with a separation distance of 3 mm and loaded into the measurement system. A precise 3 mm separation distance was maintained using a 3D-printed spacer between the two acrylic blocks. Once the blocks were secured in the measurement system, the 3D-printed spacer was gently removed. The position of the top acrylic block was jogged (step size = 0.01 mm) to ensure that the 3D-printed strain gauge was not initially loaded. Compression tests were then performed by lowering the top acrylic block by 1.5 mm at a speed of 20 mm/min [56], causing the samples to buckle. The force-time waveforms were recorded on an oscilloscope, with a sampling rate of 500 Hz, and saved for analysis. While translating at 20 mm/min, the force transducer experienced 2 Hz noise due to the stepper motors. To reduce this noise, force-time waveforms were filtered using a digital IIR bandstop filter from 1.5-2.5 Hz in MATLAB (MathWorks Inc., MA, USA). The buckling force was measured as the difference between the peak force and the initial force values. The buckling force of PtIr microwires, with a diameter of 50 µm, were also obtained for comparison with that of the polymer multielectrodes.

Theoretical Young's moduli of samples

Based on the experimentally measured buckling forces of the multielectrode and microwire samples, the theoretical Young's modulus of each sample was calculated using equation 1 [56]. Here, the buckling force (F) of the implant, clamped on both sides, is related to the Young's modulus (E), second moment of area of the beam's cross-section with respect to the axis most likely to buckle (I), and length (L) of the device. The multielectrode was modeled as a rectangular beam with a second moment of area described by equation 2, where b is the width of the shank and h is the thickness of the shank (b > h). The microwire electrode was modeled as a

cylindrical beam with a second moment of area described by equation 3, where r is the radius of the cylindrical beam.

$$F = \frac{4\pi^2 EI}{L^2} \quad (1)$$

$$I = \frac{bh^3}{12} \quad (2)$$

$$I = \frac{\pi}{4} r^4 \quad (3)$$

Bench electrochemical analysis

Polymer multielectrodes and microwire electrodes were inserted into a beaker of Dulbecco's phosphate-buffered saline (PBS) (Sigma-Aldrich, MO, USA) at room temperature. Using an electrochemical test system (MET16, Sigenics Inc., IL, USA), electrodes were assessed in a three-electrode configuration consisting of a stainless-steel counter electrode (Cooner AS632, Cooner Wire Company, CA, USA), deinsulated to expose approximately 3-5 cm, and a Ag|AgCl reference electrode. The working electrodes were assessed using electrochemical impedance spectroscopy (EIS), cyclic voltammetry (CV), and voltage transient (VT) analysis [37]. EIS was used to measure the electrode-electrolyte impedance magnitude and phase at frequencies ranging from 0.1 Hz - 10 kHz. CV was performed at sweep rates of both 50 V/s and 50 mV/s within the water window for PtIr alloys (-0.6 - 0.8 V relative to the Ag|AgCl reference electrode) [37]. Thirteen CV cycles were performed; the last three were recorded for analysis. The cathodic current was integrated with respect to time to calculate the stored cathodic charge; this charge was then averaged for each of the three recorded CV cycles and normalized by the electrode surface area to calculate the cathodal charge storage capacity (CSC_c). VT measurements were assessed with a biphasic symmetric, cathodic-leading current pulse with cathodic and anodic pulse durations of 200 µs and an interphase duration of 100 µs. Current amplitudes were increased with a step size of 25 µA until the maximum cathodic polarization (E_{mc}) was measured

just above -0.6 V relative to the Ag|AgCl reference electrode [37]; the cathodic charge resulting in E_{mc} was normalized by the electrode surface area and used to calculate the charge injection limit (CIL). If 25 µA resulted in cathodic polarizations below -0.6 V, transients at 10 µA were assessed.

Multielectrode insertion aids

Several dissolvable and rigid insertion aid methods were assessed *in vitro* and in freshly euthanized pig cadavers before settling on a half-needle shuttle design [36]. Needles (30G, 0.5" in length) were machined with a nanosecond laser to create rigid insertion shuttles (Figure 2). The top half of the needle was selectively removed from the tip of the needle for 5.2 mm along the needle shaft (Figure 2A). The remaining half-needle resembled a half-cylinder capable of surrounding the flexible polymer multielectrode during insertion *in vivo* (Figure 2B). The polymer multielectrode was secured to the insertion aid using water-soluble polyethylene glycol (PEG) 8000 (Sigma-Aldrich, MO, USA), dissolved in an equal weight of deionized water (Figure 2C). Using a set of micromanipulators, the polymer multielectrode and insertion aid were held in contact while a moderate amount of dissolved PEG solution was applied along the length of the insertion aid. After approximately 30 minutes, the PEG adhesive dried, bonding the multielectrode and insertion aid together, and the assembly was released from the micromanipulators.

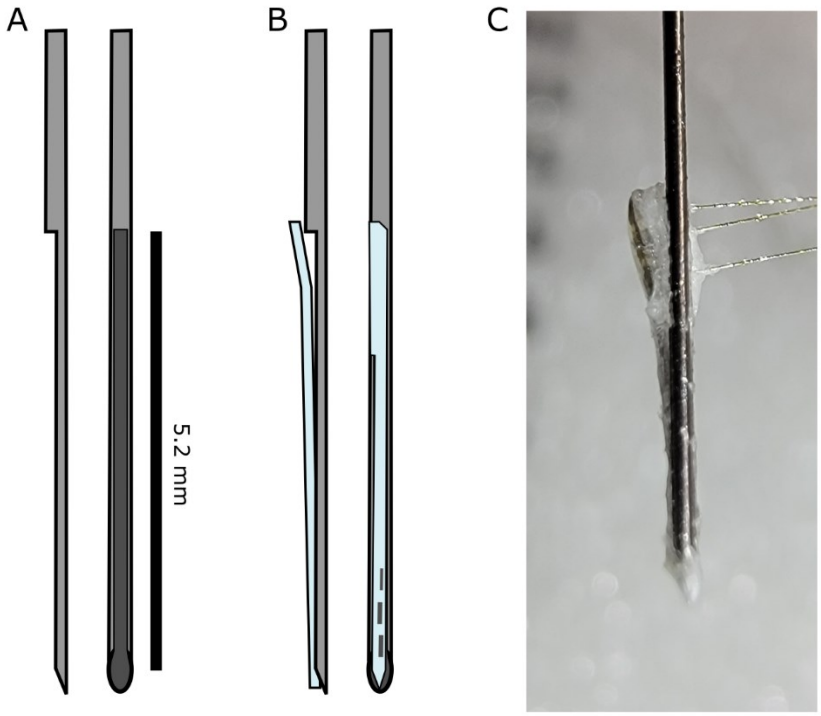

Figure 2: Half-needle insertion aids, used to implant the polymer multielectrodes into the spinal cord, are shown. (A) Needles (30G, 0.5” long) were machined with a nanosecond laser to remove the top half of the needle from the tip of the needle for 5.2 mm along the needle shaft (scale bar = 5.2 mm). (B) Conceptual images demonstrate how the multielectrodes are mounted onto the insertion aid. (C) A completed multielectrode is shown bonded to the insertion aid with PEG 8000, a biodissolvable adhesive.

Surgical and experimental procedure

All experiments were conducted under protocols approved by the University of Alberta Animal Care and Use Committee. Four neurologically intact domestic pigs were used in this study. Three pigs were utilized for assessing microwire electrochemical properties *in vivo* and for refining the multielectrode design. One pig was used for assessing refined multielectrode electrochemical properties and functionality. Pigs were sedated with an intramuscular injection of ketamine (22 mg/kg), xylazine (2.2 mg/kg), and glycopyrrolate (0.01 mg/kg). The common carotid artery and

ipsilateral external jugular vein were catheterized to allow the pigs to be perfused with 4% formalin solution after they were euthanized at the end of the experiment. Pigs were then transferred to isoflurane anesthesia and after complete sedation transitioned to a total intravenous anesthesia (TIVA) protocol, consisting of propofol (30-160 μg/kg/min), remifentanil (0.05-2.00 μg/kg/min), lidocaine (1.0-1.5 mg/kg/hr), and dexmedetomidine (0.2-0.7 μg/kg/hr) for the remainder of the experiment [62]. Vital signs were monitored continuously, and reflexes were assessed regularly to ensure the pig remained within the surgical plane of anesthesia.

A laminectomy was performed at the L4-L5 vertebral levels to expose the lumbosacral enlargement of the spinal cord [26], [62]. In the event that the enlargement was rostrally or caudally shifted, the laminectomy was extended accordingly by half a vertebral segment. The dura mater was incised and secured laterally with suture to expose the spinal cord surface. The position of the quadriceps motor pool, which was inferred from previous work in the pig [62], rhesus macaque [20], and cat [14], was located by implanting a 50 μm search microwire, with an insertion depth of approximately 5 mm, into the general area of the motor pool and stimulating with a 100 μA biphasic pulse train (40 Hz, 200 - 500 ms duration, 200 μs pulse duration) using a microelectrode stimulator (STG 4008, Multichannel Systems MCS GmbH, Germany). For the first three pigs, the 4-wire microwire array was then implanted ipsilaterally in the quadriceps motor pool and assessed electrochemically. For the fourth pig, 4 polymer multielectrodes were implanted within the quadriceps motor pools, two on the right side of the cord and two on the left, and were assessed electrochemically and functionally.

Evoked responses, joint torques, and kinematics

The hind body of the pig was supported with a surgical table extension, allowing the legs to hang freely during the experiment [62]. Reflective markers were placed on the left and right iliac crests, hips, knees, ankles, metatarsophalangeal joints, and toes. Each multielectrode stimulating site was connected to the microelectrode stimulator, and a biphasic, charge-balanced current pulse train (40 Hz, 1 s duration) with amplitudes between 50 - 300 μA was delivered to the spinal cord. The electrically evoked responses were first categorized qualitatively, as either 1) properly producing knee extension, 2) producing a reflexive synergy, 3) producing an unexpected muscle movement or synergy, or 4) producing no responses at all. After assessing the

evoked responses of each stimulating electrode, the electrodes with the best responses on both the left and right sides of the spinal cord were assessed further to analyze isometric joint torque recruitment and joint kinematics of the knee.

Isometric joint torques were measured using a force transducer with an integrated 150 lb load cell (Scottsdale, AS, USA). The force transducer was held manually just proximal to the ankle to measure knee joint torques. Pulse trains with current amplitudes from 20 - 300 μA were delivered to the spinal cord, while force transducer signals were measured and recorded at a sampling rate of 100 Hz. Three pulse trains were delivered at each current amplitude to calculate the average evoked joint torque.

After the joint torque measurements, the leg was allowed to move freely during stimulation to assess joint kinematics. The pig's ankle was partially suspended by a pulley system with a 2.5 lb counterweight. The leg was positioned such that the knee-ankle limb segment was approximately parallel to the horizontal plane. Once in this initial position, three 300 μA pulse trains were delivered to the spinal cord and leg kinematics were recorded with a camera at 120 fps (JVC Americas Corp., NJ, USA). The maximum joint angle changes for the left and right knees were calculated based on the initial and final position of the legs.

In vivo electrochemical analysis

Polymer multielectrodes and microwire electrodes were assessed *in vivo* using the MET16 electrochemical test system (see *in vitro* electrochemical analysis). Electrodes were assessed *in vivo* using a two-electrode configuration, consisting of a large-diameter needle counter electrode inserted into muscles adjacent to the spine. EIS and VT measurements were completed as described for the *in vitro* experiments. However, due to the two-electrode configuration, working electrode potentials were measured with respect to the counter electrode instead of a Ag|AgCl reference electrode. CV was not completed *in vivo*, as initial testing with electrodes implanted in the quadriceps motor pools generated large, sustained knee extensor responses that were affecting the stability of the pig on the surgical table and were deemed unsafe to continue.

Tissue perfusion and histology

At the end of the experiment, pigs were given a heparin dose (500 IU/kg) 10 minutes before euthanization and then euthanized with an intravenous injection of Euthanyl (100 mg/kg). They were then perfused with 4L of 4% formalin solution (200 mL/min) through the intracarotid catheter. Following perfusion, the spinal cord was extracted, fixed in 4% formalin solution for 24 hours and cryoprotected in gradually increasing concentrations of sucrose (10-30%) in 0.1 M phosphate buffer for 4 days. Spinal cords were cryosectioned at 20 μm and stained with a Cresyl Violet Nissl stain to assess the acute damage caused by the implants as well as to identify the location of the stimulation sites of the multielectrodes relative to the lumbar motoneuron pool.

Statistics

Statistical analyses were completed with IBM SPSS software (version 26, IBM Co., Armonk, USA). Data were found to violate assumptions of normality and homogeneity of variances, therefore nonparametric statistics were selected for the analysis. Buckling forces, Young's moduli, and acute tissue damage stemming from device insertion were compared between the polymer multielectrodes and microwires using a Mann-Whitney U Test on mean ranks. Electrochemical parameters were compared with a Kruskal-Wallis H Test on mean ranks, with Bonferroni-corrected post hoc comparisons. All values were reported as mean ± standard deviation unless explicitly stated otherwise. Significance was indicated for $p<0.05$.

RESULTS

Multielectrode and microwire microfabrication

Three-channel polymer multielectrodes were fabricated according to methods described above. An optical image of a completed multielectrode is shown in Figure 3A. The insertion depth of the multielectrodes was designed to be 4 mm based on a spinal cord neuroanatomical atlas developed by Toossi et al. [26]. The tip of the implant was designed to reach the most ventral aspect of the ventral horn in the lumbosacral spinal cord of the pig, which is approximately 4 mm deep relative to the dorsal surface of the spinal cord [26]. The three stimulating sites were

separated distally along the multielectrode shank by 400 µm center-to-center, based on the interelectrode spacing reported for cylindrical intraspinal multielectrodes [28]. All stimulating sites were deinsulated on both surfaces of the device to double the geometric surface area of the electrodes. The two deepest electrodes were machined to have one-sided geometric surface areas of 1.56×10^4 µm^2 (3.12×10^4 µm^2 with both sides deinsulated). Due to size restrictions, the most superficial stimulating site was restricted in width, thus the surface area of this electrode was reduced. The one-sided surface area of this electrode was designed to be 5.2×10^3 µm^2 (1.04×10^4 µm^2 with both sides deinsulated). To experimentally measure the deinsulated surface areas of the electrodes, large-area stimulating electrodes (n=7) and small-area stimulating electrodes (n=7) were machined into a sample of PtIr-FW insulated in PDMS/PDMS-PEG. The average deinsulated surface areas of the large stimulating electrodes and small stimulating electrodes were measured as $1.45 \pm 0.05 \times 10^4$ µm^2 (estimated to be 2.90×10^4 µm^2 with both sides deinsulated) and $4.6 \times 10^3 \pm 0.6 \times 10^3$ µm^2 (estimated to be 9.2×10^3 µm^2 with both sides deinsulated), respectively. These average area values were used for calculating the CIC_c and CIL for all the multielectrode stimulating sites.

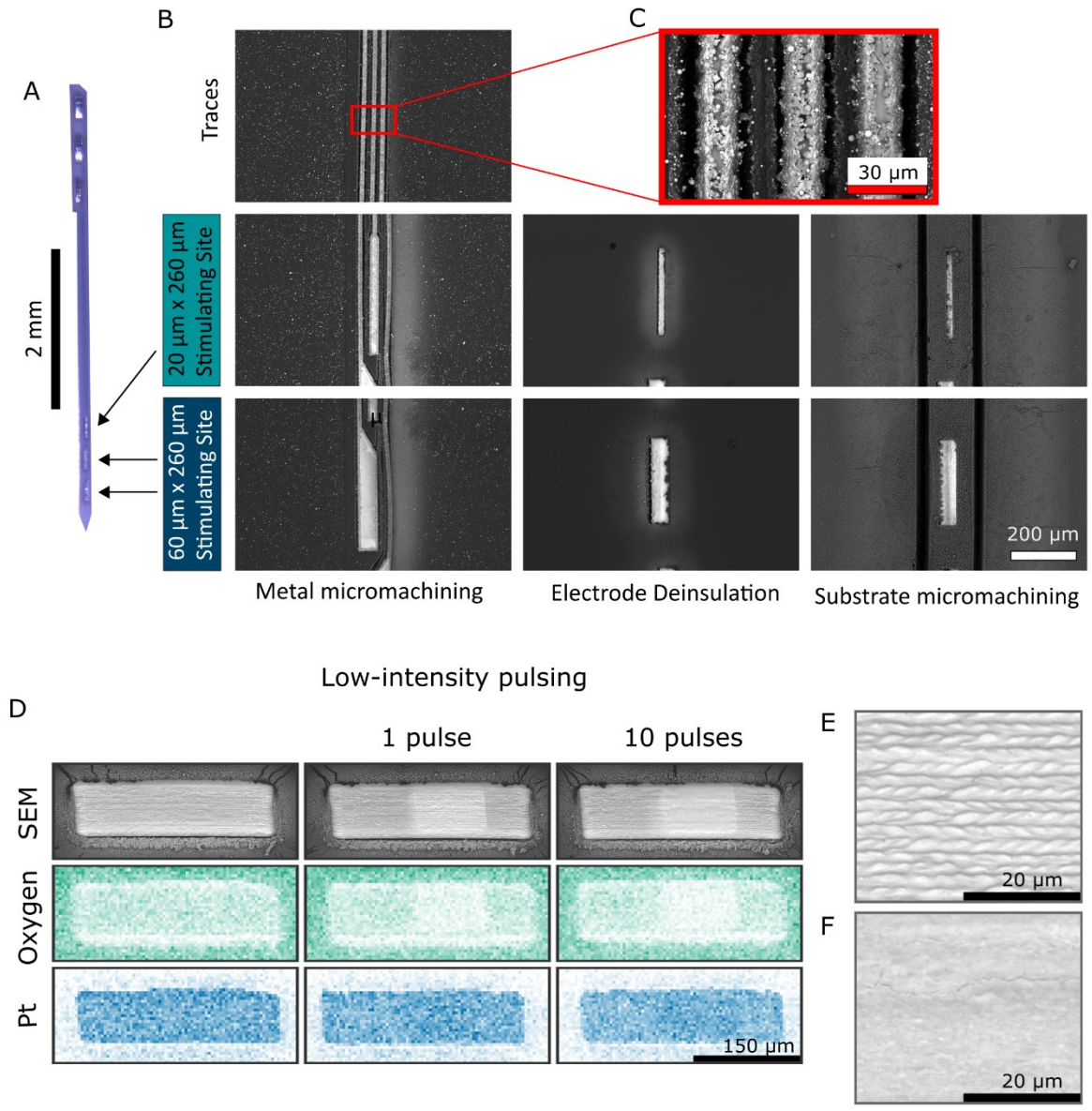

Figure 3: Images depicting polymer multielectrodes at various stages during production. (A) a completed polymer multielectrode without bonded lead wires (scale bar = 2 mm). Three stimulating electrodes, one with a one-sided nominal surface area of 20 µm x 260 µm and two with one-sided nominal surface areas of 60 µm x 260 µm, are separated dorsoventrally along the shank by 400 µm center to center. (B) SEM images of multielectrodes at various stages during manufacturing (scale bar = 200 µm). Column 1 depicts metal features machined with the nanosecond laser. Column 2 shows stimulating sites which have been deinsulated with the laser. Column 3 shows the outer edge of the electrode substrate, machined with the nanosecond laser. (C) A minimum feature size of 15 µm was achieved, seen as the trace width and trace separation

distance (scale bar = 30 μm). (D) Low-intensity laser pulses are used to remove surface oxides and contaminants from the deinsulated electrode surfaces (scale bar = 150 μm). EDS mapping shows that oxygen signals, indicative of surface oxide layers, are reduced after low intensity pulsing. Platinum signals demonstrate that the stimulating site is properly deinsulated. (E) Typical surface features of the stimulating electrodes after laser deinsulation and one low-intensity laser pulse are shown. Laser scanning produces a course, braided pattern on the electrode surface, increasing the electrochemical surface area. (F) Laser-patterned surface features are completely eliminated after 5-10 low-intensity laser pulses, leaving the surface smooth (scale bar = 20 μm).

SEM images were taken at several timepoints during manufacturing to evaluate sample quality (Figure 3B). Through extensive experimentation, laser process parameters were developed for selectively machining metal and polymer layers, as well as for removing surface contaminants from the laser machining process. These process parameters are summarized in Table 1. Using laser process parameters fine-tuned for PtIr-FW micromachining, all features of the multielectrode were machined into the PtIr-FW samples (Figure 3B, column 1). Low-intensity laser parameters were developed for selectively removing encapsulating polymer layers without damaging underlying metal surfaces to deinsulate stimulating electrodes (Figure 3B, column 2). Lastly, the outer edge of the device was machined using custom laser settings. Based on the optical measurements of 6 multielectrode samples, the width and thickness of the devices were measured to be 138 ± 1 μm and 130 ± 10 μm, respectively. A minimum feature size of 15 μm was achieved, measured as the trace width and trace separation distance (Figure 3C).

Following laser micromachining, surface contaminants obstructed all stimulating and wire-bonding sites. Low-intensity laser pulse settings were developed to clean the PtIr-FW surfaces after laser micromachining (Figure 3D). Immediately after laser deinsulation, oxide layers are observed on the stimulating electrode surface, seen as a darkened surface in the SEM image and strong oxygen signal in the EDS oxygen mapping image (Figure 3D). Platinum metal, assessed with EDS, appears to be fully deinsulated after laser deinsulation (Figure 3D). After a single low-intensity laser pulse, surface contaminants were removed. The laser-deinsulated and pulsed surface of the stimulating electrode appears course and braided, with an increased surface area

due to machining (Figure 3E). After an additional 5 - 10 low-intensity pulses, the rough surface features created through laser machining were removed and the surface appears smooth (Figure 3F). Because of this, 5-10 pulses were applied to wire-bonding sites to create smooth metal interfaces for bonding lead wires. However, a single pulse was used to clean oxide layers and surface debris from the stimulating electrode surfaces to maintain some surface roughness to improve electrochemical properties.

A population of microwire electrodes (n=8) were fabricated and measured to determine the average beveled angle and deinsulated tip length, which were found to be 18 ± 1° and 367 ± 18 μm, respectively. Based on these average dimensions, the average microwire electrode deinsulated surface area was calculated as 7.27×10^4 μm^2. This average area was used for calculating the CIC_c and CIL for all microwire electrodes.

Buckling forces and Young's moduli

The results of the compression tests can be seen in Figure 4. The custom mechanical force measurement system (Figure 4A) was calibrated with 6 weights of various sizes: 0.3893 g, 0.5068 g, 0.6261 g, 0.7030 g, 2.0213 g, and 6.5455 g. Each calibration weight was gently placed on the 3D-printed force transducer 8 times and the resulting change in voltage was measured with an oscilloscope. The force transducer operated linearly over the range of calibration weights, and the relationship between measured transducer signal [y, mV] and the applied force [x, mN] was calculated as $y = 6.7275x - 0.6975$ (Figure 4B). This equation was used to calculate the buckling force of the loaded samples during the compression tests based on the force transducer signal.

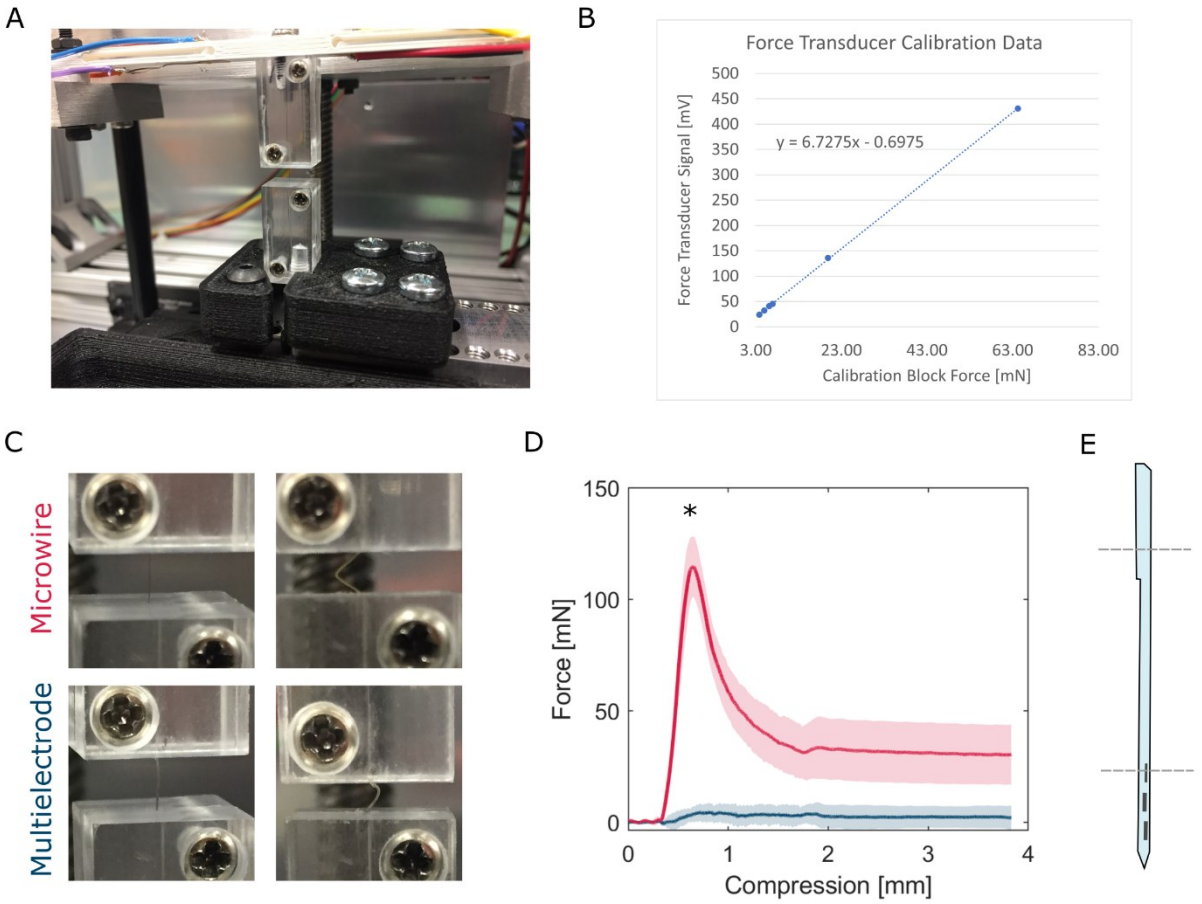

Figure 4: Buckling forces for the polymer multielectrodes (n=6) and microwires (n=6) are shown. (A) An image of the custom mechanical force measurement system. (B) Force transducer calibration data for 6 calibration weights, weighing 0.3893 g, 0.5068 g, 0.6261 g, 0.7030 g, 2.0213 g, and 6.5455 g, and the resulting average voltage signals measured by the force transducer. A linear relationship was observed over the range of calibration weights. (C) Snapshot images show multielectrodes and microwires, clamped between two acrylic blocks, before and after buckling. (D) The microwire samples exhibited significantly higher buckling forces than the multielectrode samples. (E) Approximate locations where the multielectrode samples were clamped by the acrylic blocks.

Microwire samples (n=6) and multielectrode samples (n=6) were prepared for compression testing. Each sample was clamped between two acrylic blocks and carefully loaded into the

mechanical force measurement system with a 3 mm separation distance. Using calipers, the precise separation distance of the 3D printed spacer was measured as 3.03 mm. Compression tests were completed by lowering the top acrylic block by 1.5 mm at 20 mm/min [56].

The buckling force of the microwire samples, measured as 117 ± 14 mN, was significantly greater than the buckling force of the multielectrode samples, measured as 5 ± 4 mN (U=0.000, p=0.004). Two of the six multielectrodes buckled almost immediately after the compression started, withstanding less than 1 mN of compression force, while the other 4 samples accommodated between 5 - 12 mN before buckling.

Based on the buckling forces and equations 1 - 3, the theoretical Young's modulus of the microwire samples was calculated as 89 ± 10 GPa, which was significantly greater than the theoretical Young's modulus of the multielectrode samples, calculated as 56 ± 42 MPa (U=0.000, p=0.004).

Bench electrochemical parameters

Figure 5 shows the results of the bench electrochemical analyses. Microwire samples (EIS & CV: n=12; VT: n=8) were compared against large-area multielectrode stimulating sites (n=7) and small-area multielectrode stimulating sites (n=4). One of the eight large-area multielectrode stimulating sites exhibited much larger charge injection capabilities than the other stimulating sites, possibly due to polymer-metal delamination, and was excluded from subsequent analyses. EIS results for the multielectrodes and microwire electrodes can be seen in Figure 5A and Figure 5C. At 1 kHz (Figure 5B), the microwire electrodes had an impedance magnitude of 4.9 ± 0.5 kΩ, the large-area multielectrode stimulating sites had impedance magnitudes of 8 ± 2 kΩ, and the small-area multielectrode stimulating sites had impedance magnitudes of 16 ± 8 kΩ. The impedance magnitudes differed significantly from each other (H(2)=15.324, p=0.000). Both the large-area stimulating sites (p=0.020) and the small-area stimulating sites (p=0.005) had greater impedance magnitudes than the microwire electrodes. The 1 kHz phase angles (Figure 5D) were measured as -59 ± 3°, -36 ± 6°, and -38 ± 7° for the microwires, large-area multielectrode stimulating sites, and small-area multielectrode stimulating sites, respectively. The phase angles also differed significantly from each other (H(2)=16.509, p=0.000). The large-area stimulating

sites ($p=0.002$) and the small-area stimulating sites ($p=0.024$) had more resistive phase angles than the microwire electrodes.

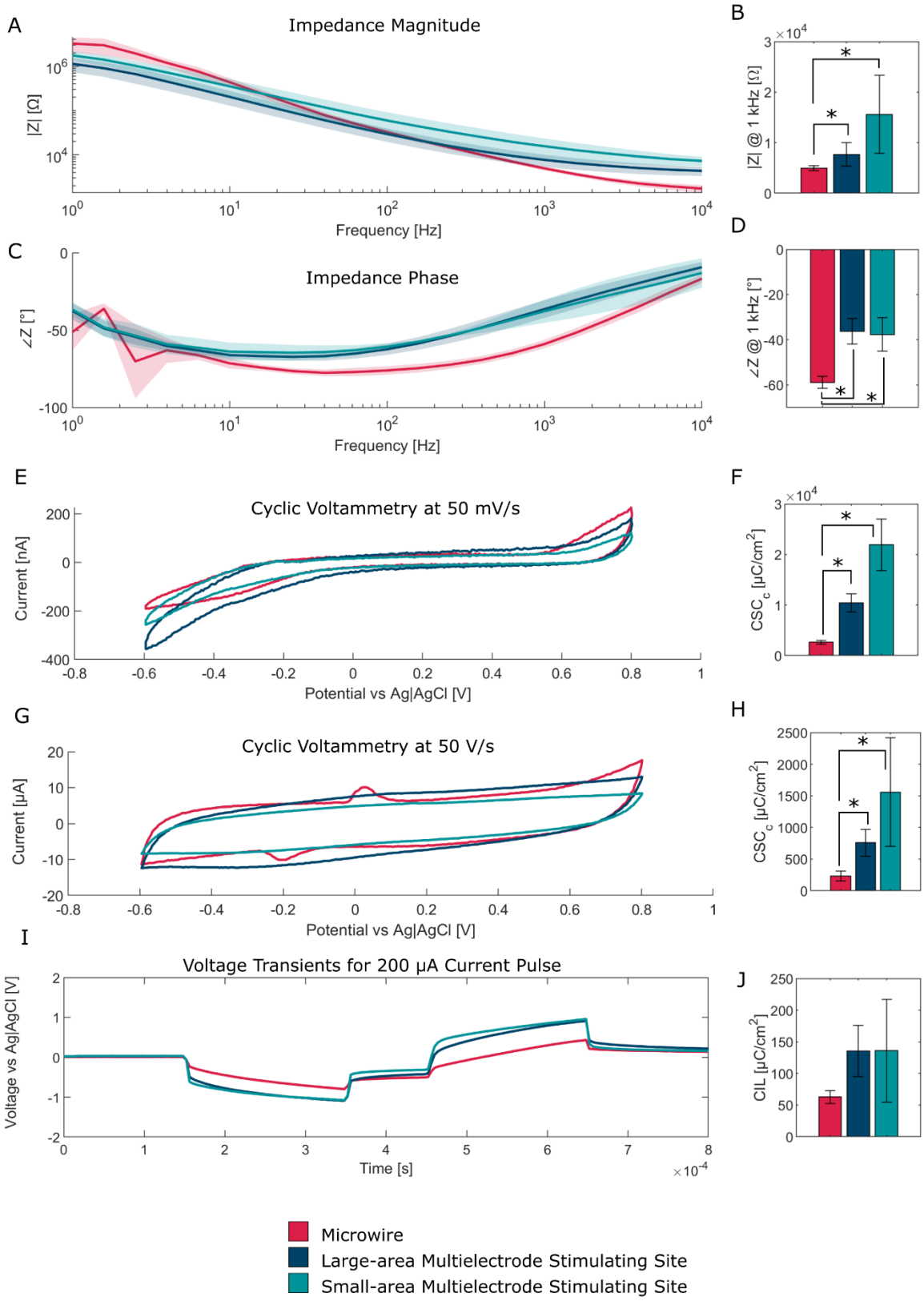
A
Impedance Magnitude
|Z| [Ω]
Frequency [Hz]
B
|Z| @ 1 kHz [Ω]
C
Impedance Phase
∠Z [°]
Frequency [Hz]
D
∠Z @ 1 kHz [°]
E
Cyclic Voltammetry at 50 mV/s
Current [nA]
Potential vs Ag|AgCl [V]
F
CSC_c [μC/cm²]
G
Cyclic Voltammetry at 50 V/s
Current [μA]
Potential vs Ag|AgCl [V]
H
CSC_c [μC/cm²]
I
Voltage Transients for 200 μA Current Pulse
Voltage vs Ag|AgCl [V]
Time [s]
J
CIL [μC/cm²]
Microwire
Large-area Multielectrode Stimulating Site
Small-area Multielectrode Stimulating Site

Figure 5: Bench electrochemical results, acquired in room temperature PBS, for the polymer multielectrode large area and small area stimulating sites and microwire electrodes are shown. (A) the electrochemical impedance magnitude and (C) phase of the electrodes are shown. (B), (D) significant differences are seen for the impedance magnitude and phase of the electrodes when assessed at 1 kHz (multielectrode large area sites: n=7; multielectrode small area sites: n=4; microwire electrodes: n=12). CV results were completed at sweep-rates of (E) 50 mV/s and (G) 50 V/s. Significant differences between the CSC_c of the electrodes at (F) 50 mV/s and (H) 50 V/s were observed (multielectrode large area sites: n=7; multielectrode small area sites: n=4; microwire electrodes: n=12). (I) VT waveforms for a 200 µA current pulse are depicted for representative polymer multielectrode stimulating sites and microwire electrodes. (J) the CIL of the electrodes observed no significant pairwise comparisons in PBS (multielectrode large area sites: n=7; multielectrode small area sites: n=4; microwire electrodes: n=8).

Slow sweep-rate 50 mV/s CV can be seen in Figure 5E. 50 mV/s CSC_c results differed significantly ($H(2)=18.174$, $p=0.000$) (Figure 5F). The CIC_c of the microwire electrodes, calculated as 2.6 ± 0.4 mC/cm^2, was significantly lower than the CIC_c of the large-area (10 ± 2 mC/cm^2) ($p=0.019$) and small-area (22 ± 5 mC/cm^2) ($p=0.001$) multielectrode stimulating sites. Fast sweep-rate 50 V/s CV results can be seen in Figure 5G. 50 V/s CSC_c results differed significantly as well ($H(2)=17.047$, $p=0.000$) (Figure 5H). The microwire electrode CSC_c was calculated as 230 ± 80 µC/cm^2, which was significantly lower than the CSC_c values of the large-area (800 ± 200 µC/cm^2) ($p=0.008$) and small-area (1600 ± 900 µC/cm^2) ($p=0.003$) multielectrode stimulating sites.

VT results for representative multielectrode stimulating sites and microwire electrodes for a 200 µA current pulse are shown in Figure 5I. In PBS, the microwire electrodes could deliver a current of 230 ± 40 µA while remaining within safe potential limits, resulting in a CIL of 60 ± 10 µC/cm^2. Large-area and small-area multielectrode stimulating sites could safely deliver currents of 200 ± 60 µA and 60 ± 40 µA in PBS, with respective CIL values of 140 ± 40 µC/cm^2 and 140 ± 80 µC/cm^2. The maximum current values differed significantly ($H(2)=9.397$, $p=0.009$), with the small-area multielectrode stimulating sites delivering significantly lower current amplitudes while remaining within safe potential limits compared to the microwire electrodes ($p=0.014$).

The maximum CIL (Figure 5J) differed significantly between the microelectrodes and the large- and small-area stimulating sites on the multielectrodes ($H(2)=6.634$, $p=0.036$), but no significant post hoc results were observed.

Evoked responses, joint torques and kinematics

The isometric joint torques and joint kinematics evoked by stimulating through the polymer multielectrodes can be seen in Figure 6. Multielectrodes were implanted into the spinal cord using half-needle insertion aids (Figure 2C). After the initial implantation, the insertion aid was released and the PEG adhesive was given time to dissolve. Within 30 seconds to 1 minute, the multielectrode detached from the insertion aid and the insertion aid was gently removed, leaving the multielectrode implanted within the spinal cord (Figure 6A). All multielectrodes were implanted into the quadriceps motor pools, two on the left side of the cord and two on the right.

Each multielectrode was connected to the stimulator and 50 µA - 300 µA biphasic current pulse trains (40 Hz, 1 s duration) were delivered into the spinal cord. An expert experimenter palpated and visually assessed the leg during electrical stimulation to judge the type and quality of the generated motor responses. For nearly all stimulating sites (n=11/12), knee extension movements were generated, indicating that the quadriceps motor pool was recruited. In one stimulating site, weak reflexive movements were observed, suggesting that current was shunting through the lead wire bonding junction. Focusing on the electrodes that produced quadriceps motor responses, weak knee extension forces were observed for all of the small-area, superficial stimulating electrodes (n=4/4) and for some of the large-area, central (n=2/3) and deep (n=2/4) stimulating electrodes. Strong quadriceps motor responses were observed for 3 of the 4 multielectrode implants at only one of the three stimulating electrodes. Two implants, implanted rostrally on the left and right sides of the spinal cord (Figure 6A), produced strong motor response when stimulating through the deepest, large-area stimulating site, while the third implant, implanted caudally on the left side of the spinal cord, generated strong motor responses through the central, large-area stimulating site. Each of these stimulating sites were selected for a thorough evaluation in terms of isometric joint torques and kinematics. However, when completing the joint torque recruitment curve for the caudal-left implant, all responses were suddenly lost, perhaps suggesting that nearby axons of passage and interneurons had succumb to tissue damage

from the inserted multielectrode. Therefore, we could only fully characterize the rostral-left and rostral-right multielectrodes.

When stimulating through the rostral-left multielectrode, isometric joint torques were recruited gradually (Figure 6B), which is a key feature of ISMS [14]. At current amplitudes of 160 μA, joint torques of 0.49 ± 0.02 Nm were evoked. When the current amplitude was increased to 300 μA, maximum joint torques of 3.7 ± 0.2 Nm were produced. For the joint kinematics, 300 μA pulse trains were able to extend the left knee by 26 ± 1° against the 2.5 lb counter-weight relative to the initial position (Figure 6D), resulting in full extension of the knee. Similar results were seen when evaluating the rostral-right multielectrode (Figure 6C). At current amplitudes of 160 μA, joint torques of 0.57 ± 0.03 Nm were produced. At 300 μA, joint torques increased to 4.4 ± 0.3 Nm. When assessing limb kinematics, 300 μA pulse trains were able to extend the right knee by 20 ± 2° relative to the initial counter-weighted position (Figure 6E), again resulting in full extension of the knee. The stimulation thresholds for the left and right rostral multielectrodes were measured to be 60 μA and 80 μA, respectively.

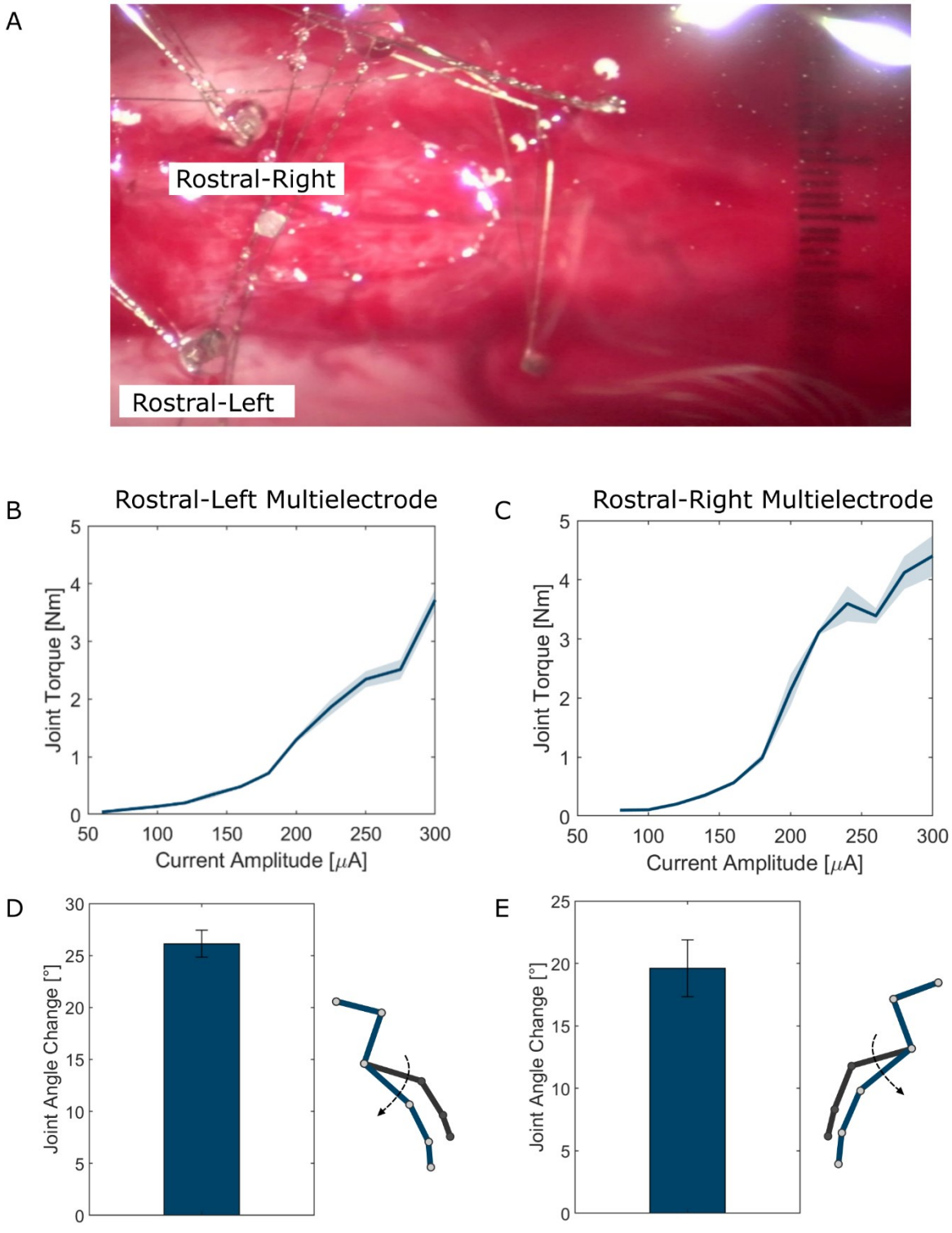

Figure 6: Images show the implanted polymer multielectrodes and the results of *in vivo* testing. (A) Four multielectrodes are shown implanted within the spinal cord. The rostrally implanted

devices (left and right) are characterized further in subsequent figures. (B), (C) Evoked isometric joint torques for the left and right legs show graded force recruitment and peak torques around 3.5-4.5 Nm. (D), (E) Joint kinematics resulting from a 300 μA pulse train for the left and right knee. The knees are shown to fully extend by approximately 19-26° during stimulation.

In vivo electrochemical parameters

Figure 7 demonstrates the electrochemical properties of the microwires and multielectrodes *in vivo*. Microwire electrodes (EIS: n=12; VT: n=8) were compared against large-area (n=7) and small-area (n=4) multielectrode stimulating electrodes. EIS magnitude and phase results are shown in Figure 7A and Figure 7C. The impedance magnitudes (Figure 7B), compared at 1 kHz, did not differ significantly ($H(2)=4.839$, $p=0.089$). The electrochemical impedance of the microwire electrodes was 26 ± 7 kΩ and the phase angle was -52 ± 6°. The 1 kHz electrochemical impedance of the large-area multielectrode stimulating sites was 23 ± 6 kΩ, with a phase of -34 ± 8°, while the impedance of the small-area multielectrode stimulating sites was 50 ± 20 kΩ, with a phase of -48 ± 3°. As seen in PBS, the impedance phase angles (Figure 7D) differed significantly ($H(2)=13.492$, $p=0.001$), as the large-area stimulating sites had significantly more resistive phase angles than the microwire electrodes ($p=0.001$).

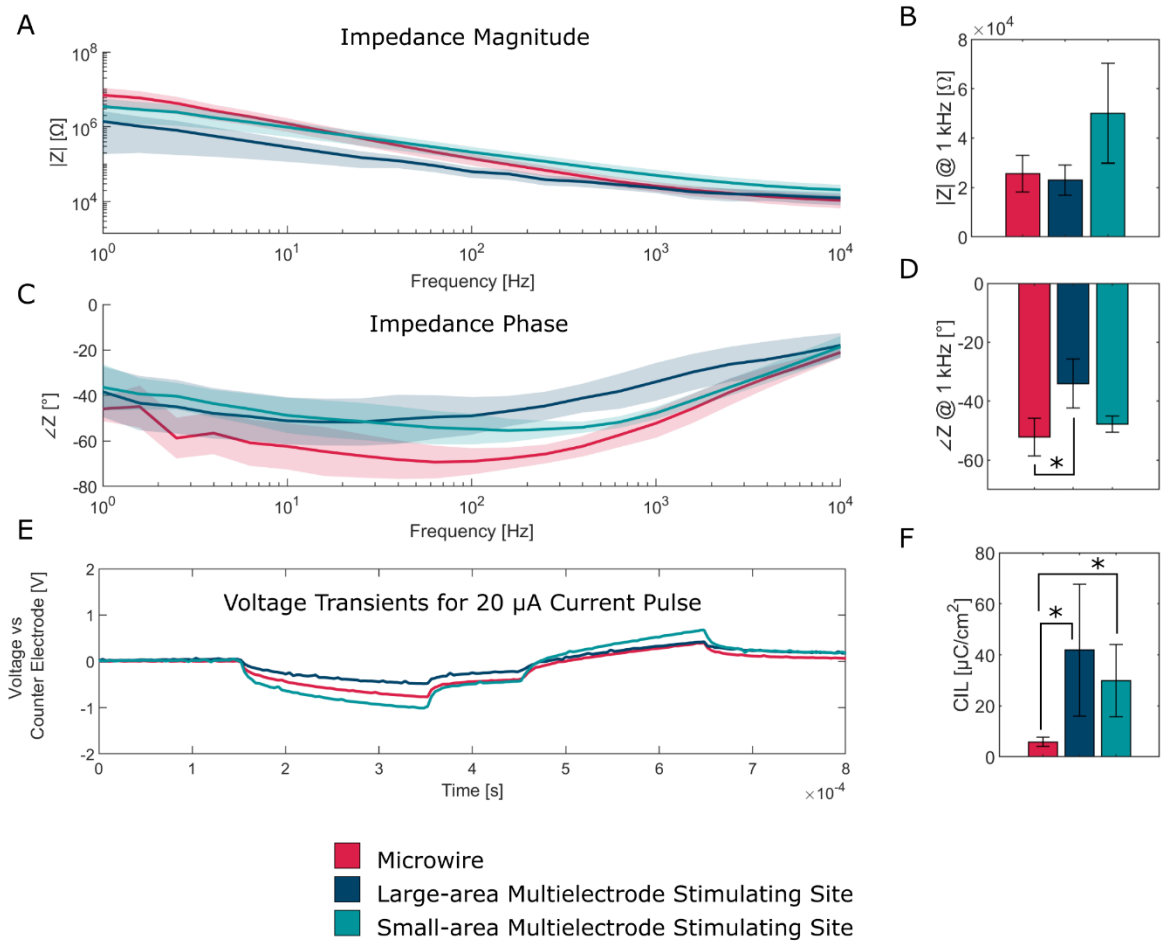

Figure 7: *In vivo* electrochemical results for the polymer multielectrodes and microwire electrodes are shown. (A) The electrochemical impedance magnitude and (C) phase of the electrodes are shown. (B) No significant differences were seen for the 1 kHz impedance magnitude, but significant differences were observed for the phase of the electrodes at 1 kHz (D) (multielectrode large area sites: n=7; multielectrode small area sites: n=4; microwire electrodes: n=12). (E) VT waveforms for a 25 µA current pulse are depicted for representative polymer multielectrode stimulating sites and microwire electrodes. (F) the *in vivo* CIL of the electrodes was significantly different, with higher CIL calculated for the polymer multielectrodes (multielectrode large area sites: n=7; multielectrode small area sites: n=4; microwire electrodes: n=8).

Representative VT waveforms of multielectrode and microwire electrodes delivering a 25 µA biphasic current pulse are shown (Figure 7E). In terms of VT measurements, microwire electrodes were able to pass current amplitudes of 21 ± 6 µA while remaining within safe potential limits, while the large-area and small-area multielectrode stimulating sites were able to safely deliver current amplitudes of 60 ± 40 µA and 10 ± 6 µA, respectively. This corresponded to CIL values of 6 ± 2 µC/cm^2 for the microwire electrodes, 40 ± 30 µC/cm^2 for the large-area multielectrodes stimulating sites, and 30 ± 10 µC/cm^2 for the small-area multielectrode stimulating sites. The maximum current amplitude which could be safely delivered differed significantly between the electrode subtypes ($H(2)=9.874$, $p=0.007$). The large-area stimulating sites were capable of injecting significantly higher current amplitudes than the small-area stimulating electrodes ($p=0.017$). And the CIL (Figure 7F) differed significantly among the electrode subtypes as well ($H(2)=13.730$, $p=0.001$). The large-area stimulating sites ($p=0.005$) and the small-area stimulating sites ($p=0.030$) had significantly greater CIL than the microwire electrodes.

Histology

Histological analyses were conducted to determine all multielectrode positions within the spinal cord and to qualitatively assess tissue damage resulting from the multielectrodes and half-needle insertion aids (Figure 8). All the multielectrodes displayed relatively straight insertion paths into the spinal cord, suggesting that proper ventral horn targeting was achieved. To assess acute tissue damage caused by the multielectrode insertion, insertion track widths were measured and compared against the track widths of microwire electrodes. Typical acute tissue damage for the polymer multielectrodes and half-needle insertion aids can be seen in Figure 8A. An example of tissue damage caused by a microwire electrode can be seen in Figure 8B. The average track width of the multielectrode samples and half-needle insertion aids ($n=4$) was 270 ± 90 µm, which was significantly greater than the average track width of identified microwire electrode tracks ($n=4$), measured as 60 ± 20 µm ($U=0.000$, $p=0.021$) (Figure 8C). Tissue disruption and bleeding within the insertion track could be seen in some cases up to 200 µm rostral or caudal to the center of the implant track. Although much more noticeable than damage induced by microwire implants, this damage may be expected considering the that the insertion aid was 312

μm wide. By using insertion aids with smaller dimensions [54], acute tissue damage could likely be reduced.

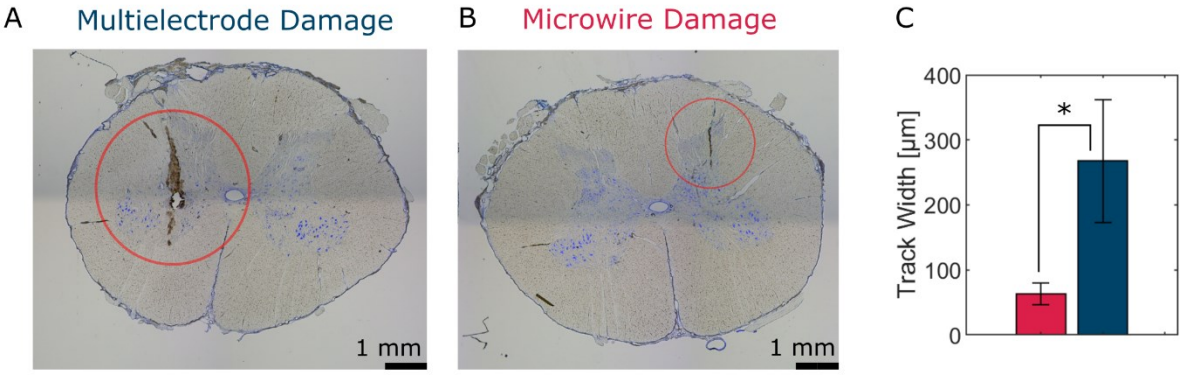

Figure 8: Histological images showing the acute damage caused by multielectrodes (n=4), fixed in half-needle insertion aids, and microwire electrodes (n=4). (A) a typical track from a multielectrode/half-needle insertion aid is shown. (B) a typical microwire electrode track is shown. (C) The track width and acute tissue damage caused by the multielectrode and insertion aid was significantly higher than the acute tissue damage caused by microwire electrodes.

DISCUSSION

Polymer multielectrodes exhibit greater mechanical flexibility than microwire electrodes

The polymer multielectrodes were observed to be significantly more flexible than the microwire electrodes based on their lower buckling force and decreased theoretical Young's modulus. This result is not surprising because the multielectrodes were primarily made from PDMS, which is known to have a Young's modulus as low as 100 kPa [45]. Although the multielectrodes had larger cross-sectional dimensions than the microwires, the microwires remained stiffer because they were constructed almost entirely from platinum and iridium (80%/20%), which have Young's moduli as high as 172 GPa and 545 GPa, respectively [63], [64]. For similar reasons, the polymer multielectrodes would also likely be much more flexible than optical fiber-based intraspinal multielectrodes [28] or silicon-based microelectrode arrays [29], [31] due to the

greater tensile stiffness of the materials used to create those devices. In our experiments, the theoretical Young's modulus of the microwire implants was lower than values typically reported for platinum [63] or iridium [64], yet still significantly stiffer than the modulus of the multielectrodes. A possible reason for this discrepancy could be errors in mounting the microwires properly in the force measurement system. If the microwires were positioned at a slight angle, the buckling force may have been reduced, which would in turn reduce the calculated theoretical Young's modulus.

With their enhanced flexibility, the polymer multielectrodes are significantly closer to matching the mechanical properties of the spinal cord, which has a Young's modulus as low as 5 kPa [46], compared to other rigid microwire or multielectrode implants. Because of this, polymer multielectrodes would likely reduce mechanically-induced FBR *in vivo* [35], [36], improving the biocompatibility of the device. Despite clear improvements in flexibility over the microwire electrodes, the Young's modulus of the polymer multielectrodes was still much higher (i.e., stiffer) than that of PDMS. This was likely due to the stiff PtIr conductors embedded in the substrate. In future work, trace thickness could be reduced, or metal conductors could be replaced with flexible conductive materials such as conductive polymers [36], to improve device flexibility further. Additionally, although device flexibility was significantly improved, these devices may still impart harmful tissue strains because of tethering forces caused by the bonded lead wires [33]. In future iterations of this technology, mechanically-induced tissue strain may be reduced further by also modifying the lead connections to the device. This may be achieved with lead-wire strain relief systems [32] or by utilizing fully wireless designs [34].

Laser-deinsulated stimulating sites exhibit greater charge injection capabilities than platinum-iridium microwire electrodes in bench and *in vivo* assessments

When assessing the PtIr microwire electrodes and polymer multielectrode stimulating sites in PBS and *in vivo*, clear differences emerged in terms of the electrochemical properties and charge injection capabilities of the two classes of electrodes. Although the impedance magnitudes of both the large-area and small-area multielectrode stimulating sites were greater than that of the microwire electrodes in PBS, the large-area and small-area electrodes demonstrated significantly greater CSC_c values in PBS and significantly higher CIL values *in vivo* compared to the

microwire electrodes. These electrochemical improvements were likely due to laser-induced micropatterning of the multielectrode stimulating surfaces, which has been shown to notably increase electrochemical surface area and improve the electrochemical properties of stimulating electrodes [49], [65], [66]. Modest improvements in CIL have been reported by creating hatched patterns in stimulating electrode surfaces via laser micromachining [65], while significantly greater improvements can be attained by using nanoscale laser patterning techniques such as structured laser interference patterning (SLIP) [49], [65] or laser-induced periodic surface structuring (LIPSS) [66]. In the case of this study, deinsulating the multielectrode stimulating sites with laser micromachining roughened the stimulating surface, resulting in the observed improvements in CSC_c and CIL. The CIL of the microwire electrodes in PBS was comparable to values reported in the literature for platinum electrodes. Rose & Robblee reported that the CIL of platinum electrodes is between 100 - 150 $\mu C/cm^2$ when assessed using 200 µs pulse durations [70]. Other groups, however, have reported lower charge injection capabilities of around 40 $\mu C/cm^2$ for platinum electrodes assessed with similar pulse durations, suggesting that pulse frequency may also play an important role in determining CIL [42].

In vivo, the CIL of all electrodes decreased relative to measurements in PBS. This phenomenon has commonly been reported in the literature for stimulating electrodes. Leung et al. demonstrated that the charge injection capabilities of platinum electrodes can decrease by as much as 10x *in vivo* [42], likely due to tissue obstruction and differences in ionic conductivity compared to bench testing environments [67]. Notably, when assessed *in vivo*, all the microwire electrodes and nearly all the multielectrode stimulating electrodes were unable to safely deliver current amplitudes required by ISMS. Typically, ISMS requires current amplitudes of up to 100 µA to evoke functional motor responses [22], [60]. Yet microwire electrodes were only capable of delivering 21 µA of current while remaining within the safe potential limits for platinum-iridium, and only two (n=2/8) of the large-area stimulating electrodes were capable of safely delivering current amplitudes above 100 µA while remaining within safe potentials limits. At the electrode-tissue interface, operating beyond the safe potential limits for PtIr would inevitably lead to the generation of toxic electrochemical byproducts which may induce tissue damage [37] - [39]. However, tissue damage stemming from intraspinal electrical stimulation has been rarely observed in previous chronic experiments [15], [25], which may imply that the spinal cord is capable of tolerating these electrochemical byproducts. To improve the electrochemical

properties of multielectrode stimulating sites, surface modifications could be employed for future chronic implementations. This may include coating the devices in electroactive materials, such as PEDOT [41], laser-patterning the electrode surfaces with SLIP or LIPSS techniques [65], [66], employing activated oxide coatings on the stimulating electrodes [40], or a combination of multiple approaches [68]. In the case of laser-patterned surfaces, Green et al. showed that laser-patterned surfaces exhibited sustained improvements over bare platinum electrodes even after the application of 150 million stimulation pulses, indicating that the electrochemical advantages of laser surface patterning may be maintained at chronic timepoints [65].

Dorsoventral targeting is improved with polymer multielectrodes

All four of the multielectrode samples that were tested *in vivo* were able to recruit quadriceps motor responses through at least 2 of the 3 stimulating electrodes. Importantly, proper motor responses were attained after the device was first implanted, without the need for device repositioning or multiple spinal cord penetrations. By including multiple electrical stimulation sites along the shank of the polymer multielectrodes, the likelihood that a proper locomotor target would be reached after the first spinal cord penetration was increased by 3x compared to microwire electrodes, which can only stimulate one focal region within the spinal cord. This reduced the need for multiple spinal cord penetrations to attain proper locomotor responses, which has been commonly observed for microwire electrodes.

Evoked response amplitudes also changed depending on the dorsoventral position of the stimulating electrode on each multielectrode. For two of the multielectrodes, the greatest locomotor responses were generated by the deepest stimulating sites, whereas one electrode produced strong locomotor responses through the central stimulating site. For this multielectrode design, stimulating electrodes were separated by only 400 μm from center to center and only 140 μm from edge to edge. Considering that adjacent electrodes evoked considerably different motor response amplitudes, this reaffirms that functional responses generated by ISMS are highly sensitive to correct targeting within the spinal cord, especially in the dorsoventral axis, and that correct targeting of the implanted electrode is critical for the successful implementation of ISMS [20].

Evoked joint torques and kinematics, characterized thoroughly for two of the multielectrodes, appeared strong and were within ranges previously observed in the pig when stimulating with microwire electrodes under propofol anesthesia (approximate interquartile range: 1 - 8 Nm), demonstrating that polymer multielectrodes can produce similar functional responses to those produced by microwire electrodes when stimulating within the spinal cord [62]. However, the stimulation threshold of the multielectrodes, measured as 60-80 μA, was much higher than values reported for microwire electrodes in the pig [62]. Toossi et al. reported that microwire stimulation thresholds are typically around 12.5 μA in pig models under propofol anesthesia [62]. Additionally, the multielectrodes required higher charge injection levels to produce equivalent joint torques evoked by microwire electrodes [62]. These differences could have been due to the different geometries of the devices. The sharp edges of the beveled microwire electrodes would experience higher current densities than the flat surfaces of the polymer multielectrode stimulating sites [37], perhaps leading to differences in neuronal activation near the different implanted devices.

Lastly, in addition to improving dorsoventral targeting in the spinal cord, polymer multielectrodes may also permit the recruitment of distinct locomotor responses through separate stimulating sites on a single device. In this experiment, all electrodes were implanted rostrally within the quadriceps motor pool, which was known to be large in the cat [47] and rhesus macaque [20]. In this region of the lumbar enlargement, there is not significant overlap between separate motor pools and it is unlikely that adjacent stimulating sites could produce different functional responses. But in the caudal lumbar enlargement, which has multiple overlapping motor pools [20], improved dorsoventral targeting with multiple stimulation sites may allow a single implanted device to activate distinct functional movements and synergies through adjacent stimulation sites. Similar advantages have been demonstrated by Pikov et al. with silicon microelectrode arrays, where it was shown that intraspinal microstimulation within the sacral spinal cord produced distinct bladder and external urethral sphincter responses when stimulating through electrodes that were separated by sub-millimeter distances [31].

Acute tissue damage from half-needle insertion aids

Due to the inherent flexibility of the polymer multielectrodes, a rigid insertion aid was required for implanting the devices into the spinal cord. This is a common challenge for polymer microelectrodes, where researchers have used strategies such as temporary insertion guides or shuttles [52], [54], dissolvable stiffeners [55] - [57], smart polymers or shape memory polymers that exhibit lower moduli after insertion [35], [58], or tunable liquid metal probes [53] to help insert these devices into the nervous system. In this case, the half-needle insertion aid, which had an outer diameter of 312 μm, was much larger than the 50 μm microwire electrodes typically used for ISMS, and therefore resulted in significantly more tissue damage than a single microwire electrode. Additionally, the PEG glue used to adhere the multielectrode to the insertion aid appeared to have a rough, textured surface, which may have contributed to the increased tissue damage. Acutely, this presents a major limitation for polymer multielectrodes. Despite improvements in functionality and chronic biocompatibility, the initial insertion damage caused by the multielectrode and insertion aid is much greater than the damage caused by a single microwire electrode. It is unclear how the spinal cord would tolerate this acute insertion damage, although Biran et al. reported that the cortex was resilient to acute, stab-wound injuries, and that FBR was mostly observed around chronically implanted electrodes [69]. In terms of the proposed polymer multielectrodes, which are expected to decrease FBR when implanted chronically, it remains to be determined if the greater initial insertion trauma will be negated by decreases in FBR at chronic time points when compared to microwire electrodes. In future research, thinner silicon insertion aids [54] or small diameter tungsten insertion aids which may produce less acute tissue damage should be explored in the spinal cord as an alternative to the half-needle insertion aid used in this study. Additionally, methods to reduce the surface roughness of the PEG adhesive, such as by using PDMS molds for casting the PEG [56], could be explored as a way to decrease insertion-related tissue damage.

CONCLUSION

For the first time, we have developed and characterized a flexible, PDMS-substrate intraspinal multielectrode for generating locomotor function after severe spinal cord injury. This design

exhibits similar advantages to rigid multielectrodes [28] or microelectrode arrays [31], in that it has multiple stimulating electrodes on a single shank, in order to increase the number of regions within the spinal cord that can be stimulated with a single device. However, our device has been fabricated with a novel, flexible PDMS-based substrate to improve biointegration by reducing the mechanical mismatch between the device and the spinal cord. We have shown that PDMS multielectrodes can electrically stimulate 3x more locations within the spinal cord than a single microwire electrode. Additionally, the PDMS multielectrodes were significantly more flexible than microwire electrodes, which may reduce FBR at chronic timepoints. The laser-roughened stimulating electrodes of the PDMS multielectrodes demonstrated improved charge storage capacities in PBS and charge injection limits than microwire electrodes *in vivo* and produced functional joint torques and joint kinematics when assessed *in vivo*. Although this device was designed specifically for the spinal cord, similarly fabricated PDMS-substrate multielectrodes may be equally beneficial in the cortex or peripheral nerves for improving biointegration and device functionality. Overall, this provides a new multielectrode design that may improve targeting, functionality and biointegration in chronic models of spinal cord injury.

Acknowledgements

The authors thank Mr. Rod Gramlich for developing the surgical table extension and joint torque force transducer used in this study. The authors also thank the staff of the Surgical Medical Research Institute at the University of Alberta for their assistance during the animal surgeries. This work was funded by CIHR, the University Hospital Foundation through donations by Nancy and Jim Hutton and Leo Broks, and the Canada Foundation for Innovation. DAR was supported by an NSERC Graduate Scholarship and an Alberta Graduate Excellence Scholarship. VKM is a Canada Research Chair in Functional Restoration.

References

[1] A. Gökaltun, Y. B. A. Kang, M. L. Yarmush, O. B. Usta, and A. Asatekin, "Simple surface modification of poly(dimethylsiloxane) via surface segregating smart polymers for biomicrofluidics," *Scientific Reports*, vol. 9, 7377, 2019.

[2] C. S. Ahuja, J. R. Wilson, S. Nori, M. R. N. Kotter, C. Druschel, A. Curt, and M. G. Fehlings, "Traumatic spinal cord injury," *Nature Reviews Disease Primers*, vol. 3, no. 1, Apr., pp. 1-21, 2017.

[3] A. Singh, L. Tetreault, S. Kalsi-Ryan, A. Nouri, and M. G. Fehlings, "Global prevalence and incidence of traumatic spinal cord injury," *Clinical Epidemiology*, vol. 6, Sep., pp. 309-331, 2014.

[4] R. Sweis, and José Biller, "Systemic complications of spinal cord injury," *Current Neurology and Neuroscience Reports*, vol. 17, art. 8, Feb., pp. 1-8, 2017.

[5] National Spinal Cord Injury Statistical Center, Facts and Figures at a Glance, Birmingham, AL: University of Alabama at Birmingham, 2016.

[6] I. H. Tsai, D. E. Graves, W. Chan, C. Darkoh, M-S. Lee, and L. A. Pompeii, "Environmental barriers and social participation in individuals with spinal cord injury," *Rehabilitation Psychology*, vol. 62, no. 1, Feb., pp. 36-44, 2017.

[7] H. Krueger, V. K. Noonan, L. M. Trenaman, P. Joshi, and C. S. Rivers, "The economic burden of traumatic spinal cord injury in Canada," *Chronic diseases and injuries in Canada*, vol. 33, no. 3, June, pp. 1-26, 2013.

[8] L. A. Simpson, J. J. Eng, J. T. C. Hsieh, D. L. Wolfe, and the SCIRE Research Team, "The health and life priorities of individuals with spinal cord injury: A systematic review," *Journal of Neurotrauma*, vol. 29, no. 8, May, pp. 1548-1555, 2012.

[9] F. B. Wagner, J-B. Mignardot, C. G. Le Goff-Mignardot, R. Demesmaeker, S. Komi, M. Capogrosso, A. Rowald, I. Seáñez, M. Caban, E. Pirondini, M. Vat, L. A. McCracken, R. Heimgartner, I. Fodor, A. Watrin, P. Seguin, E. Paoles, K. Van Den Keybus, G. Eberle, B. Schurch, E. Pralong, F. Becce, J. Prior, N. Buse, R. Buschman, E. Neufeld, N. Kuster, S. Carda, J. von Zitzewitz, V. Delattre, T. Denison, H. Lambert, K. Minassian, J. Bloch, and G. Courtine, "Targeted neurotechnology restores walking in humans with spinal cord injury," *Nature*, vol. 563, Oct., pp. 65-71, 2018.

[10] R. J. Triolo, S. N. Bailey, M. E. Miller, L. M. Rohde, J. S. Anderson, J. A. Jr. Davis, J. J. Abbas, L. A. DiPonio, G. P. Forrest, D. R. Jr. Gater, and L. J. Yang, "Longitudinal performance of a surgically implanted neuroprosthesis for lower extremity exercise,

standing, and transfers after spinal cord injury," *Arch Phys Med Rehabil.*, vol. 93, no. 5, May, pp. 896-904, 2012.

[11] D. Guiraud, T. Stieglitz, K. P. Koch, J. L. Divoux, and P. Rabischong, "An implantable neuroprosthesis for standing and walking in paraplegia: 5-year patient follow-up," *J. Neural Eng.*, vol. 3, no. 4, Sept., pp. 269-275, 2006.

[12] M. L. Gill, P. J. Grahn, J. S. Calvert, M. B. Linde, I. A. Lavrov, J. A. Strommen, L. A. Beck, D. G. Sayenko, M. G. Van Straaten, D. I. Drubach, D. D. Veith, A. R. Thoreson, C. Lopez, Y. P. Gerasimenko, V. R. Edgerton, K. H. Lee, and K. D. Zhao, "Neuromodulation of lumbosacral spinal networks enables independent stepping after complete paraplegia," *Nature Medicine*, vol. 24, Nov., pp. 1677-1682, 2018.

[13] C. A. Angeli, M. Boakye, R. A. Morton, J. Vogt, K. Benton, Y. Chen, C. K. Ferreira, and S. J. Harkema, "Recovery of over-ground walking after chronic motor complete spinal cord injury," *New England Journal of Medicine*, vol. 379, Sep., pp. 1244-1250, 2018.

[14] V. K. Mushahwar and K. W. Horch, "Muscle recruitment through electrical stimulation of the lumbo-sacral spinal cord," *IEEE Trans. Rehabil. Eng.*, vol. 8, no. 1, Mar., pp. 22-29, 2000.

[15] V. K. Mushahwar, D. F. Collins, and A. Prochazka, "Spinal cord microstimulation generates functional limb movements in chronically implanted cats," *Experimental Neurology*, vol. 163, Feb., pp. 422-429, 2000.

[16] L. Guevremont, C. G. Renzi, J. A. Norton, J. Kowalczewski, R. Saigal, and V. K. Mushahwar, "Locomotor-related networks in the lumbosacral enlargement of the adult spinal cat: Activation through intraspinal microstimulation," *IEEE Trans. Neural Syst. Rehabil. Eng.*, vol. 14, no. 3, Sep., pp. 266-272, 2006.

[17] V. K. Mushahwar, and K. W. Horch, "Selective activation of muscle groups in the feline hindlimb through electrical microstimulation of the ventral lumbo-sacral spinal cord," *IEEE Trans. Rehabil. Eng.*, vol. 8, no. 1, Mar., pp. 11-21, 2000.

[18] J. A. Bamford, C. T. Putman, and V. K. Mushahwar, "Intraspinal microstimulation preferentially recruits fatigue-resistant muscle fibres and generates gradual force in rat," *J. Physiol*, vol. 569, no. 3, Dec., pp. 873-884, 2005.

[19] J. T. Hachmann, J. H. Jeong, P. J. Grahn, G. W. Mallory, L. Q. Evertz, A. J. Bieber, D. A. Lobel, K. E. Bennet, K. H. Lee, and J. L. Lujan, "Large animal model for development of functional restoration paradigms using epidural and intraspinal stimulation," *PLoS ONE*, vol. 8, no. 12, Dec., pp. 1-7, 2013.

[20] A. Toossi, D. G. Everaert, S. I. Perlmutter, and V. K. Mushahwar, "Functional organization of motor networks in the lumbosacral spinal cord of non-human primates," *Scientific Reports*, vol. 9, Sept., pp. 1-16, 2019.

[21] B. Lau, L. Guevremont, and V. K. Mushahwar, “Strategies for generating prolonged functional standing using intramuscular stimulation or intraspinal microstimulation,” *IEEE Trans. Neural Syst. Rehabil. Eng.*, vol. 15, no. 2, June, pp. 273-285, 2007.

[22] B. J. Holinski, K. A. Mazurek, D. G. Everaert, A. Toossi, A. M. Lucas-Osma, P. Troyk, R. Etienne-Cummings, R. B. Stein, and V. K. Mushahwar, “Intraspinal microstimulation produces over-ground walking in anesthetized cats,” *J. Neural Eng.*, vol. 13, no. 5, Sept., pp. 1-17, 2016.

[23] J. A. Bamford, R. M. Lebel, K. Parseyan, and V. K. Mushahwar, “The fabrication, implantation, and stability of intraspinal microwire arrays in the spinal cord of cat and rat,” *IEEE Trans. Neural Syst. Rehabil. Eng.*, vol. 25, no. 3, Mar., pp. 287-296, 2017.

[24] P. J. Grahn, K. H. Lee, A. Kasasbeh, G. W. Mallory, J. T. Hachmann, J. R. Dube, C. J. Kimble, D. A. Lobel, A. Bieber, J. H. Jeong, K. E. Bennet, and J. L. Lujan, “Wireless control of intraspinal microstimulation in a rodent model of paralysis,” *J. Neurosurg.*, vol. 123, Jul., pp. 232-242, 2015.

[25] J. A. Bamford, K. G. Todd, and V. K. Mushahwar, “The effects of intraspinal microstimulation on spinal cord tissue in the rat,” *Biomaterials*, vol. 31, Apr., pp. 5552-5563, 2010.

[26] A. Toossi, B. Bergin, M. Marefatallah, B. Parhizi, N. Tyreman, D. G. Everaert, S. Rezaei, P. Seres, J. C. Gatenby, S. I. Perlmutter, and V. K. Mushahwar, “Comparative neuroanatomy of the lumbosacral spinal cord of the rat, cat, pig, monkey, and human,” *Scientific Reports*, vol. 11, Jan., pp. 1-15, 2021.

[27] A. Toossi, D. G. Everaert, P. Seres, J. L. Jaremko, K. Robinson, C. C. Kao, P. E. Konrad, and V. K. Mushahwar, “Ultrasound-guided spinal stereotactic system for intraspinal implants,” *J. Neurosurg Spine*, vol., 29, Sept., pp. 292-305, 2018.

[28] S. Snow, S. C. Jacobsen, D. L. Wells, and K. W. Horch, “Microfabricated cylindrical multielectrodes for neural stimulation,” *IEEE Trans. Biomed. Eng.*, vol. 53, no. 2, Feb., pp. 320-326, 2006.

[29] V. Pikov, L. Bullara, and D. B. McCreery, “Intraspinal stimulation for bladder voiding in cats before and after chronic spinal cord injury,” *J. Neural Eng.*, vol. 4, no. 4, Dec., pp. 356-368, 2007.

[30] S. Shahdoost, S. B. Frost, D. J. Guggenmos, J. A. Borrell, C. Dunham, S. Barbay, R. J. Nudo, and P. Mohseni, “A brain-spinal interface (BSI) system-on-chip (SoC) for closed-loop cortically-controlled intraspinal microstimulation,” *Analog Integrated Circuits and Signal Processing*, vol. 95, Jan., pp. 1-16, 2018.

[31] V. Pikov, D. B. McCreery, and M. Han, “Intraspinal stimulation with a silicon-based 3D chronic microelectrode array for bladder voiding in cats,” *Journal of Neural Engineering*, vol. 17, Dec., pp. 1-13, 2020.

[32] A. Toossi, D. G. Everaert, A. Azar, C. R. Dennison, and V. K. Mushahwar, “Mechanically stable intraspinal microstimulation implants for human translation,” *Annals of Biomedical Engineering*, vol. 45, no. 3, Mar., pp. 681-694, 2017.

[33] J. Thelin, H. Jörntell, E. Psouni, M. Garwicz, J. Schouenborg, N. Danielsen, and C. E. Linsmeier, “Implant size and fixation mode strongly influence tissue reactions in the CNS,” *PLoS ONE*, vol. 6, no. 1, Jan., 2011.

[34] A. Abdo, M. Sahin, D. S. Freedman, E. Cevik, P. S. Spuhler, and M. S. Unlu, “Floating light-activated micro electrical stimulators tested in the rat spinal cord,” *Journal of Neural Engineering*, vol. 5, no. 5, Oct., pp. 1-21, 2011.

[35] J. K. Nguyen, D. J. Park, J. L. Skousen, A. E. Hess-Dunning, D. J. Tyler, S. J. Rowan, C. Weder, and J. R. Capadona, “Mechanically-compliant intracortical implants reduce the neuroinflammatory response,” *Journal of Neural Engineering*, vol. 11, no. 5, Aug., pp. 1-15, 2014.

[36] Z. J. Du, C. L. Kolarcik, T. D. Y. Kozai, S. D. Luebben, S. A. Sapp, X. S. Zheng, J. A. Nabity, and X. T. Cui, “Ultrasoft microwire neural electrodes improve chronic tissue integration,” *Acta Biomaterialia*, vol. 53, Apr., pp. 46-58, 2017.

[37] S. F. Cogan, “Neural Stimulation and Recording Electrodes,” *Annu. Rev. Biomed. Eng.*, vol. 10, Apr., pp. 275-309, 2008.

[38] D. R. Merrill, M. Bikson, and J. G. R. Jefferys, “Electrical stimulation of excitable tissue: Design of efficacious and safe protocols,” *J. Neurosci. Methods*, vol. 141, pp. 171-198, 2005.

[39] S. F. Cogan, K. A. Ludwig, C. G. Welle, and P. Takmakov, “Tissue damage thresholds during therapeutic electrical stimulation,” *Journal of Neural Engineering*, vol. 13, no. 2, Jan., pp. 1-13, 2016.

[40] S. F. Cogan, P. R. Troyk, J. Ehrlich, and T. D. Plante, “In vitro comparison of the charge-injection limits of activated iridium oxide (AIROF) and platinum-iridium microelectrodes,” *IEEE Trans. Biomed. Eng.,* vol. 52, no. 9, Sep., pp. 1612-1614, 2005.

[41] H. Vara and J. E. Collazos-Castro, “Enhanced spinal cord microstimulation using conducting polymer-coated carbon microfibers,” *Acta Biomaterialia*, vol. 90, May, pp. 71-86, 2019.

[42] R. T. Leung, M. N. Shivdasani, D. A. X. Nayagam, and R. K. Shepherd, "In Vivo and in vitro comparison of the charge injection capacity of platinum macroelectrodes," *IEEE Trans. Biomed. Eng.*, vol. 62, no. 3, Mar., pp. 849-857, 2015.

[43] K. M. Szostak, L. Grand, and T. G. Constandinou, "Neural interfaces for intracortical recording: Requirements, fabrication methods, and characteristics," *Frontiers in Neuroscience*, vol. 11, art. 665, pp. 1-27, 2017.

[44] A. Weltman, J. Yoo, and E. Meng, "Flexible, penetrating brain probes enabled by advances in polymer microfabrication," *Micromachines*, vol. 7, no. 10, Oct., pp. 1-36, 2016.

[45] C. Hassler, T. Boretius, and T. Steiglitz, "Polymers for neural implants," *Polymer Physics*, vol. 49, pp. 18-33, 2011.

[46] H. Ozawa, T. Matsumoto, T. Ohashi, M. Sato, and S. Kokubun, "Mechanical properties and function of the spinal pia mater," *J. Neurosurg. Spine*, vol. 1, Jul., pp. 122-127, 2004.

[47] V. K. Mushahwar, D. M. Gillard, M. J. A. Gauthier, and A. Prochazka, "Intraspinal microstimulation generates locomotor-like and feedback-controlled movements," *IEEE Trans. Neural Syst. Rehabil. Eng.*, vol. 10, no. 1, Mar., pp. 68-81, 2002.

[48] K. C. Cheung, P. Renaud, H. Tanila, and K. Djupsund, "Flexible polyimide microelectrode array for in vivo recordings and current source density analysis," *Biosensors and Bioelectronics*, vol. 22, pp. 1783-1790, 2007.

[49] M. Mueller, N. de la Oliva, J. del Valle, I. Delgado-Martínez, X. Navarro, and T. Stieglitz, "Rapid prototyping of flexible intrafascicular electrode arrays by picosecond laser structuring," *Journal of Neural Engineering*, vol. 14, no. 6, Nov., pp. 1-11, 2017.

[50] I. R. Minev, P. Musienko, A. Hirsch, Q. Barraud, N. Wenger, E. M. Moraud, J. Gandar, M. Capogrosso, T. Milekovic, L. Asboth, R. F. Torres, N. Vachicouras, Q. Liu, N. Pavlova, S. Duis, A. Larmagnac, J. Vörös, S. Micera, Z. Suo, G. Courtine, and S. P. Lacour, "Electronic dura mater for long-term multimodal neural interfaces," *Science*, vol. 347, no. 6218, Jan., pp. 159-163, 2015.

[51] J. M. Kim, D. R. Oh, J. Sanchez, S. H. Kim, and J. M. Seo, "Fabrication of polydimethylsiloxane (PDMS) - based multielectrode array for neural interface,"*35th Annual International Conference of the IEEE EMBS*, Jul., pp. 1716-1719, 2013.

[52] T. D. Y. Kozai, and D. R. Kipke, "Insertion shuttle with carboxyl terminated self-assembled monolayer coatings for implanting flexible polymer neural probes in the brain," *J. Neurosci. Methods*, vol. 184, no. 2, Nov., pp. 199-205, 2009.

[53] X. Wen, B. Wang, S. Huang, T. Liu, M. -S. Lee, P. -S. Chung, Y. T. Chow, I. -W. Huang, H. G. Monbouquette, N. T. Maidment, and P. -Y. Chiou, "Flexible,

multifunctional neural probe with liquid metal enabled, ultra-large tunable stiffness for deep-brain chemical sensing and agent delivery," *Biosens Bioelectron.*, vol. 131, Apr., pp. 37-45, 2019.

[54] S. H. Felix, K. G. Shah, V. M. Tolosa, H. J. Sheth, A. C. Tooker, T. L. Delima, S. P. Jadhav, L. M. Frank, and S. S. Pannu, "Insertion of flexible neural probes using rigid stiffeners attached with biodissolvable adhesive," *Journal of Visualized Experiments*, vol. 79, 50609, 2013.

[55] J. Agorelius, F. Tsanakalis, A. Friberg, P. T. Thorbergsson, L. M. E. Pettersson, and G. Schouenborg, "An array of highly flexible electrodes with a tailored configuration locked by gelatin during implantation - initial evaluation in cortex cerebri of awake rats," *Frontiers in Neuroscience*, vol. 9, art. 331, Sep., pp. 1-12, 2015.

[56] A. Lecomte, V. Castagnola, E. Descamps, L. Dahan, M. C. Blatché, T. M. Dinis, E. Leclerc, C. Egles, and C. Bergaud, "Silk and PEG as means to stiffen a parylene probe for insertion in the brain: Toward a double time-scale tool for local drug delivery," *J. Micromech. Microeng.*, vol. 25, 125003, 2015.

[57] Z. Zhao, X. Li, F. He, X. Wei, S. Lin, and C. Xie, "Parallel, minimally-invasive implantation of ultra-flexible neural electrode arrays," *J. Neural Eng.*, vol. 16, no. 3, Jun., 035001, 2019.

[58] A. M. Stiller, J. O. Usoro, J. Lawson, B. Araya, M. A. González-González, V. R. Danda, W. E. Voit, B. J. Black, and J. J. Pancrazio, "Mechanically robust, softening shape memory polymer probes for intracortical recording," *Micromachines*, vol. 11, no. 6, art. 619, Jun., 2020.

[59] M. Schuettler, B. V. King, and G. J. Suaning, "Fabrication of implantable microelectrode arrays by laser cutting of silicone rubber and platinum foil," *Journal of Neural Engineering*, vol. 2, no. 1, Feb., pp. S121-S128, 2005.

[60] A. N. Dalrymple, D. A. Roszko, R. S. Sutton, and V. K. Mushahwar, "Pavlovian control of intraspinal microstimulation to produce over-ground walking," *Journal of Neural Engineering*, vol. 17, no. 3, May, 036002, 2020.

[61] J. Qu, Q. Wu, T. Clancy, Q. Fan, X. Wang, and X. Liu, "3D-printed strain-gauge micro force sensors," *IEEE Sensors Journal*, vol. 20, no. 13, Jul., pp. 6971-6978, 2020.

[62] A. Toossi, D. G. Everaert, R. R. E. Uwiera, D. S. Hu, K. Robinson, F. S. Gragasin, and V. K. Mushahwar, "Effect of anesthesia on motor responses evoked by spinal neural prostheses during intraoperative procedures," *Journal of Neural Engineering*, vol. 16, Mar., pp. 1-18, 2019.

[63] AZoMaterials, “Platinum - Properties and Applications,” *azom.com*. [Online]. Available: https://www.azom.com/properties.aspx?ArticleID=601. [Accessed Jul. 16, 2021].

[64] AZoMaterials, “Iridium - Properties and Applications,” *azom.com*. [Online]. Available: https://www.azom.com/properties.aspx?ArticleID=1700. [Accessed Jul. 16, 2021].

[65] R. A. Green, P. B. Matteucci, C. W. D. Dodds, J. Palmer, W. F. Dueck, R. T. Hassarati, P. J. Byrnes-Preston, N. H. Lovell, and G. J. Suaning, “Laser patterning of platinum electrodes for safe neurostimulation,” *Journal of Neural Engineering*, vol. 11, no. 5, Sept., 056017, 2014.

[66] A. Kelly, N. Farid, K. Krukiewicz, N. Belisle, J. Grorke, E. M. Waters, A. Trotier, F. Laffir, M. Kilcoyne, G. M. O’Connor, and M. J. Biggs, “Laser-induced periodic surface structure enhances neuroelectrode charge transfer capabilities and modulates astrocyte function,” *ACS Biomater. Sci. Eng.*, vol. 6, Mar., pp. 1449-1461, 2020.

[67] S. F. Cogan, “In vivo and in vitro differences in the charge-injection and electrochemical properties of iridium oxide electrodes,” In Proc. IEEE EMBS Annual International Conference, 2006, pp. 882-885.

[68] M. Schuettler, “Electrochemical properties of platinum electrodes in vitro: comparison of six different surface qualities,” In Proc. 29th Annual International Conference of the IEEE EMBS, 2007, pp. 186-189.

[69] R. Biran, D. C. Martin, and P. A. Tresco, “Neuronal cell loss accompanies the brain tissue response to chronically implanted silicon microelectrode arrays,” *Experimental Neurology*, vol. 195, pp. 115-126, 2005.

[70] T. L. Rose and L. S. Robblee, “Electrical stimulation with Pt electrodes. VIII. Electrochemically safe charge injection limits with 0.2 ms pulses,” *IEEE Trans. Biomed. Eng.*, vol. 37, no. 11, Nov., pp. 1118-1120, 1990.

Chapter 3: Conclusion and Future Directions

General Discussion and Conclusions

The overall goal of this research work was to design, fabricate, and characterize new polymer multielectrodes for the spinal cord in an effort to improve the functionality and biocompatibility of technologies used to implement intraspinal microstimulation (ISMS). Firstly, these newly developed penetrating polymer multielectrodes, fabricated with a flexible PDMS-based substrate and used in the spinal cord for the first time, were shown to be significantly more flexible than microwire electrodes (and by extension other rigid multielectrodes or microelectrode arrays) traditionally used to implement ISMS, thus satisfying the first aim of my thesis. Because of this improved flexibility, polymer multielectrodes may be better suited for mechanically matching the compliance of the spinal cord, which has been reported to be as low as 5 kPa [1]. In the cortex, other flexible implants have demonstrated pronounced decreases in foreign body responses (FBR) at chronic timepoints compared to rigid implants [2], [3]. For the spinal cord, this suggests that the PDMS-substrate polymer multielectrodes created through this research would generate decreased FBR compared to other rigid intraspinal implants, thus improving chronic tissue integration and device functionality. Although device tethering forces may still impart some harmful strains at the implant-tissue interface, this could be addressed in future research by employing lead wire strain relief systems [4] or entirely wireless designs [5]. Secondly, multielectrode stimulating electrodes, machined with laser microfabrication techniques, were shown to have higher charge injection capabilities than the microwire electrodes, addressing the second aim of my thesis. Laser-deinsulated polymer multielectrode stimulating sites, with geometric surface areas approximately 1/3 the surface area of microwire electrodes, not only matched the electrochemical properties of PtIr microwire electrodes, but in fact exceeded them. Because of laser-induced micropatterning, which has been shown to drastically improve the electrochemical properties of stimulating electrodes [6] - [8], the multielectrode stimulating sites exhibited significantly higher charge storage capacities in bench testing and significantly higher charge injection limits *in vivo* compared to the microwire electrodes used in this study. In bench testing, the large-area multielectrode stimulating sites were capable of safely delivering similar current amplitudes as the microwire electrodes, despite having only 1/3 the geometric surface area compared to the microwire electrodes. *In vivo*, the large-area and small-area multielectrode stimulating sites were both capable of safely delivering

similar current amplitudes as the microwire electrodes while remaining within safe potential limits [9]. Interestingly, the microwire electrodes used in this study were not capable of safely delivering current amplitudes typically required for ISMS, despite having similar dimensions to microwire electrodes used in previous ISMS research [10], [11], [25]. These microwire electrodes were only capable of delivering 21 ± 6 μA, while the maximum required current amplitudes to implement ISMS effectively have been reported as 100 μA [10] or even 130 μA [11]. Tissue damage stemming from toxic electrochemical byproducts has not been observed in chronic implementations of ISMS [12], [13]; however, if the microwire tip exposure areas used in this study were to be utilized, these electrodes may require electrochemical enhancements of their surface areas, such as nanopatterned surfaces [6], [8], activated oxide coatings [14], or conductive polymer coatings [15], to safely deliver the required current amplitudes. Thirdly, some of the polymer multielectrode stimulating sites were capable of producing isometric joint torques and joint kinematics similar to responses previously demonstrated by microwire electrodes in the pig, satisfying the third aim of my thesis. Considering that the PDMS multielectrodes had more stimulating electrodes per device than the microwire electrodes and that the multielectrode stimulating sites were capable of producing functional responses similar to those observed by microwire electrodes, the polymer multielectrodes may in the future provide an advantage over microwire implants in the context of ISMS or other penetrating devices in the nervous system.

Future research

In future research, the design of the PDMS multielectrodes could be altered to further improve device functionality and biocompatibility. Flexibility could be improved by reducing the dimensions of the device or by using more flexible materials to manufacture the device. In terms of dimensions, the thickness and width of the multielectrodes, measured as 130 ± 10 μm and 138 ± 1 μm, respectively, were unavoidably large because of the laser microfabrication methods used. As the nanosecond laser was used to machine the metal features of the multielectrode, the laser would cut through underlying polymer layers as well. It was seen experimentally (data not shown) that if the underlying polymer layers were thinner than ~60-80 μm, the nanosecond laser would completely cut through the polymer layer and the release layer, ruining the sample entirely. Therefore, the underlying polymer layer was intentionally made thicker (80 μm or

thicker) to improve device fabrication success rates. This limitation may be eliminated with the use of a femtosecond laser to fabricate these devices. Moreover, if traditional photolithographic techniques were instead used to deposit conductive elements on the bottom polymer layer, such as with physical vapor deposition and electrodeposition [16], conductive traces could be formed without the need for a thick underlying polymer layer, thus reducing the size of the device. Reducing trace thickness and trace width, both possible with standard electrodeposition and photolithographic methods [16], could also be used to reduce metal trace dimensions, thus reducing implant stiffness. Alternatively, mechanical conductors could be entirely replaced by conductive hydrogels or polymers [3], [17] or with liquid metal conductors [18] to greatly reduce the stiffness of the device. Although nanosecond laser microfabrication was very successful for machining these polymer multielectrode prototypes, improving the multielectrodes further will likely require the use of other manufacturing techniques and materials, such as with traditional clean-room technologies [16] or by using experimental printing methods for conductive inks or conductive polymers [19], [20].

Insertion methods for the device could also be improved. A half-needle insertion shuttle design [3] was selected for inserting the PDMS multielectrodes into the spinal cord due to its simplicity and effectiveness. However, the insertion aid created considerable tissue displacement and damage *in vivo*, potentially hindering advantages in chronic biocompatibility. Other insertion aid techniques, such as thin silicon insertion aids [21], mechanically tunable materials [2], [18], or dissolvable silk fibroin stiffeners [22] may prove more effective in selectively stiffening the device while reducing the initial insertion trauma.

The electrochemical properties of the devices, although greater than those of the microwire electrodes used in this study, could also be improved further through the application of surface treatments or coatings [6], [8], [14], [15]. The multielectrodes must be assessed chronically *in vivo* to confirm that their enhanced flexibility truly improves tissue biocompatibility and device functionality compared to other intraspinal devices.

Finally, a key aspect of this multielectrode design, which I did not have time to personally assess, was the addition of PDMS-PEG BCP in the PDMS substrate. This substrate modification was reported to significantly improve PDMS surface hydrophilicity and decrease protein and cell adhesion *in vitro* for biomicrofluidics devices [23]. In parallel to my thesis research, I only had

time to assess this surface modification preliminarily in mixed mouse glial cell cultures in collaboration with Christopher Tsui in Dr. Kathryn Todd's laboratory. At 7 and 14 days, we have so far seen that the addition of PDMS-PEG markedly reduces astrocyte and microglia cell adhesion on the implant surfaces, which may serve to cloak the multielectrode from the nervous system [24] and decrease FBR even more. I regret that I did not have time to evaluate this further, although this remains an interesting avenue to explore in future research.

References

[1] H. Ozawa, T. Matsumoto, T. Ohashi, M. Sato, and S. Kokubun, "Mechanical properties and function of the spinal pia mater," *J. Neurosurg. Spine*, vol. 1, Jul., pp. 122-127, 2004.

[2] J. K. Nguyen, D. J. Park, J. L. Skousen, A. E. Hess-Dunning, D. J. Tyler, S. J. Rowan, C. Weder, and J. R. Capadona, "Mechanically-compliant intracortical implants reduce the neuroinflammatory response," *Journal of Neural Engineering*, vol. 11, no. 5, Aug., pp. 1-15, 2014.

[3] Z. J. Du, C. L. Kolarcik, T. D. Y. Kozai, S. D. Luebben, S. A. Sapp, X. S. Zheng, J. A. Nabity, and X. T. Cui, "Ultrasoft microwire neural electrodes improve chronic tissue integration," *Acta Biomaterialia*, vol. 53, Apr., pp. 46-58, 2017.

[4] A. Toossi, D. G. Everaert, A. Azar, C. R. Dennison, and V. K. Mushahwar, "Mechanically stable intraspinal microstimulation implants for human translation," *Annals of Biomedical Engineering*, vol. 45, no. 3, Mar., pp. 681-694, 2017.

[5] A. Abdo, M. Sahin, D. S. Freedman, E. Cevik, P. S. Spuhler, and M. S. Unlu, "Floating light-activated micro electrical stimulators tested in the rat spinal cord," *Journal of Neural Engineering*, vol. 5, no. 5, Oct., pp. 1-21, 2011.

[6] R. A. Green, P. B. Matteucci, C. W. D. Dodds, J. Palmer, W. F. Dueck, R. T. Hassarati, P. J. Byrnes-Preston, N. H. Lovell, and G. J. Suaning, "Laser patterning of platinum electrodes for safe neurostimulation," *Journal of Neural Engineering*, vol. 11, no. 5, Sept., 056017, 2014.

[7] M. Mueller, N. de la Oliva, J. del Valle, I. Delgado-Martínez, X. Navarro, and T. Stieglitz, "Rapid prototyping of flexible intrafascicular electrode arrays by picosecond laser structuring," *Journal of Neural Engineering*, vol. 14, no. 6, Nov., pp. 1-11, 2017.

[8] A. Kelly, N. Farid, K. Krukiewicz, N. Belisle, J. Grorke, E. M. Waters, A. Trotier, F. Laffir, M. Kilcoyne, G. M. O'Connor, and M. J. Biggs, "Laser-induced periodic surface structure enhances neuroelectrode charge transfer capabilities and modulates astrocyte function," *ACS Biomater. Sci. Eng.*, vol. 6, Mar., pp. 1449-1461, 2020.

[9] S. F. Cogan, "Neural Stimulation and Recording Electrodes," *Annu. Rev. Biomed. Eng.*, vol. 10, Apr., pp. 275-309, 2008.

[10] B. J. Holinski, K. A. Mazurek, D. G. Everaert, A. Toossi, A. M. Lucas-Osma, P. Troyk, R. Etienne-Cummings, R. B. Stein, and V. K. Mushahwar, "Intraspinal microstimulation produces over-ground walking in anesthetized cats," *J. Neural Eng.*, vol. 13, no. 5, Sept., pp. 1-17, 2016.

[11] A. N. Dalrymple, D. A. Roszko, R. S. Sutton, and V. K. Mushahwar, "Pavlovian control of intraspinal microstimulation to produce over-ground walking," *Journal of Neural Engineering*, vol. 17, no. 3, May, 036002, 2020.

[12] V. K. Mushahwar, D. F. Collins, and A. Prochazka, "Spinal cord microstimulation generates functional limb movements in chronically implanted cats," *Experimental Neurology*, vol. 163, Feb., pp. 422-429, 2000.

[13] J. A. Bamford, K. G. Todd, and V. K. Mushahwar, "The effects of intraspinal microstimulation on spinal cord tissue in the rat," *Biomaterials*, vol. 31, Apr., pp. 5552-5563, 2010.

[14] S. F. Cogan, P. R. Troyk, J. Ehrlich, and T. D. Plante, "In vitro comparison of the charge-injection limits of activated iridium oxide (AIROF) and platinum-iridium microelectrodes," *IEEE Trans. Biomed. Eng.,* vol. 52, no. 9, Sep., pp. 1612-1614, 2005.

[15] H. Vara and J. E. Collazos-Castro, "Enhanced spinal cord microstimulation using conducting polymer-coated carbon microfibers," *Acta Biomaterialia*, vol. 90, May, pp. 71-86, 2019.

[16] K. M. Szostak, L. Grand, and T. G. Constandinou, "Neural interfaces for intracortical recording: Requirements, fabrication methods, and characteristics," *Frontiers in Neuroscience*, vol. 11, art. 665, pp. 1-27, 2017.

[17] C. M. Tringides, N. Vachicouras, I. de Lázaro, H. Wang, A. Trouillet, B. R. Seo, A. Elosegui-Artola, F. Fallegger, Y. Shin, C. Casiraghi, K. Kostarelos, S. P. Lacour, and D. J. Mooney, "Viscoelastic surface electrode arrays to interface with viscoelastic tissues," *Nat. Nanotechnol.*, Jun., pp. 1-11, 2021.

[18] X. Wen, B. Wang, S. Huang, T. Liu, M. -S. Lee, P. -S. Chung, Y. T. Chow, I. -W. Huang, H. G. Monbouquette, N. T. Maidment, and P. -Y. Chiou, "Flexible, multifunctional neural probe with liquid metal enabled, ultra-large tunable stiffness for deep-brain chemical sensing and agent delivery," *Biosens Bioelectron.*, vol. 131, Apr., pp. 37-45, 2019.

[19] D. Afanasenkau, D. Kalinina, V. Lyakhovetskii, C. Tondera, O. Gorsky, S. Moosavi, N. Pavlova, N. Merkulyeva, A. V. Kalueff, I. R. Minev, and P. Musienko, "Rapid prototyping of soft bioelectronic implants for use as neuromuscular interfaces," *Nat Biomed. Eng.,* vol. 4, Sept., pp. 1010-1022, 2020.

[20] H. Yuk, B. Lu, S. Lin, K. Qu, J. Xu, J. Luo, and X. Zhao, "3D printing of conducting polymers," *Nat. Comm.*, vol. 11, Mar., 1604, 2020.

[21] S. H. Felix, K. G. Shah, V. M. Tolosa, H. J. Sheth, A. C. Tooker, T. L. Delima, S. P. Jadhav, L. M. Frank, and S. S. Pannu, "Insertion of flexible neural probes using rigid

stiffeners attached with biodissolvable adhesive," *Journal of Visualized Experiments*, vol. 79, 50609, 2013.

[22] A. Lecomte, V. Castagnola, E. Descamps, L. Dahan, M. C. Blatché, T. M. Dinis, E. Leclerc, C. Egles, and C. Bergaud, "Silk and PEG as means to stiffen a parylene probe for insertion in the brain: Toward a double time-scale tool for local drug delivery," *J. Micromech. Microeng.*, vol. 25, 125003, 2015.

[23] A. Gökaltun, Y. B. A. Kang, M. L. Yarmush, O. B. Usta, and A. Asatekin, "Simple surface modification of poly(dimethylsiloxane) via surface segregating smart polymers for biomicrofluidics," *Scientific Reports*, vol. 9, 7377, 2019.

[24] T. D. Y. Kozai, N. B. Langhals, P. R. Patel, X. Deng, H. Zhang, K. L. Smith, J. Lahann, N. A. Kotov, and D. R. Kipke, "Ultrasmall implantable composite microelectrodes with bioactive surfaces for chronic neural interfaces," *Nat. Mater.*, vol. 11, no. 12, Dec., pp. 1065-1073, 2012.

[25] A. Toossi, D. G. Everaert, R. R. E. Uwiera, D. S. Hu, K. Robinson, F. S. Gragasin, and V. K. Mushahwar, "Effect of anesthesia on motor responses evoked by spinal neural prostheses during intraoperative procedures," *Journal of Neural Engineering*, vol. 16, Mar., pp. 1-18, 2019.

Bibliography

[1] C. S. Ahuja, J. R. Wilson, S. Nori, M. R. N. Kotter, C. Druschel, A. Curt, and M. G. Fehlings, "Traumatic spinal cord injury," *Nature Reviews Disease Primers*, vol. 3, no. 1, Apr., pp. 1-21, 2017.

[2] V. K. Noonan, M. Fingas, A. Farray, D. Baxter, A. Singh, M. G. Fehlings, and M. F. Dvorak, "Incidence and prevalence of spinal cord injury in Canada: A national perspective," *Neuroepidemiology*, vol. 38, no. 4, June, pp. 219-226, 2012.

[3] R. Sweis, and José Biller, "Systemic complications of spinal cord injury," *Current Neurology and Neuroscience Reports*, vol. 17, art. 8, Feb., pp. 1-8, 2017.

[4] I. H. Tsai, D. E. Graves, W. Chan, C. Darkoh, M-S. Lee, and L. A. Pompeii, "Environmental barriers and social participation in individuals with spinal cord injury," *Rehabilitation Psychology*, vol. 62, no. 1, Feb., pp. 36-44, 2017.

[5] H. Krueger, V. K. Noonan, L. M. Trenaman, P. Joshi, and C. S. Rivers, "The economic burden of traumatic spinal cord injury in Canada," *Chronic diseases and injuries in Canada*, vol. 33, no. 3, June, pp. 1-26, 2013.

[6] L. A. Simpson, J. J. Eng, J. T. C. Hsieh, D. L. Wolfe, and the SCIRE Research Team, "The health and life priorities of individuals with spinal cord injury: A systematic review," *Journal of Neurotrauma*, vol. 29, no. 8, May, pp. 1548-1555, 2012.

[7] M. G. Fehlings, L. A. Tetreault, J. R. Wilson, B. K. Kwon, A. S. Burns, A. R. Martin, G. Hawryluk, and J. S. Harrop, "A clinical practice guideline for the management of acute spinal cord injury: Introduction, rationale, and scope," *Global Spine Journal*, vol. 7, no. 3, Sep., pp. 84S-94S, 2017.

[8] A. K. Varma, A. Das, G. Wallace IV, J. Barry, A. A. Vertegel, S. K. Ray, and N. L. Banik, "Spinal cord injury: A review of current therapy, future treatments, and basic science frontiers," *Neurochemical Research*, vol. 38, Mar., pp. 895-905, 2013.

[9] M. M. Zavvarian, A. Toossi, M. Khazaei, J. Hong, and M. G. Fehlings, "Novel innovations in cell and gene therapies for spinal cord injury," *F1000Research*, vol. 9, Apr., pp. 1-11, 2020.

[10] K. E. Musselman, M. Shah, and J. Zariffa, "Rehabilitation technologies and interventions for individuals with spinal cord injury: Translational potential of current trends," *Journal of NeuroEngineering and Rehabilitation*, vol. 15, art. 40, May., pp. 1-8, 2018.

[11] C. H. Ho, R. J. Triolo, A. L. Elias, K. L. Kilgore, A. F. DiMarco, K. Bogie, A. H. Vette, M. Audu, R. Kobetic, S. R. Chang, K. M. Chan, S. Dukelow, D. J. Bourbeau, S. W. Brose, K. J. Gustafson, Z. Kiss, and V. K. Mushahwar, "Functional electrical stimulation

and spinal cord injury," *Phys Med Rehabil Clin N Am.*, vol. 25, no. 3, Aug., pp. 1-30, 2014.

[12] F. B. Wagner, J-B. Mignardot, C. G. Le Goff-Mignardot, R. Demesmaeker, S. Komi, M. Capogrosso, A. Rowald, I. Seáñez, M. Caban, E. Pirondini, M. Vat, L. A. McCracken, R. Heimgartner, I. Fodor, A. Watrin, P. Seguin, E. Paoles, K. Van Den Keybus, G. Eberle, B. Schurch, E. Pralong, F. Becce, J. Prior, N. Buse, R. Buschman, E. Neufeld, N. Kuster, S. Carda, J. von Zitzewitz, V. Delattre, T. Denison, H. Lambert, K. Minassian, J. Bloch, and G. Courtine, "Targeted neurotechnology restores walking in humans with spinal cord injury," *Nature*, vol. 563, Oct., pp. 65-71, 2018.

[13] R. J. Triolo, S. N. Bailey, M. E. Miller, L. M. Rohde, J. S. Anderson, J. A. Jr. Davis, J. J. Abbas, L. A. DiPonio, G. P. Forrest, D. R. Jr. Gater, and L. J. Yang, "Longitudinal performance of a surgically implanted neuroprosthesis for lower extremity exercise, standing, and transfers after spinal cord injury," *Arch Phys Med Rehabil.*, vol. 93, no. 5, May, pp. 896-904, 2012.

[14] D. Guiraud, T. Stieglitz, K. P. Koch, J. L. Divoux, and P. Rabischong, "An implantable neuroprosthesis for standing and walking in paraplegia: 5-year patient follow-up," *J. Neural Eng.*, vol. 3, no. 4, Sept., pp. 269-275, 2006.

[15] E. Henneman, G. Somjen, and D. O. Carpenter, "Functional significance of cell size in spinal motoneurons," *J. Neurophys.*, vol. 28, no. 3, May, pp. 560-580, 1965.

[16] T. S. Barss, E. N. Ainsley, F. C. Claveria-Gonzalez, M. J. Luu, D. J. Miller, M. J. Wiest, and D. F. Collins, "Utilizing physiological principles of motor unit recruitment to reduce fatigability of electrically-evoked contractions: A narrative review," *Archives of Physical Medicine and Rehabilitation*, vol. 99, no. 4, Apr., pp. 779-791, 2018.

[17] R. B. North and J. P. Prager, "Chapter 45: History of spinal cord stimulation," in *Neuromodulation, 2nd Ed.*, E. S. Krames, P. H. Peckham, and A. R. Rezai, Eds. Elsevier, 2018, pp-587-596.

[18] R. Herman, J. He, S. D'Luzansky, W. Willis, and S. Dilli, "Spinal cord stimulation facilitates functional walking in a chronic, incomplete spinal cord injured," *Spinal Cord*, vol. 40, no. 2, Feb., pp. 65-68, 2002.

[19] M. R. Carhart, J. He, R. Herman, S. D'Luzansky, and W. T. Willis, "Epidural spinal-cord stimulation facilitates recovery of functional walking following incomplete spinal-cord injury," *IEEE Trans. Neural Syst. Rehabil. Eng.*, vol. 12, no. 1, Mar., pp. 32-42, 2004.

[20] M. L. Gill, P. J. Grahn, J. S. Calvert, M. B. Linde, I. A. Lavrov, J. A. Strommen, L. A. Beck, D. G. Sayenko, M. G. Van Straaten, D. I. Drubach, D. D. Veith, A. R. Thoreson, C. Lopez, Y. P. Gerasimenko, V. R. Edgerton, K. H. Lee, and K. D. Zhao, "Neuromodulation of lumbosacral spinal networks enables independent stepping after complete paraplegia," *Nature Medicine*, vol. 24, Nov., pp. 1677-1682, 2018.

[21] C. A. Angeli, M. Boakye, R. A. Morton, J. Vogt, K. Benton, Y. Chen, C. K. Ferreira, and S. J. Harkema, "Recovery of over-ground walking after chronic motor complete spinal cord injury," *New England Journal of Medicine*, vol. 379, Sep., pp. 1244-1250, 2018.

[22] V. K. Mushahwar and K. W. Horch, "Muscle recruitment through electrical stimulation of the lumbo-sacral spinal cord," *IEEE Trans. Rehabil. Eng.*, vol. 8, no. 1, Mar., pp. 22-29, 2000.

[23] V. K. Mushahwar, D. F. Collins, and A. Prochazka, "Spinal cord microstimulation generates functional limb movements in chronically implanted cats," *Experimental Neurology*, vol. 163, Feb., pp. 422-429, 2000.

[24] L. Guevremont, C. G. Renzi, J. A. Norton, J. Kowalczewski, R. Saigal, and V. K. Mushahwar, "Locomotor-related networks in the lumbosacral enlargement of the adult spinal cat: Activation through intraspinal microstimulation," *IEEE Trans. Neural Syst. Rehabil. Eng.*, vol. 14, no. 3, Sep., pp. 266-272, 2006.

[25] R. A. Guant, A. Prochazka, V. K. Mushahwar, L. Guevremont, and P. H. Ellaway, "Intraspinal microstimulation excites multisegmental sensory afferents at lower stimulus levels than local α-motoneuron responses," *J. Neurophysiol*, vol. 96, no. 6, Dec., pp. 2995-3005, 2006.

[26] D. Barthélemy, H. Leblond, and S. Rossignol, "Characteristics and mechanisms of locomotion induced by intraspinal microstimulation and dorsal root stimulation in spinal cats," *J. Neuophysiol*, vol. 97, no. 3, Mar., pp. 1986-2000, 2007.

[27] V. K. Mushahwar, and K. W. Horch, "Selective activation of muscle groups in the feline hindlimb through electrical microstimulation of the ventral lumbo-sacral spinal cord," *IEEE Trans. Rehabil. Eng.*, vol. 8, no. 1, Mar., pp. 11-21, 2000.

[28] J. A. Bamford, C. T. Putman, and V. K. Mushahwar, "Intraspinal microstimulation preferentially recruits fatigue-resistant muscle fibres and generates gradual force in rat," *J. Physiol*, vol. 569, no. 3, Dec., pp. 873-884, 2005.

[29] J. T. Hachmann, J. H. Jeong, P. J. Grahn, G. W. Mallory, L. Q. Evertz, A. J. Bieber, D. A. Lobel, K. E. Bennet, K. H. Lee, and J. L. Lujan, "Large animal model for development of functional restoration paradigms using epidural and intraspinal stimulation," *PLoS ONE*, vol. 8, no. 12, Dec., pp. 1-7, 2013.

[30] A. Toossi, D. G. Everaert, S. I. Perlmutter, and V. K. Mushahwar, "Functional organization of motor networks in the lumbosacral spinal cord of non-human primates," *Scientific Reports*, vol. 9, Sept., pp. 1-16, 2019.

[31] B. Lau, L. Guevremont, and V. K. Mushahwar, "Strategies for generating prolonged functional standing using intramuscular stimulation or intraspinal microstimulation," *IEEE Trans. Neural Syst. Rehabil. Eng.*, vol. 15, no. 2, June, pp. 273-285, 2007.

[32] B. J. Holinski, K. A. Mazurek, D. G. Everaert, A. Toossi, A. M. Lucas-Osma, P. Troyk, R. Etienne-Cummings, R. B. Stein, and V. K. Mushahwar, "Intraspinal microstimulation produces over-ground walking in anesthetized cats," *J. Neural Eng.*, vol. 13, no. 5, Sept., pp. 1-17, 2016.

[33] D. B. Popovic, "Functional electrical stimulation for lower extremities," in *Neural Prostheses: Replacing Motor Function After Disease or Disability*, R. B. Stein, P. H. Peckham, and D. B. Popovic, Eds. New York: Oxford Univ. Press, 1992, pp. 233-251.

[34] R. Saigal, C. Renzi, and V. K. Mushahwar, "Intraspinal microstimulation generates functional movements after spinal-cord injury," *IEEE Trans. Neural Syst. Rehabil. Eng.*, vol. 12, no. 4, Dec., pp. 430-440, 2004.

[35] J. A. Bamford, R. M. Lebel, K. Parseyan, and V. K. Mushahwar, "The fabrication, implantation, and stability of intraspinal microwire arrays in the spinal cord of cat and rat," *IEEE Trans. Neural Syst. Rehabil. Eng.*, vol. 25, no. 3, Mar., pp. 287-296, 2017.

[36] P. J. Grahn, K. H. Lee, A. Kasasbeh, G. W. Mallory, J. T. Hachmann, J. R. Dube, C. J. Kimble, D. A. Lobel, A. Bieber, J. H. Jeong, K. E. Bennet, and J. L. Lujan, "Wireless control of intraspinal microstimulation in a rodent model of paralysis," *J. Neurosurg.*, vol. 123, Jul., pp. 232-242, 2015.

[37] J. A. Bamford, K. G. Todd, and V. K. Mushahwar, "The effects of intraspinal microstimulation on spinal cord tissue in the rat," *Biomaterials*, vol. 31, Apr., pp. 5552-5563, 2010.

[38] D. R. Merrill, M. Bikson, and J. G. R. Jefferys, "Electrical stimulation of excitable tissue: Design of efficacious and safe protocols," *J. Neurosci. Methods*, vol. 141, pp. 171-198, 2005.

[39] S. F. Cogan, "Neural Stimulation and Recording Electrodes," *Annu. Rev. Biomed. Eng.*, vol. 10, Apr., pp. 275-309, 2008.

[40] A. Toossi, B. Bergin, M. Marefatallah, B. Parhizi, N. Tyreman, D. G. Everaert, S. Rezaei, P. Seres, J. C. Gatenby, S. I. Perlmutter, and V. K. Mushahwar, "Comparative neuroanatomy of the lumbosacral spinal cord of the rat, cat, pig, monkey, and human," *Scientific Reports*, vol. 11, Jan., pp. 1-15, 2021.

[41] P. J. Grahn, S. J. Goerss, J. L. Lujan, G. W. Mallory, B. A. Kall, A. A. Mendez, J. K. Trevathan, J. P. Felmlee, K. E. Bennet, and K. H. Lee, "MRI-guided stereotactic system for delivery of intraspinal microstimulation," *SPINE*, vol. 41, no. 13, July, pp. E806-E813, 2016.

[42] A. Toossi, D. G. Everaert, P. Seres, J. L. Jaremko, K. Robinson, C. C. Kao, P. E. Konrad, and V. K. Mushahwar, "Ultrasound-guided spinal stereotactic system for intraspinal implants," *J. Neurosurg Spine*, vol., 29, Sept., pp. 292-305, 2018.

[43] S. Snow, S. C. Jacobsen, D. L. Wells, and K. W. Horch, "Microfabricated cylindrical multielectrodes for neural stimulation," *IEEE Trans. Biomed. Eng.*, vol. 53, no. 2, Feb., pp. 320-326, 2006.

[44] V. Pikov, L. Bullara, and D. B. McCreery, "Intraspinal stimulation for bladder voiding in cats before and after chronic spinal cord injury," *J. Neural Eng.*, vol. 4, no. 4, Dec., pp. 356-368, 2007.

[45] S. Shahdoost, S. B. Frost, D. J. Guggenmos, J. A. Borrell, C. Dunham, S. Barbay, R. J. Nudo, and P. Mohseni, "A brain-spinal interface (BSI) system-on-chip (SoC) for closed-loop cortically-controlled intraspinal microstimulation," *Analog Integrated Circuits and Signal Processing*, vol. 95, Jan., pp. 1-16, 2018.

[46] V. Pikov, D. B. McCreery, and M. Han, "Intraspinal stimulation with a silicon-based 3D chronic microelectrode array for bladder voiding in cats," *Journal of Neural Engineering*, vol. 17, Dec., pp. 1-13, 2020.

[47] R. Biran, D. C. Martin, and P. A. Tresco, "The brain tissue response to implanted silicon microelectrode arrays is increased when the device is tethered to the skull," *J. Biomed. Mater. Res. A.*, vol. 82, no. 1, Jul., pp. 169-178, 2007.

[48] A. Abdo, M. Sahin, D. S. Freedman, E. Cevik, P. S. Spuhler, and M. S. Unlu, "Floating light-activated micro electrical stimulators tested in the rat spinal cord," *Journal of Neural Engineering*, vol. 5, no. 5, Oct., pp. 1-21, 2011.

[49] F. Lotti, F. Ranieri, G. Vadalà, L. Zollo, and G. Di Pino, "Invasive intraneural interfaces: Foreign body reaction issues," *Frontiers in Neuroscience*, vol. 11, art. 497, Sept., 2017.

[50] V. S. Polikov, P. A. Tresco, and W. M. Reichert, "Response of brain tissue to chronically implanted neural electrodes," *Journal of Neuroscience Methods*, vol. 148, Aug., pp. 1-18, 2005.

[51] S. Sommakia, J. L. Rickus, and K. J. Otto, "Glial cells, but not neurons, exhibit a controllable response to a localized inflammatory microenvironment *in vitro*," *Frontiers in Neuroengineering*, vol. 7, art. 41, Nov., 2014.

[52] S. Sridar, M. A. Churchward, V. K. Mushahwar, K. G. Todd, and A. L. Elias, "Peptide modification of polyimide-insulated microwires: Towards improved biocompatibility through reduced glial scarring," *Acta Biomaterialia*, vol. 60, Jul., pp. 154-166, 2017.

[53] Y. Zhong, and R. V. Bellamkonda, "Dexamethasone coated neural probes elicit attenuated inflammatory response and neuronal loss compared to uncoated neural probes," *Brain Res.*, vol. 1148, May, pp. 15-27, 2007.

[54] J. Thelin, H. Jörntell, E. Psouni, M. Garwicz, J. Schouenborg, N. Danielsen, and C. E. Linsmeier, "Implant size and fixation mode strongly influence tissue reactions in the CNS," *PLoS ONE*, vol. 6, no. 1, Jan., 2011.

[55] S. Mirkiani, D. A. Roszko, R. Fox, P. R. Troyk, and V. K. Mushahwar, "Stretchable lead wires for long-term intraspinal microstimulation," presented at Neural Interfaces 2021: The NANS-NIC Joint Meeting (virtual), 2021.

[56] A. Toossi, D. G. Everaert, A. Azar, C. R. Dennison, and V. K. Mushahwar, "Mechanically stable intraspinal microstimulation implants for human translation," *Annals of Biomedical Engineering*, vol. 45, no. 3, Mar., pp. 681-694, 2017.

[57] J. K. Nguyen, D. J. Park, J. L. Skousen, A. E. Hess-Dunning, D. J. Tyler, S. J. Rowan, C. Weder, and J. R. Capadona, "Mechanically-compliant intracortical implants reduce the neuroinflammatory response," *Journal of Neural Engineering*, vol. 11, no. 5, Aug., pp. 1-15, 2014.

[58] D. B. McCreery, W. G. Agnew, T. G. H. Yuen, and L. Bullara, "Charge density and charge per phase as cofactors in neural injury induced by electrical stimulation," *IEEE Trans. Biomed. Eng.*, vol. 37, no. 10, Oct., pp. 996-1001, 1990.

[59] R. V. Shannon, "A model of safe levels for electrical stimulation," *IEEE Trans. Biomed. Eng.*, vol. 39, no. 4, Apr., pp. 424-426, 1992.

[60] S. F. Cogan, K. A. Ludwig, C. G. Welle, and P. Takmakov, "Tissue damage thresholds during therapeutic electrical stimulation," *Journal of Neural Engineering*, vol. 13, no. 2, Jan., pp. 1-13, 2016.

[61] D. McCreery, V. Pikov, and P. R. Troyk, "Neuronal loss due to prolonged controlled-current stimulation with chronically implanted microelectrodes in the cat cerebral cortex," *Journal of Neural Engineering*, vol. 7, no. 3, May, pp. 1-9, 2010.

[62] S. F. Cogan, P. R. Troyk, J. Ehrlich, and T. D. Plante, "In vitro comparison of the charge-injection limits of activated iridium oxide (AIROF) and platinum-iridium microelectrodes," *IEEE Trans. Biomed. Eng.,* vol. 52, no. 9, Sep., pp. 1612-1614, 2005.

[63] H. Vara and J. E. Collazos-Castro, "Enhanced spinal cord microstimulation using conducting polymer-coated carbon microfibers," *Acta Biomaterialia*, vol. 90, May, pp. 71-86, 2019.

[64] A. N. Dalrymple, U. A. Robles, M. Huynh, B. A. Nayagam, R. A. Green, L. A. Poole-Warren, J. B. Fallon, and R. K. Sheperd, "Electrochemical and biological performance of chronically stimulated conductive hydrogel electrodes," *Journal of Neural Engineering*, vol. 17, Apr., pp. 1-17, 2020.

[65] R. T. Leung, M. N. Shivdasani, D. A. X. Nayagam, and R. K. Shepherd, "In Vivo and in vitro comparison of the charge injection capacity of platinum macroelectrodes," *IEEE Trans. Biomed. Eng.*, vol. 62, no. 3, Mar., pp. 849-857, 2015.

[66] Z. J. Du, C. L. Kolarcik, T. D. Y. Kozai, S. D. Luebben, S. A. Sapp, X. S. Zheng, J. A. Nabity, and X. T. Cui, "Ultrasoft microwire neural electrodes improve chronic tissue integration," *Acta Biomaterialia*, vol. 53, Apr., pp. 46-58, 2017.

[67] K. M. Szostak, L. Grand, and T. G. Constandinou, "Neural interfaces for intracortical recording: Requirements, fabrication methods, and characteristics," *Frontiers in Neuroscience*, vol. 11, art. 665, pp. 1-27, 2017.

[68] A. Weltman, J. Yoo, and E. Meng, "Flexible, penetrating brain probes enabled by advances in polymer microfabrication," *Micromachines*, vol. 7, no. 10, Oct., pp. 1-36, 2016.

[69] C. H. Thompson, T. A. E. Riggins, P. R. Patel, C. A. Chestek, W. Li, and E. Purcell, "Toward guiding principles for the design of biologically-integrated electrodes for the central nervous system," *J. Neural Eng.*, vol. 17, no. 2, Mar., 2020.

[70] C. Hassler, T. Boretius, and T. Steiglitz, "Polymers for neural implants," *Polymer Physics*, vol. 49, pp. 18-33, 2011.

[71] H. Ozawa, T. Matsumoto, T. Ohashi, M. Sato, and S. Kokubun, "Mechanical properties and function of the spinal pia mater," *J. Neurosurg. Spine*, vol. 1, Jul., pp. 122-127, 2004.

[72] K. C. Cheung, P. Renaud, H. Tanila, and K. Djupsund, "Flexible polyimide microelectrode array for in vivo recordings and current source density analysis," *Biosensors and Bioelectronics*, vol. 22, pp. 1783-1790, 2007.

[73] M. Mueller, N. de la Oliva, J. del Valle, I. Delgado-Martínez, X. Navarro, and T. Stieglitz, "Rapid prototyping of flexible intrafascicular electrode arrays by picosecond laser structuring," *Journal of Neural Engineering*, vol. 14, no. 6, Nov., pp. 1-11, 2017.

[74] S. Shin, J. H. Kim, J. Jeong, T. M. Gwon, S. H. Lee, and S. J. Kim, "Novel four-sided neural probe fabricated by a thermal lamination process of polymer films," *J. Neurosci. Methods*, vol. 278, pp. 25-35, 2017.

[75] R. T. Rihani, A. M. Stiller, J. O. Usoro, H. Lawson, H. Kim, B. J. Black, V. R. Danda, J. Maeng, V. D. Varner, T. H. Ware, and J. J. Pancrazio, "Deployable, liquid crystal elastomer-based intracortical probes," *Acta Biomaterialia*, vol. 111, pp. 54-64, 2020.

[76] J. M. Kim, D. R. Oh, J. Sanchez, S. H. Kim, and J. M. Seo, "Fabrication of polydimethylsiloxane (PDMS) - based multielectrode array for neural interface,"*35th Annual International Conference of the IEEE EMBS*, Jul., pp. 1716-1719, 2013.

[77] I. R. Minev, P. Musienko, A. Hirsch, Q. Barraud, N. Wenger, E. M. Moraud, J. Gandar, M. Capogrosso, T. Milekovic, L. Asboth, R. F. Torres, N. Vachicouras, Q. Liu, N. Pavlova, S. Duis, A. Larmagnac, J. Vörös, S. Micera, Z. Suo, G. Courtine, and S. P. Lacour, "Electronic dura mater for long-term multimodal neural interfaces," *Science*, vol. 347, no. 6218, Jan., pp. 159-163, 2015.

[78] T. D. Y. Kozai, and D. R. Kipke, "Insertion shuttle with carboxyl terminated self-assembled monolayer coatings for implanting flexible polymer neural probes in the brain," *J. Neurosci. Methods*, vol. 184, no. 2, Nov., pp. 199-205, 2009.

[79] X. Wen, B. Wang, S. Huang, T. Liu, M. -S. Lee, P. -S. Chung, Y. T. Chow, I. -W. Huang, H. G. Monbouquette, N. T. Maidment, and P. -Y. Chiou, "Flexible, multifunctional neural probe with liquid metal enabled, ultra-large tunable stiffness for deep-brain chemical sensing and agent delivery," *Biosens Bioelectron.*, vol. 131, Apr., pp. 37-45, 2019.

[80] S. H. Felix, K. G. Shah, V. M. Tolosa, H. J. Sheth, A. C. Tooker, T. L. Delima, S. P. Jadhav, L. M. Frank, and S. S. Pannu, "Insertion of flexible neural probes using rigid stiffeners attached with biodissolvable adhesive," *Journal of Visualized Experiments*, vol. 79, 50609, 2013.

[81] J. Agorelius, F. Tsanakalis, A. Friberg, P. T. Thorbergsson, L. M. E. Pettersson, and G. Schouenborg, "An array of highly flexible electrodes with a tailored configuration locked by gelatin during implantation - initial evaluation in cortex cerebri of awake rats," *Frontiers in Neuroscience*, vol. 9, art. 331, Sep., pp. 1-12, 2015.

[82] A. Lecomte, V. Castagnola, E. Descamps, L. Dahan, M. C. Blatché, T. M. Dinis, E. Leclerc, C. Egles, and C. Bergaud, "Silk and PEG as means to stiffen a parylene probe for insertion in the brain: Toward a double time-scale tool for local drug delivery," *J. Micromech. Microeng.*, vol. 25, 125003, 2015.

[83] Z. Zhao, X. Li, F. He, X. Wei, S. Lin, and C. Xie, "Parallel, minimally-invasive implantation of ultra-flexible neural electrode arrays," *J. Neural Eng.*, vol. 16, no. 3, Jun., 035001, 2019.

[84] A. M. Stiller, J. O. Usoro, J. Lawson, B. Araya, M. A. González-González, V. R. Danda, W. E. Voit, B. J. Black, and J. J. Pancrazio, "Mechanically robust, softening shape memory polymer probes for intracortical recording," *Micromachines*, vol. 11, no. 6, art. 619, Jun., 2020.

[85] M. Schuettler, B. V. King, and G. J. Suaning, "Fabrication of implantable microelectrode arrays by laser cutting of silicone rubber and platinum foil," *Journal of Neural Engineering*, vol. 2, no. 1, Feb., pp. S121-S128, 2005.

[86] C. W. D. Dodds, M. Schuettler, T. Guenther, N. H. Lovell, and G. J. Suaning, "Advancements in electrode design and laser techniques for fabricating micro-electrode

arrays as part of a retinal prosthesis," *2011 Annual International Conference of the IEEE Engineering in Medicine and Biology Society*, Aug., pp. 636-639, 2011.

[87] H. T. Lancashire, A. Canhoestenberghe, C. J. Pendegrass, Y. A. Ajam, E. Magee, N. Donaldson, and G. W. Blunn, "Microchannel neural interface manufacture by stacking silicone and metal foil laminae," *Journal of Neural Engineering*, vol. 13, no. 3, Mar., pp. 1-9, 2016.

[88] W. Shen, L. Karumbaiah, X. Liu, T. Saxena, S. Chen, R. Patkar, R. V. Bellamkonda, and M. G. Allen, "Extracellular matrix-based intracortical microelectrodes: Toward a microfabricated neural interface based on natural materials," *Microsystems & Nanoengineering*, vol. 1, art. 15010, Jun., pp. 1-12, 2015.

[89] R. A. Green, J. S. Ordonez, M. Schuettler, L. A. Poole-Warren, N. H. Lovell, and G. J. Suaning, "Cytotoxicity of implantable microelectrode arrays produced by laser micromachining," *Biomaterials*, vol. 31, no. 5, Feb., pp. 886-893, 2010.

[90] A. Kelly, N. Farid, K. Krukiewicz, N. Belisle, J. Grorke, E. M. Waters, A. Trotier, F. Laffir, M. Kilcoyne, G. M. O'Connor, and M. J. Biggs, "Laser-induced periodic surface structure enhances neuroelectrode charge transfer capabilities and modulates astrocyte function," *ACS Biomater. Sci. Eng.*, vol. 6, Mar., pp. 1449-1461, 2020.

[91] A. Gökaltun, Y. B. A. Kang, M. L. Yarmush, O. B. Usta, and A. Asatekin, "Simple surface modification of poly(dimethylsiloxane) via surface segregating smart polymers for biomicrofluidics," *Scientific Reports*, vol. 9, 7377, 2019.

[92] G. Chryssolouris, *Laser Machining: Theory and Practice*. New York: Springer Science+Business Media, 1991.

[93] J. Qu, Q. Wu, T. Clancy, Q. Fan, X. Wang, and X. Liu, "3D-printed strain-gauge micro force sensors," *IEEE Sensors Journal*, vol. 20, no. 13, Jul., pp. 6971-6978, 2020.

[94] A. Toossi, D. G. Everaert, R. R. E. Uwiera, D. S. Hu, K. Robinson, F. S. Gragasin, and V. K. Mushahwar, "Effect of anesthesia on motor responses evoked by spinal neural prostheses during intraoperative procedures," *Journal of Neural Engineering*, vol. 16, Mar., pp. 1-18, 2019.

[95] R. A. Green, P. B. Matteucci, C. W. D. Dodds, J. Palmer, W. F. Dueck, R. T. Hassarati, P. J. Byrnes-Preston, N. H. Lovell, and G. J. Suaning, "Laser patterning of platinum electrodes for safe neurostimulation," *Journal of Neural Engineering*, vol. 11, no. 5, Sept., 056017, 2014.

[96] A. N. Dalrymple, D. A. Roszko, R. S. Sutton, and V. K. Mushahwar, "Pavlovian control of intraspinal microstimulation to produce over-ground walking," *Journal of Neural Engineering*, vol. 17, no. 3, May, 036002, 2020.

[97] C. M. Tringides, N. Vachicouras, I. de Lázaro, H. Wang, A. Trouillet, B. R. Seo, A. Elosegui-Artola, F. Fallegger, Y. Shin, C. Casiraghi, K. Kostarelos, S. P. Lacour, and D. J. Mooney, "Viscoelastic surface electrode arrays to interface with viscoelastic tissues," *Nat. Nanotechnol.*, Jun., pp. 1-11, 2021.

[98] H. Yuk, B. Lu, S. Lin, K. Qu, J. Xu, J. Luo, and X. Zhao, "3D printing of conducting polymers," *Nat. Comm.*, vol. 11, Mar., 1604, 2020.

[99] D. Afanasenkau, D. Kalinina, V. Lyakhovetskii, C. Tondera, O. Gorsky, S. Moosavi, N. Pavlova, N. Merkulyeva, A. V. Kalueff, I. R. Minev, and P. Musienko, "Rapid prototyping of soft bioelectronic implants for use as neuromuscular interfaces," *Nat Biomed. Eng.,* vol. 4, Sept., pp. 1010-1022, 2020.

[100] T. D. Y. Kozai, N. B. Langhals, P. R. Patel, X. Deng, H. Zhang, K. L. Smith, J. Lahann, N. A. Kotov, and D. R. Kipke, "Ultrasmall implantable composite microelectrodes with bioactive surfaces for chronic neural interfaces," *Nat. Mater.*, vol. 11, no. 12, Dec., pp. 1065-1073, 2012.

[101] A. Singh, L. Tetreault, S. Kalsi-Ryan, A. Nouri, and M. G. Fehlings, "Global prevalence and incidence of traumatic spinal cord injury," *Clinical Epidemiology*, vol. 6, Sep., pp. 309-331, 2014.

[102] National Spinal Cord Injury Statistical Center, Facts and Figures at a Glance, Birmingham, AL: University of Alabama at Birmingham, 2016.

[103] V. K. Mushahwar, D. M. Gillard, M. J. A. Gauthier, and A. Prochazka, "Intraspinal microstimulation generates locomotor-like and feedback-controlled movements," *IEEE Trans. Neural Syst. Rehabil. Eng.*, vol. 10, no. 1, Mar., pp. 68-81, 2002.

[104] AZoMaterials, "Platinum - Properties and Applications," *azom.com*. [Online]. Available: https://www.azom.com/properties.aspx?ArticleID=601. [Accessed Jul. 16, 2021].

[105] AZoMaterials, "Iridium - Properties and Applications," *azom.com*. [Online]. Available: https://www.azom.com/properties.aspx?ArticleID=1700. [Accessed Jul. 16, 2021].

[106] S. F. Cogan, "In vivo and in vitro differences in the charge-injection and electrochemical properties of iridium oxide electrodes," In Proc. IEEE EMBS Annual International Conference, 2006, pp. 882-885.

[107] M. Schuettler, "Electrochemical properties of platinum electrodes in vitro: comparison of six different surface qualities," In Proc. 29th Annual International Conference of the IEEE EMBS, 2007, pp. 186-189.

[108] R. Biran, D. C. Martin, and P. A. Tresco, “Neuronal cell loss accompanies the brain tissue response to chronically implanted silicon microelectrode arrays,” *Experimental Neurology*, vol. 195, pp. 115-126, 2005.

[109] T. L. Rose and L. S. Robblee, “Electrical stimulation with Pt electrodes. VIII. Electrochemically safe charge injection limits with 0.2 ms pulses,” *IEEE Trans. Biomed. Eng.*, vol. 37, no. 11, Nov., pp. 1118-1120, 1990.

[110] E. Schmidt, P. Raposo, R. Vavrek, and K. Fouad, “Inducing inflammation following subacute spinal cord injury in female rats: A double-edged sword to promote motor recovery,” *Brain, Behavior, and Immunity*, vol. 93, Mar., pp. 55-65, 2021.

[111] A. N. Dalrymple, M. Huynh, U. A. Robles, J. B. Marroquin, C. D. Lee, A. Petrossians, J. J. Whalen III, D. Li, H. C. Parkington, J. S. Forsythe, R. A. Green, L. A. Poole-Warren, R. K. Shepherd, and J. B. Fallon, “Electrochemical and mechanical performance of reduced graphene oxide, conductive hydrogel, and electrodeposited Pt-Ir coated electrodes: an active in vitro study,” *Journal of Neural Engineering*, vol. 17, Dec., 016015, 2019.

[112] K. A. Mazurek, B. J. Holinski, D. G. Everaert, R. B. Stein, R. Etienne-Cummings, and V. K. Mushahwar, “Feed forward and feedback control for over-ground locomotion in anaesthetized cats,” *Journal of Neural Engineering*, vol. 9, Apr., 026003, 2012.